Master Thesis in Geosciences

Structural Analysis of the Troms-Finnmark Fault Complex, SW Barents Sea

Waqas Ahmed

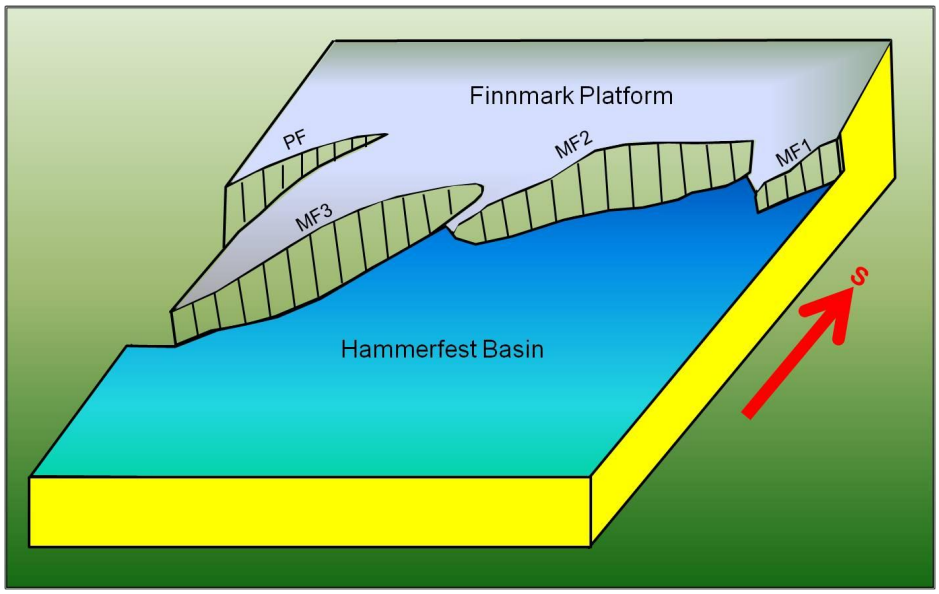

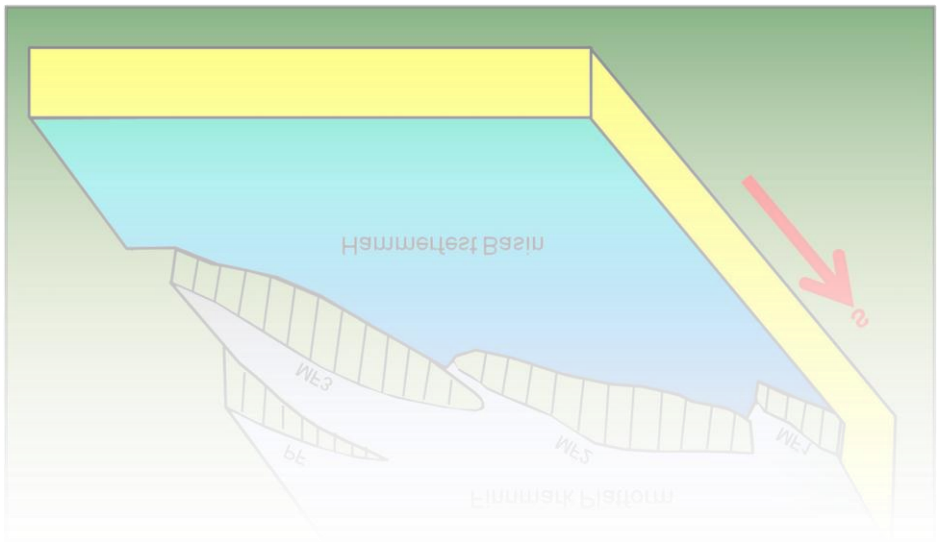

UNIVERSITY OF OSLO
FACULTY OF MATHEMATICS AND NATURAL SCIENCES

Structural Analysis of the Troms-Finnmark Fault Complex, SW Barents Sea

Waqas Ahmed

Master Thesis in Geosciences

Discipline: Petroleum Geology and Geophysics

Department of Geosciences

Faculty of Mathematics and Natural Sciences

UNIVERSITY OF OSLO

February, 2012

Abstract

Detailed structural analysis of the Troms-Finnmark Fault Complex is implemented in order to understand the associated structural configuration and the stress apparatus responsible for the present day architecture of the area under investigation. The en-echelon array of the fault complex is composed of three constituent, softly-linked fault strands named as MF1, MF2 & MF3. This fault complex registers repeated episodes of reactivation since its inception in the late Paleozoic. Late Paleozoic fault dating is constrained by making use of "Expansion Index" analysis which indicates growth of strata belonging to this age. Stratigraphic dating provides control on the age-bracketing of the fault movement during the middle-late Mesozoic. The master fault strands MF2 and MF3, on the basis of stratigraphic age dating reveals a bicyclic kinematic behavior.

The profile view of these fault strands (MF1, MF2 & MF3) display a wide variety of the master fault geometries which range from the planar through the slightly curved to the typical listric normal fault, which all show a down-to-the-North displacement. On the basis of the basement-involvement and degree of reactivation, the three fault strands are termed as ***"First-Class"*** faults. The maximum fault displacement is associated with the central fault strand MF2 where the displacement values surpass 2.7 km towards the central part, while the greatest displacement values for the fault segment MF3 are slightly above 1.5 km at the intra Permian level.

Several instances of positive structural inversion are documented in the study area. The analysis of kinematic indicators of such features suggests that the compressive stress system acting perpendicular to the master faults is responsible for their development. Their analysis further yields information on the age of inversion structures and this episodic event is placed in the mid-late Jurassic to the late Cretaceous.

The first order estimate of the paleo-stress orientations is carried out. During the Permian, the WNW-ESE oriented σ_3 is interpreted to have influenced the study area. The stress regime shifted to the NE-SW oriented σ_3 during the mid-Jurassic and the orientation of minimum principal stress direction is interpreted to be NW-SE for the early Cretaceous. These local stress vectors do not conform to the regional stress orientations determined by previous workers, however, the NW-SE oriented σ_3 during the Tertiary, shows agreement with the regional interpretations.

Acknowledgements

I express special appreciation to my supervisor Professor Roy Helge Gabrielsen for his invaluable input and thought-provoking discussions during the course of this study. He has been tremendously supportive in shaping my thoughts to carry out this work within the time frame. I am also grateful to Professor Jan Inge Faleide for his significant input in this study especially, while improving the manuscript. His comments and suggestions were very constructive and useful. I owe special thanks to Dr. Michel Heeremans, co-supervisor, who helped in data management.

I particularly want to acknowledge TGS-Nopec for providing the seismic data for this study.

I thank my entire family for their patience, support and love throughout my stay in Oslo. Finally, I would like to extend gratitude to my friends, who made the stay in Norway worth-remembering.

W.A

Contents

Chapter 1
Introduction

The area under investigation lies in the the SW Barents Sea *(Fig. 1.1).* The Barents Sea comprises the north-western corner of the Eurasian continental shelf (Faleide et al., 1993a). Svalbard archipelago and Franz Josef Land marks the northern extent of the Barents Sea while Kola peninsula and Norwegian mainland are located to its south. Eastern boundary of the Barents Shelf is defined by Novaya Zemlya while the western limit is demarcated by the oceanic crust of Norwegian-Greenland Sea *(Fig. 1.1)* (Faleide et al., 1984).

The SW Barents Sea encompasses some of the world's deepest sedimentary basins. These were formed as a consequence of various regional tectonics episodes within the North Atlantic-Arctic region, eventually ending-up with continental separation of Eurasia and Greenland and formation of the oceanic crust (Norwegian-Greenland Sea) in the Early Tertiary (Faleide et al., 1993a). A relatively complete sedimentary package ranging in age from the late Paleozoic to the Quaternary is preserved in the Barents Shelf which exceeds in thickness of above 15 km at places (Gudlaugsson et al., 1998).

Structurally, the Barents Shelf is composed of a mosaic of basins, fault complexes and intra-basinal highs with their orientations largely derived from pre-existing structural grain, related to Caledonian and older orogenies affecting the area *(Fig. 2.1)* (Gabrielsen et al., 1990). Evidences of the late Palaeozoic to Cenozoic tectonic activity are well documented in the western Barents Sea. It was later concluded that recurring reactivation of the major fault zones with each new tectonic acitivity is an obvious phenomenon of this area (Gabrielsen, 1984; Gabrielsen et al., 1997; Gabrielsen et al., 2011). The Troms-Finnmark Fault Complex runs parallel to the coastline of Troms and Finnmark counties *(Fig. 2.3)* between 69°20'N, 16°E and $71^0$40'N, $23^0$40'E (Gabrielsen et al., 1990). This extensional fault complex serves as a structural division between the Finnmark Platform in the south-southeast and northward basins such as Harstad, Tromsø and Hammerfest basins (Gabrielsen et al., 1990) (detailed description presented in Chapter 2).

The main aim of present study is to analyze the structural configuration and evolution of the Troms-Finnmark Fault Complex through time. Details derived from this study are then contested in a regional context and their mutual temporal and spatial relationship is evaluated.

Figure 1.1: Location Map of study area in yellow higlighted rectangle points to the approximate location of the Troms- Finnmark Fault Complex located in SW Barents Sea (modified from www.wikipedia.org).

Detailed structural analysis is done by employing three fundamental techniques of structural geology which includes descriptive, kinematic and dynamic analysis. All of these tend to look at the same geological phenomenon from a different perspective. ***Descriptive analysis (Chapter 3)*** is related to recognition and description of structures and recording their orientations. ***Kinematic analysis(Chapter 4)*** concentrates on understanding the deformational movements that result in the formation of structures while ***dynamic analysis (Chapter 4)*** primarily deals with deformational movements in the terminology of stresses and forces that make and shape the structures (Davis, 1984).

Data utilized during course of the present study includes 2D seismic reflection data while borehole data is incorporated for stratigraphic calibration. Seismic interpretation is carried out using Schlumberger's Petrel software. In order to understand the structural configuration of the Troms-Finnmark Fault Complex, interpretation of regional 2D seismic lines is carried out at the very beginning in order to gain an insight on the regional structural setting of the area. It was

followed by a cautious seismic-to-well tie procedure, to accomplish stratigraphic calibration, only after which detailed interpretation of different pre-decided reflections became possible *(section 3.4)*. Detailed interpretation involved faults' interpretation and reflections' interpretation and this initial interpretation served as basis for the construction of time-structure maps, fault maps and time-thickness maps *(Fig. 3.1)*. All the data sets were then integrated to resolve the following:

a. Classification of the fault complex by utilizing the time-structure maps, fault maps and the selected cross-sections (Chapter 3).
b. Fault Dating and analysis of the hangingwall accommodation structures (Chapter 4).
c. Comprehending the structural architecture of the fault complex and the governing stress system at different stages of the fault evolution (Chapter 3&4).
d. Comparison of the outcomes of the present study with the regional geological framework of the Barents Sea (Chapter 4).

These aspects together constitute the core of present structural analysis on comprehending the temporal and spatial evolution of the Troms-Finnmark Fault Complex which is the most significant underlying purpose of this study.

Chapter 2
Regional Tectonics & Stratigraphic Framework

2.1 Regional Tectonics

The Barents Shelf has an intracratonic setting that underwent various episodes of tectonic activity since Caledonian Orogeny (Gabrielsen et al., 1990). Ziegler (1986) explained that the crystalline basement of Western and Central Europe is composed of a range of crustal elements that were consolidated during pre-Grenvillian, the Grenvillian-Dalslandian, Morarian, Cadomian, Caledonian and Hercynian orogenies. Closure of the Iapetus Ocean and the consequent collision of Greenland, Norway and Spitsbergen in early Paleozoic is referred to as the Caledonian Orogeny and metamorphic basement of the Barents Sea belongs to this tectonic event (Dengo & Røssland, 1992). Structural features related to this orogeny show a north-east trend in northern mainland Norway (Sturt et al., 1978; Townsend, 1987) while a north-west strike of structural features predominates Spitsbergen (Harland, 1985; Dengo & Røssland 1992). Extensional basins that formed in the subsequent rifting episodes bear strong resemblance with the orientation of pre-existing fracture system pointing that orientation of younger extensional features were controlled largely by the pre-existing structural grain (Gabrielsen, 1984; Gabrielsen et al., 1990; Dengo & Røssland 1992).

Gabrielsen et al. (1990) argued that most of the known major structural trends may have been shaped by the Devonian and some significant features could be linked with the Caledonian Orogeny itself. They further commented that Archean to late Precambrian deformation in Svalbard and northern Norway established N-S to NNW-SSE and WNW-ESE to NW-SE structural trends (Harland, 1969; Harland et al., 1974; Beckinsale et al., 1975; Kjøde et al., 1978; Berthelsen & Marker, 1986; Rider, 1988). While the Caledonian deformation resulted in ENE-WSW to NE-SW striking structural features (Roberts, 1971; Roberts, 1972; Worthing, 1984) and subsequent reactivation of WNW-ESE trending pre-existing faults like the Trollfjord-Komagelv Fault (Johnson et al.,1978; Kjøde et al., 1978; Jensen & Broks, 1988; as cited in Gabrielsen et al., 1990). Erosion followed the Caledonian Orogeny in late Silurian - early Devonian, resulting in thick succession of continental clastic sediments known as Old Red Sandstone (Roberts &Sturt, 1980; Dengo & Røssland, 1992).

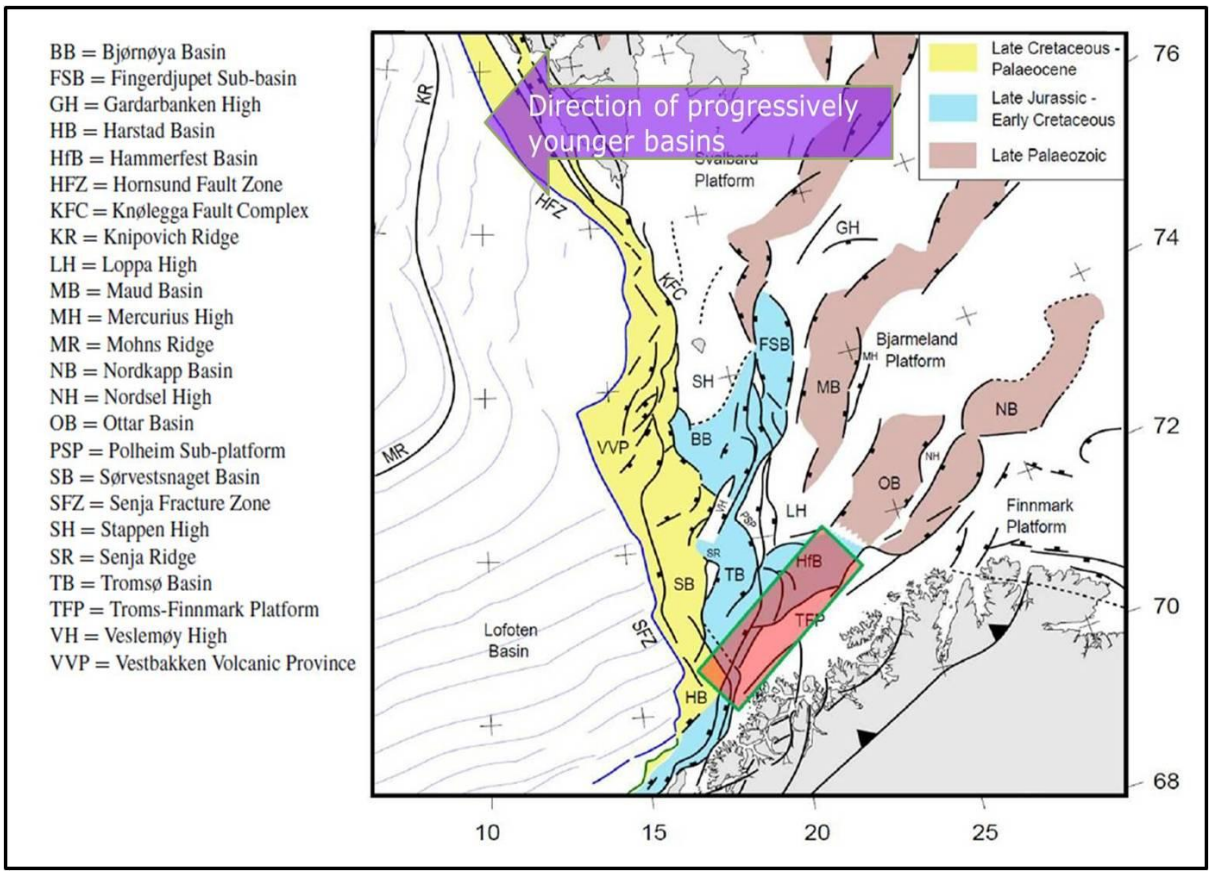

Figure 2.1: Main structural elements of Barents Sea, basins become yourngger from east towards west, red highlighted box points to the location of Troms-Finnmark Fault Complex (modified from Faleide et al., 2010).

Gudlaugsson et al. (1998) suggested post-Caledonian extensional collapse towards the southeast of Bjørnøya while the Devonian graben of Spitsbergen related to this extensional collapse is presented as a field analogue (cited in Barrere et al., 2009). However, such Devonian grabens have not been found on the entire SW Barents Shelf (Johansen et al.,1994). The post-Caledonian geological evolution of the western Barents Sea is controlled by three distinctive rifting periods, Late Devonian?-Carboniferous, Middle Jurassic-Early Cretaceous, and early Tertiary. These major rift periods are further comprised of various short-lived tectonic pulses (Faleide et al., 2010). According to Gudlaugsson et al. (1998), the late Paleozoic tectonic framework can be summarized as follow:

i) Development of the Caledonian basement.

ii) Coupled extensional and compressional stress system of the Devonian, found in Svalbard only.

iii) Main rifting episode during the Carboniferous and the Permian.

iv) Thermal subsidence during the Permian.

As the result of initial rifting, several half-graben structures were formed which served as depocentres for the alluvial fan and floodplain clastic sediments together with the carbonates (Steel & Worsley, 1984; Dengo & Røssland 1992). These half-graben included Tromsø, Bjørnøya, Hammerfest and Nordkapp basins where basement-involved normal faulting was the dominant deformation mechanism (Dengo & Røssland, 1992). Tectonic reconstructions performed by Harland (1969) and Ziegler (1988) served as basis for Rønnevik & Jacobsen (1984) and Faleide et al. (1984) to propose that first rifting phase in the western Barents Sea was the consequence of movements along the sinistral stike-slip fault in the western Barents Sea and a conjugate dextral strike-slip fault present in central Barents Shelf. However, Dengo & Røssland (1992) differ on this account and suggest that deformational mechanism governing the structural development of the Barents Sea during initial phase of crustal extension is dominantly dip-slip normal faulting with little evident strike-slip component.

Eastern and northeastern parts of the Barents Sea have been tectonically less acitve since the late Carboniferous whereas, the western part has remained the focus of deformation throughout the Mesozoic and the Cenozoic (Gabrielsen et al., 1990). Regional subsidence was followed by active continental stretching in the late Carboniferous however, Gabrielsen et al. (1990) are skeptical of any regional influence of rifting episode occuring in the late Devonian to the early Carboniferous yet they agree with only such instance of the Bjørnøya Basin . Permian period through most of its interval, witnessed thermal subsidence (Dengo & Røssland, 1992). Major structural features that have controlled the subsequent structural architecture of the Barents Sea may have been established by the end of the late Paleozoic (Gabrielsen et al., 1990). Towards the East, Uralian Sea closure took place from the late Permian to the early Triassic and Barents Sea assumed the form of a distal foreland basin to the Uralian Orogeny thereby, receiving huge sediment influx that reactivated certain basement involved normal faults due to sediment loading (Dengo & Røssland, 1992).

The Triassic to the early Jurassic is termed as the period of tectonic quiescence, however, the Stappen and the Loppa highs were influenced by tilting while eastern parts of the Barents Shelf experienced subsidence during this time (Gabrielsen et al., 1990). Nevertheless, major rifting

event between Norway and Greenland was initiated which became more significant during the late Jurassic to the early Cretaceous and the main zone of deformation remained west of the Loppa High (Dengo & Røssland, 1992). Block faulting during this period was terminated with the development of now well known major basins and highs *(Fig. 2.1)* (Gabrielsen et al., 1990). However, tectonic development during this rifting phase is rather complex with high rates of subsidence witnessed by the Tromsø Basin and western part of the Bjørnøya Basin in the early Cretaceous while hints of local inversion along the Ringvassøy-Loppa Fault Complex and its junction with the Asterias Fault Complex are chronologically equivalent (Gabrielsen et al., 1990).

Deformation during Tertiary is related to opening of the North Atlantic and the Arctic Oceans. However, continental breakup took place at the Paleocene – Eocene transition. Mohns Ridge existed in the Norwegian-Greenland Sea through Eocene and onwards. While further northward, the Knipovich Ridge was not established until Miocene (Faleide et al., 1993a). Deformation mostly occurred west of the Loppa High and the Senja Ridge along the pre-existing zones of weakness whereas, towards east of the Loppa High, stable conditions prevailed (Dengo & Røssland, 1992). An uplift of the magnitude of 1000-1500 m in the south-western part of the Barents Shelf duing the post-Paleocene was proposed by Nyland et al. (1992). Western boundary of Barents Sea developed as a sheared margin following the sea floor spreading during the Eocene, with upto 550 km of dextral strike-slip movement on the Hornsund Fault (Faleide et al., 1991; Myhre et al., 1982; as cited in Dengo & Røssland, 1992). While since the mid Miocene to the present, the western Barents Shelf is experiencing a regional uplift (Dengo & Rossland, 1992).

2.2 Stratigraphic Framework

Boreholes on the Barents Shelf have penetrated down to the Permian strata while Permo-Carboniferous rocks in the region are thought to be similar as those of Svalbard, Bjørnøya and Northeast Greenland (Faleide et al., 1993). Borehole and deep seismic reflection/refraction data suggest the presence of the late Paleozoic strata in southwestern Barents Sea *(Fig. 2.2)* (Jackson et al., 1990; Faleide et al., 1991; Faleide et al., 1993). Transgressive-regressive deposition of substantial Triassic succession is present throughout the Barents Sea (Mørk et al., 1989; Faleide

et al., 1993). Sandstone of the lower-middle Jurassic are present throughout the Hammerfest Basin which probably increased in thickness toward the Tromsø Basin (Faleide et al., 1993b).

During the middle-late Jurassic, sedimentation was rift-related and predominant deposition was that of shales and claystones with subordinate marly dolomitc limestone and rarely occuring siltstone and sandstone, that point to deposition in the deep basinal enviroment (Worsley et al., 1988; Faleide et al., 1993). In the early Cretaceous, marine depositional environments prevailed leading to the depositon of shales and claystones (Faleide et al., 1993). The late Cretaceous witnessed clastic sedimentation (mainly claystones) in the Tromsø Basin reflecting open marine, deep shelf environment. While the western part of the Hammerfest Basin transformed into more calcareous-dominated towards the East showing a shallow detritus-starved shelfal environment (Worsley et al., 1988; Faleide et al., 1993).

Paleogene sedimentation is dominated by claystones with thin interbedded siltstones, tuffs and carbonates and depositonal environment is interpreted to be an open to deep marine shelf (Faleide et al., 1993). Lower Paleogene is present throughout the south-western Barents Shelf with lateral variation in lithology while the younger sequence is preserved only in the Tromsø, Harstad and Sørvestsnaget basins (Faleide et al., 1993). Neogene-Quaternary stratigraphic succession makes unconformable contact with the underlying Paleogene and the Mesozoic sequence (Faleide et al., 1993). Glacial sediments that are 100-200m thick in the Hammerfest Basin increase to more than 700m at Senja Ridge and their thickness increases westward towards the Lofoten Basin, where they attain a thickness of as much as 4000 m (Faleide et al., 1993; Faleide et al., 1996).

2.3 Troms-Finnmark Fault Complex – A Review

Gabrielsen et al. (1990) have given a comprehensive description of the Troms-Finnmark Fault Complex and discussed its genesis in temporal and spatial context. According to them, this fault complex was originally defined by Moe (1974). Later, various workers have discussed this fault in their work, which includes but not limited to the authors such as, Syrstad et al. (1976); Rønnevik et al. (1982); Gabrielsen (1984); Rønnevik & Jacobsen (1984); Faleide et al. (1984); Gabrielsen et al. (1984); Berglund et al. (1986); Sund et al. (1986); Ziegler et al. (1986); Townsend (1987); Gabrielsen & Færseth (1989); Gabrielsen et al. (1990) and Dengo & Røssland

(1992). The Troms-Finnmark Fault Complex runs parallel to the coastline of Troms and Finnmark counties *(Fig. 2.3)* between 69°20'N, 16°E and 71^{0}40'N, 23^{0}40'E (Gabrielsen et al., 1990).

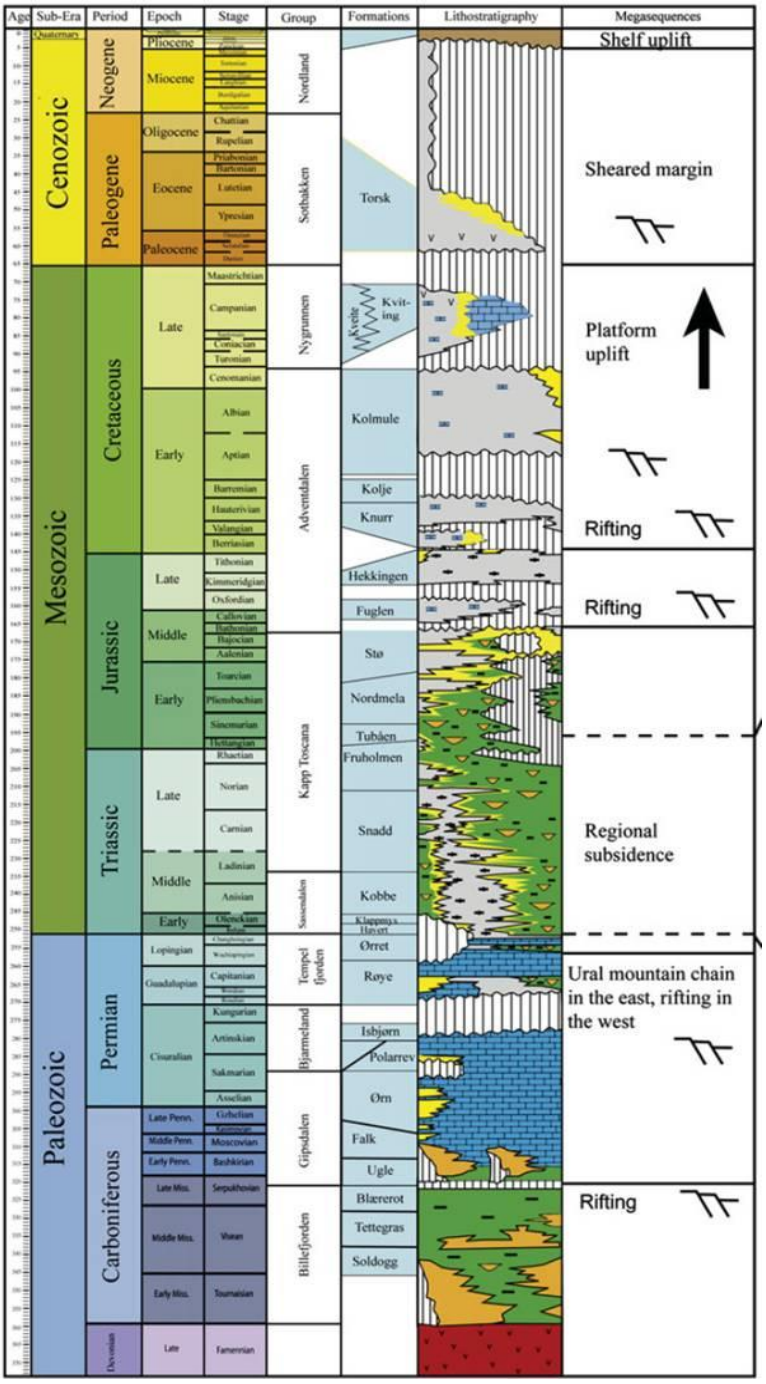

Figure 2.2: Generalized stratigraphy of the Barents Shelf, accompanying regional tectonic events and megasequences are also shown in the figure (modified from Glørstad-Clark et al., 2010).

It serves as a structural division between the Finnmark Platform in the south-southeast and northward basins such as Harstad Basin, Tromsø Basin and Hammerfest Basin *(Fig. 2.3)* (Gabrielsen et al., 1990).

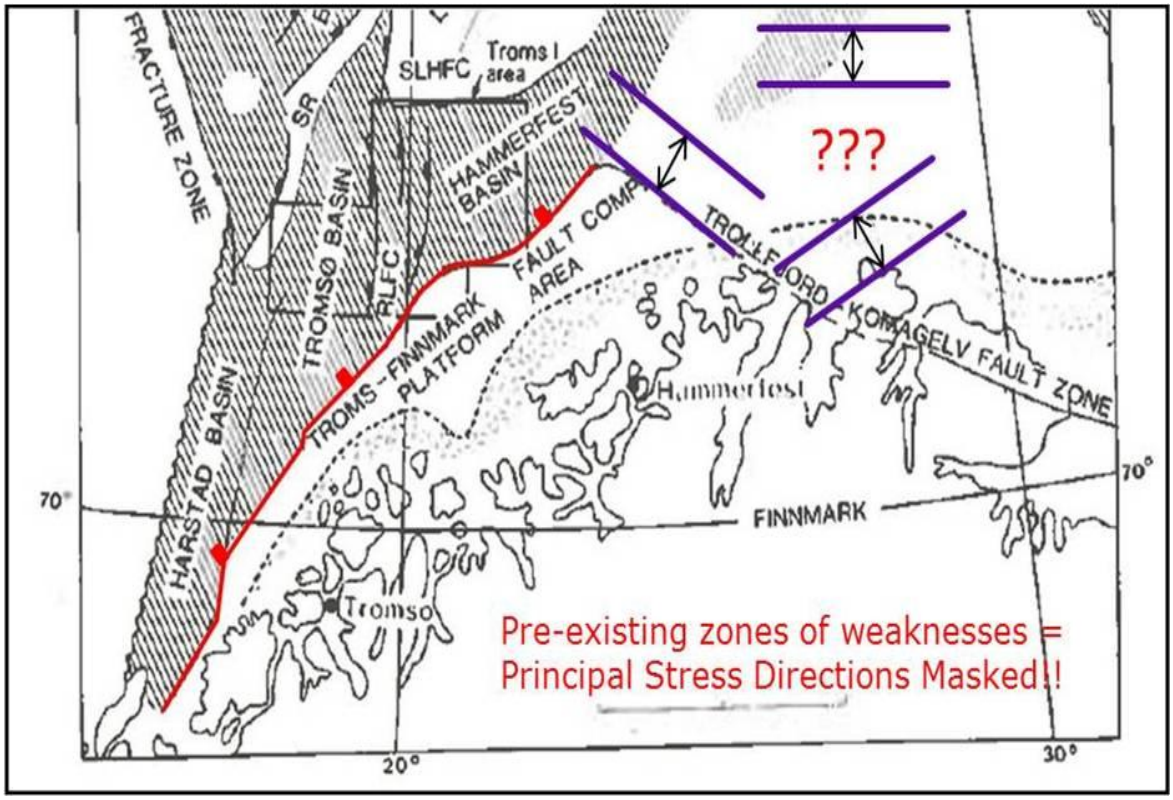

Figure 2.3: Red-colour line represents trace of NE-SW striking Troms-Finnmark Fault Complex with a dog-leg trend towards its north-eastern extremity (modified from Berglund et al., 1986). Stretching directions in violet colour indicate that the orientation of σ_3 would be masked in the presence of the pre-existing zone of weakness.

At its southern extremity, this fault complex shows a structural trend of NNE-SSW to NE-SW, while it changes its strike to more ENE-WSW at about $19^0$20'E (Gabrielsen et al., 1990). On smaller scale however, this fault complex shows NE-SW and E-W to ESE-WNW trending segments that together constitute a dog-leg style (Berglund et al., 1986). Cumulative throw of more than1.5s (twt) is estimated for this fault complex (Gabrielsen 1984). Towards northeast, it terminates along the offshore extension of Trollfjord-Komagelv Fault Zone exhibiting a WNW-ESE trend *(Fig. 2.4)* (Gabrielsen, 1984; Berglund et al., 1986; Ziegler et al., 1986; Gabrielsen & Færseth, 1989; Gabrielsen et al., 1990).

According to Siedlecka and Siedlicki (1972), Trollfjord-Komagelv Fault separates Baltica (the Barents Sea region allochthon) and the Timan Range (Vendian/Lower Palaeozoic cover) along its strike (as cited in Johansen et al.,1994). This fault at first was interpreted to be a thrust without significant displacement along strike (Siedlecka, 1975; cited in Johansen et al., 1994). Based on structural style (Roberts, 1972; Johnson et al., 1978), stratigraphic record, differential thickness across the fault, presence of 640 m.a old basic intrusions to the north of fault (Beckinsale et al., 1975) and available palaeomagnetic data (Kjøde et al., 1978), it has been proposed that large-scale dextral strike-slip movement along the fault zone took place during Early Ordovican to Early Carboniferous *(Fig. 2.4)* (Roberts, 1972; Johnson et al., 1978; Kjøde et al., 1978; as cited in Johansen et al., 1994).

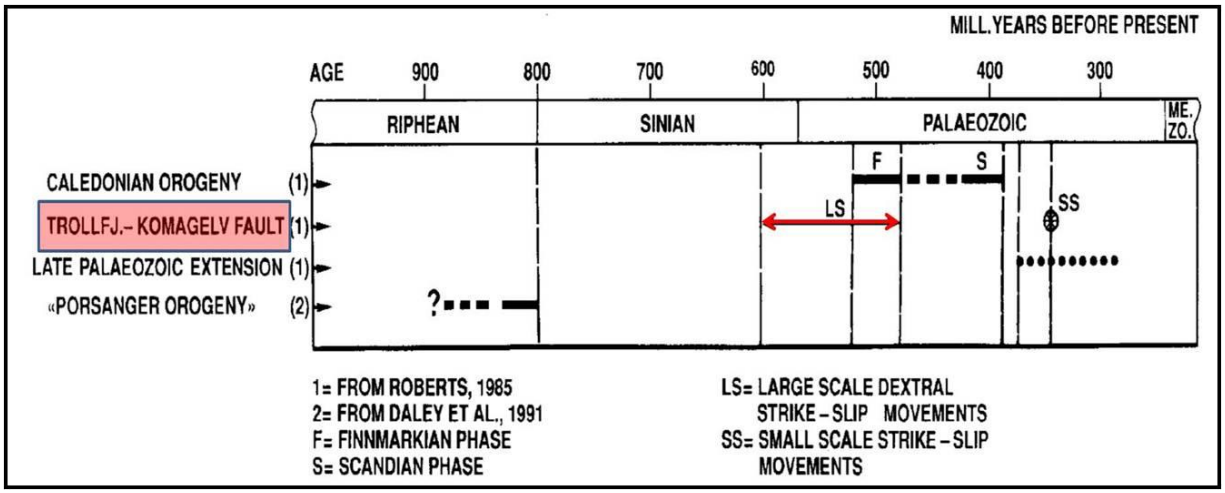

Figure 2.4: Pre-Mesozoic tectonic events in the Barents Sea, representing the Finnmarkian and the Scandian deformational phases of Caledonian Orogeny while the Trollfjord-Komagelv Fault represents the large scale dextral strike-slip fault (modified from Johansen et al., 1994).

The Troms-Finnmark Fault Complex display listric fault geometry with normal dip-slip while the hanging wall is associated with roll-over anticlines and antithetic faults *(Fig. 2.5)* (Fønstelien & Horvei 1979; Gabrielsen, 1984; Faleide et al., 1984; Berglund et al., 1986; Ziegler et al., 1986; Gabrielsen et al., 1990). This fault complex is believed to have established on a pre-existing zone of weakness (Gabrielsen et al., 1990). Handin (1969) explained that critical stress level needed to initiate faulting along pre-existing fracture surface is less than that required to break the un-fractured specimen of the same lithology (as cited in Davis, 1984). Hence, if a young episode of

faulting occurs through reactivation of old zones of weakness, the minimum principal stress direction (σ_3), cannot be inferred from the available geometric data *(Fig. 2.3)* (Davis, 1984).

Pre-Permian sequence shows some activity in the north-eastern segment of the fault complex but activity along this fault may be coeval with the Vargsundet Fault present on the mainland Norway (Berglund et al., 1986; Gabrielsen & Færseth, 1989; Gabrielsen et al., 1990) which is believed to be activated during Caledonian Orogeny (Roberts, 1971 & 1985; Worthing, 1984; Gabrielsen et al., 1990). Later, tectonic phases reactivated the Troms-Finnmark Fault Complex, several times till Eocene while the most notable subsidence along this fault complex took place during Late Jurassic - Early Cretaceous crustal extension (Gabrielsen et al., 1990). This fault complex belongs to Class-1, *sensu* Gabrielsen (1984), implying that it is a basement involved structure with a regional significance.

Different genetic models have been put forth to explain the structural development of the Troms-Finnmark Fault Complex. Gabrielsen (1984) explained that this fault complex is a consequence of normal faulting which is a deep rooted fault (Gabrielsen et al., 1990). North-eastern segment is suggested to have experienced sinistral strike-slip displacement in mid-Jurassic time (Rønnevik et al., 1982; Rønnevik & Jacobsen, 1984; Gabrielsen et al., 1990); similarly, geometry of the north-eastern segment could be attributed to mild inversion (Gabrielsen et al., 1990).

Reactivation of this fault complex by sinistral strike-slip in Late Cretaceous to Early Tertiary is proposed by Ziegler et al. (1986) and Gabrielsen & Farseth (1989) seem to be in agreement with this proposal (Gabrielsen et al., 1990).

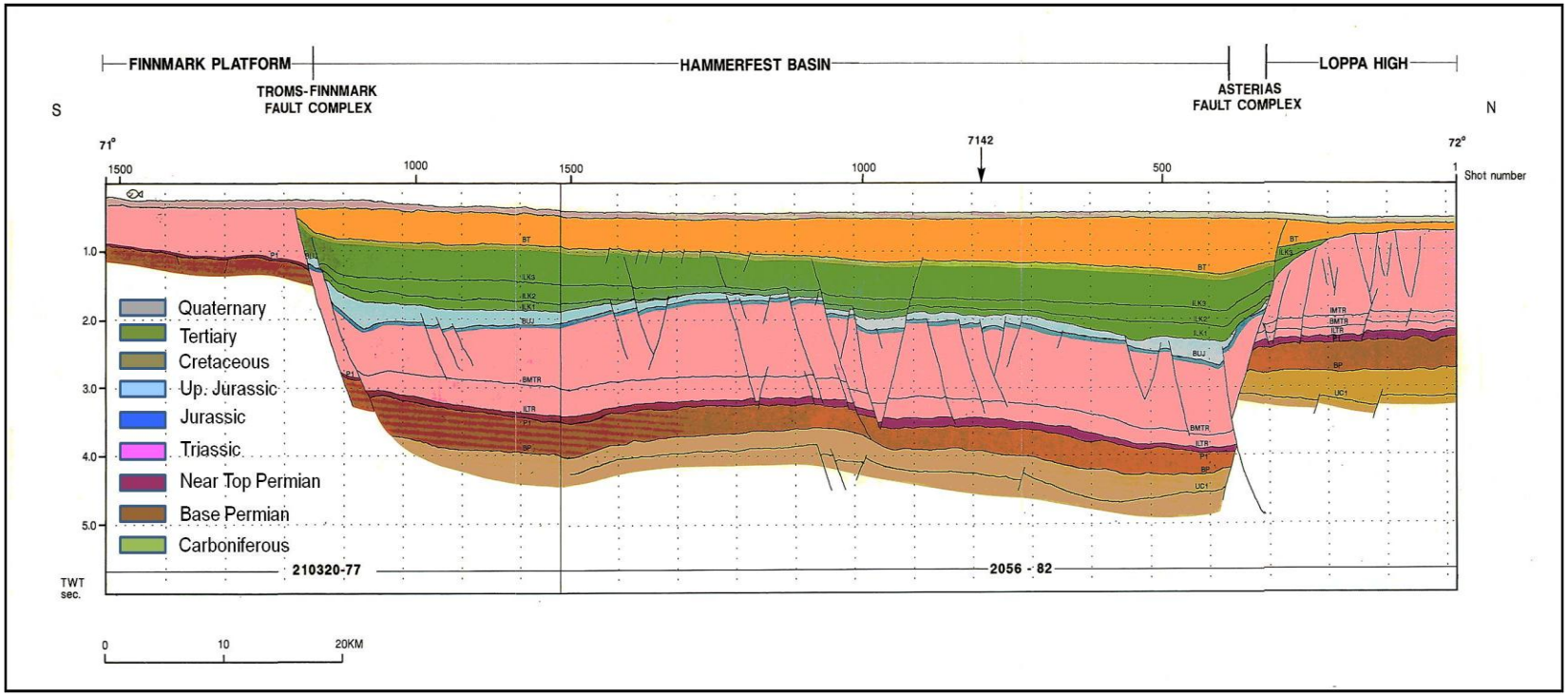

Figure 2.5: Interpreted Composite seismic line, showing Troms-Finnmark Fault Complex in the South and Hammerfest Basin in the North bounding the Hammerfest Basin, planar normal fault geometry of the Troms-Finnmark Fault Complex with its synthetic splay dipping towards north is evident, colour code for interpreted lithology is also shown (modified from Gabrielsen et al., 1990).

Berglund et al. (1986) proposed that structural configuration of this fault complex is typical of a listric normal fault that flattens within deeper stratigraphic levels and hangingwall of the fault complex has developed reverse drag and counter/antithetic fault beside presence of prominent synthetic faults *(Fig. 2.6)*.

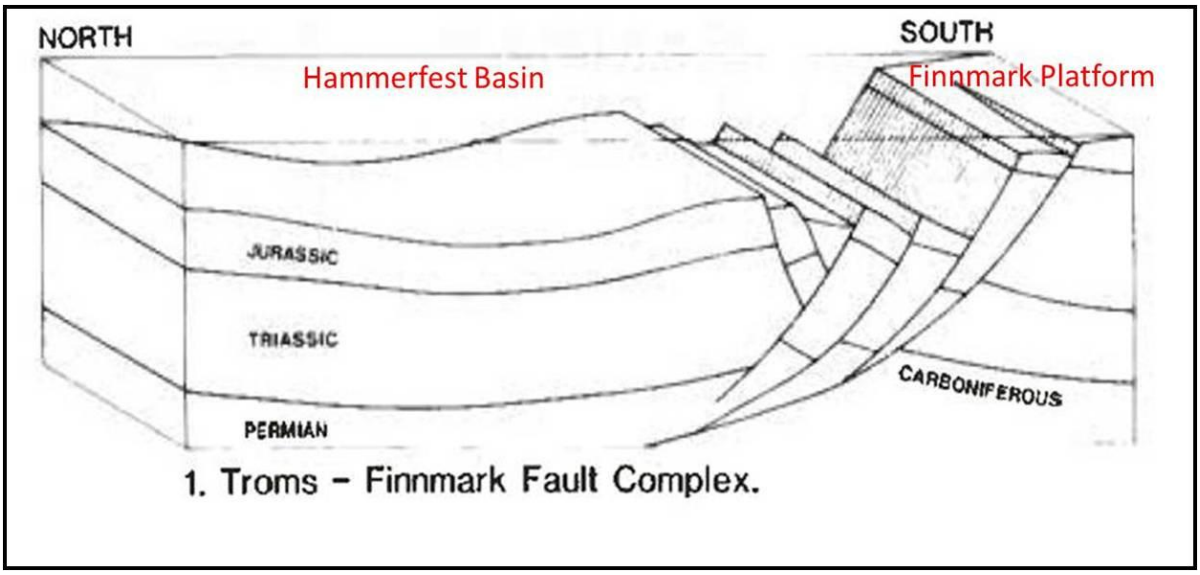

Figure 2.6: Listric normal fault geometry of the Troms-Finnmark Fault Complex with north dipping, concave-upward fault plane and antithetic faults in the hanging wall block (modified from Berglund et al., 1986).

A brief review of structural elements which are related to the Troms-Finnmark Fault Complex as basin/platform delineating feature, is presented in the following section. However, it is important to note that the present study only incorporates part of the Troms-Finnmark Fault Complex that separates the Hammerfest Basin and part of the Finnmark Platform.

2.4 Finnmark Platform

Norwegian mainland Caledonides outcrop towards the south of the Finnmark Platform *(Fig. 2.3)* (Gabrielsen et al., 1990), while its western limit is marked by the southernmost extension of Ringvassøy-Loppa Fault Complex (Larsen et al., 2002). Towards its western extremity, the Jurassic strata directly underlies base of the Quaternary (Vorren et al., 1986; as cited in Gabrielsen et al., 1990). The Hammerfest and Nordkapp basins are located towards the north and the eastern part of the Finnmark Platform in the Norwegian sector is marked by underlying rift

topography with fault blocks containing siliciclastic sediments that belong to the early Carboniferous (Larssen et al., 2002). These sediments were onlapped in the mid-Carboniferous and the overlying sequence is carbonate-dominated, with little evaporite sedimentation at some intervals. This type of geological development continues further eastwards, paralleling the Kola Peninsula and the Timan-Pechora Basin, which defines a consistent development (Johansen et al., 1993 as cited in Larssen et al., 2002). Faults with small vertical separation have been mapped in the portion of the platform sequence that is younger than the late Carboniferous (Vorren et al., 1986). During the Permian, the more stable western platform area (west of approx. 25^0E) was transgressed and the resultant sedimentation is defined by mix siliciclastic and carbonate deposits. Late Jurassic movements along pre-existing faults later modified the platform, and uplift during late Tertiary modified the platform in its present shape with a gentle northward tilt (Larssen et al., 2002).

The Finnmark Platform signifies a structural element in the Barents Shelf that has been stable since the late Paleozoic (Gabrielsen et al., 1990). Precambrian and Paleozoic rocks underlying the platform are believed to have affected by the Caledonian Orogeny. It is shown by a characteristic rift topography dominated by NE-SW striking faults – orientation typical of Caledonian orogeny. Faulting is less evident towards eastern parts of the platform. Thick clastic sedimentation resulted from rapid subsidence during first phase of crustal extension of Barents Shelf while a tectonically stable platform started to emerge in Late Carboniferous (Gabrielsen et al., 1990).

2.5 Hammerfest Basin

It is a composite sedimentary basin, 70 km wide and 150 km long that was developed during the second rift phase (Mesozoic) in Barents Shelf (Berglund et al., 1986). It is a relatively shallow basin showing ENE-WSW orientation *(Fig. 2.3).* Towards the South lies the Finnmark Platform which is separated by the Troms-Finnmark Fault Complex and the Asterias Fault Complex separates it from the Loppa High to the north. Its western border towards the Tromsø Basin is marked by the presence of southernmost segment of the Rignvassøy-Loppa Fault Complex, while its eastern limit is developed as a flexure against the Bjarmeland Platform (Larssen et al., 2002). On the basis of NW-SE striking offshore extension of Trollfjord-Komagelv Fault, the

Hammerfest Basin may be subdivided into a western and an eastern sub-basin (Ziegler et al., 1986; Gabrielsen & Færseth, 1989; Gabrielsen et al., 1990).

The western part of the Hammerfest Basin shows a gentle westward dip towards the Tromsø Basin. Internal fault system of the basin is composed of E-W, ENE-WSW and WNW-ESE trending faults which are informally termed as the Hammerfest Basin fault system by Gabrielsen (1984). The Hammerfest Basin includes both deep, high-angle faults along the basin margins and listric normal faults detached above the Permian sequence, situated more centrally in the basin (Berglund et al., 1986). Extensional deformation led to major structural development of the Hammerfest Basin while several workers have opined that deformational style indicates reactivation by strike-slip in Late Jurassic to Early Cretaceous as well (Berglund et al., 1986; Sund et al., 1986; Gabrielsen & Færseth, 1989; Gabrielsen et al., 1990). The eastern part of the basin is generally less influenced by faulting and characterizes the features of a sag basin. The depth to basement is the Hammerfest Basin has been calculated to 6-7 km (Roufosse, 1987, as cited in Gabrielsen et al., 1990).

Separation of the Hammerfest Basin from the Finnmark Platform occurred during Late Carboniferous. In the Triassic to Early Jurassic, the Tromsø and Hammerfest basins were probably inter-related parts of a broader epeirogenic depositonal system, although the Hammerfest Basin can be identified as a distinct entity already during Late Scythian time (Berglund et al., 1986, as cited in Gabrielsen et al., 1990). Since the Middle Jurassic, the outline of the Hammerfest Basin developed as it is now identified and the domal feature present in the central segment of the basin, started to develop from mid-Jurassic to Barremian (Rønnevik & Jacobsen, 1984; Gabrielsen et al., 1990). Inversion along some faults has also been documented which is attributed to the Late Jurassic - Early Cretaceous (Berglund et al., 1986; Sund et al., 1986; Gabrielsen & Færseth, 1988,1989), or Late Cretaceous - Early Tertiary reactivation (Ziegler et al., 1986; Gabrielsen et al., 1990).

The Hammerfest Basin has been explained as an aulacogen, a failed rift in a triple junction system (Talleraas, 1979, as cited in Gabrielsen et al., 1990). Rønnevik et al. (1982) and Rønnevik & Jacobsen (1984) highlighted the impact of strike-slip faulting in the structural development of the fault complexes surrounding the basin (Gabrielsen et al., 1990). This has been followed up by arguments that the structural history of the Hammerfest Basin may be

linked with transfer-faulting related to major gravity-induced movements (Ziegler et al., 1986), and rotation of regional fault blocks around a vertical axis (Gabrielsen & Færseth 1988; Gabrielsen et al., 1990).

2.6 Tromsø Basin

The Tromsø Basin is located north of the town of Tromsø, from 71^0-72^0 15'N and 17^0 30'-19^0N 50'E *(Fig. 2.3).* Senja Ridge lies towards its west and its eastern limit is marked by the Ringvassøy-Loppa Fault Complex. Towards the southeast, it terminates against the Troms-Finnmark Fault Complex, whereas the southwestern margin at present is less understood. In the North, it is separated from the Bjørnøya Basin by an inter-basinal high, the Veslemøy High (Gabrielsen et al., 1990). The Tromsø Basin is a NNE-SSW trending structural feature which contains a series of salt diapirs linked by a smooth flexure and related with a system of detached faults (informally known as the Tromsø Basin Fault System by Gabrielsen, 1984) in the central part of southern area (Gabrielsen et al., 1990). The depth to the basin floor can only be estimated in the northern segment of the basin which corresponds to 7.5 s (twt) (Brekke & Riis, 1987, as cited in Gabrielsen et al., 1990). However, based upon gravity data, depth to "basement" has been estimated to 10-13 km (Roufosse, 1987, as cited in Gabrielsen et al., 1990).

NE-SW trending structural features of Late Devonian to Early Carboniferous that have been identified east of the Tromsø Basin are absent here. This may be due to masking effect of thick Cretaceous sequence present in the basin. Thick sequences of Late Paleozoic salt are also found, but it has been suggested that the pre-Mesozoic sequence found today in the Tromsø Basin is thin (Gudlaugsson et al., 1987) and hence the basin did not exist prior to deposition of the evaporites (Gabrielsen et al., 1990). A continuous basin constituting the later Tromsø, Bjørnøya and Hammerfest basins might have existed in Late Triassic to Early Jurassic times (Rønnevik et al., 1982; Gabrielsen et al., 1990). During the Early Cretaceous the Tromsø Basin was separated from the Hammerfest Basin towards the East (Gabrielsen et al., 1990). Towards North, there are clues that the Tromsø Basin existed as a separate basin in the Paleozoic, but that it was united with the Bjørnøya Basin. The two basins separated during the Late Cretaceous when horizontal movements along the Bjørnøyrenna Fault Complex occurred. Effects of faulting related to halokinesis have been documented as late as the Eocene (Gabrielsen, 1984), and some later activity is likely as well (Gabrielsen et al., 1990).

Unlike the Hammerfest Basin, halokinesis has played a significant role in structuring the Tromsø Basin and the effect of salt has been used to describe the great subsidence that occurred during Cretaceous (Øvrebø & Talleraas, 1976, 1977, as cited in Gabrielsen et al., 1990). However, other models explain the Mesozoic and Cenozoic development of the Tromsø Basin in connection with large-scale extensional (Talleraas, 1979; Hanisch, 1984a, b) or shear (Rønnevik & Jacobsen, 1984; Brekke & Riis 1987) movements and suggest that the crust came near to break-up in this area (Gudlaugsson et al., 1987; Gabrielsen et al., 1990).

2.7 Harstad Basin

The Harstad Basin is located north of Andøya, between 69^0 20' and 71^0 N, and 16^0 30' and 17^0 45' E, adjacent to the shelf edge. The basin is oriented in a NNE-SSW style *(Fig. 2.3).* The southernmost part of the Troms-Finnmark Fault Complex makes the eastern boundary of this basin, and the western boundary is marked with the transition to oceanic crust. Towards its South lies a system of E-W trending normal faults north of Andøya and its northern boundary is marked by a likely deep-seated fault system located in the extension of of the Troms-Finnmark Fault Complex (Gabrielsen et al., 1990). Extensional faulting related to the second rift phase experienced by the Barents Shelf has affected the basin which probably started in the mid Jurassic and remained active during the period of major subsidence in the early Cretaceous. However, Late Cretaceous is marked with renewed normal faulting along with inversion of some major faults. This basin is believed to be located on the same axis of subsidence as the Tromsø Basin and both may be genetically linked with each other. The Harstad Basin is also marked by considerable subsidence during the Cretaceous and the top of the Jurassic succession has been estimated at 5 sec (twt) or more (Brekke & Riis, 1987, as cited in Gabrielsen et al., 1990).

Southern part of the Harstad Basin is affected by large-scale listric faults trending E-W towards south and NNE-SSW trend dominates towards the north (Brekke & Riis 1987, as cited in Gabrielsen et al., 1990). Large-scale roll-over anticlines are associated with these listric normal faults. Towards north of the Harstad Basin, effect of this structuration is less intense and extensional features are overprinted by compressional features (Gabrielsen et al., 1990).

Chapter 3

Descriptive Analysis

Descriptive analysis is related to recognition and description of the structures and measuring their orientations. Description of geological structures and their associated features / sub-features are of fundamental importance as the foundation of detailed structural analysis including the kinematic & dynamic analysis is anchored in the descriptive part (Davis, 1984).

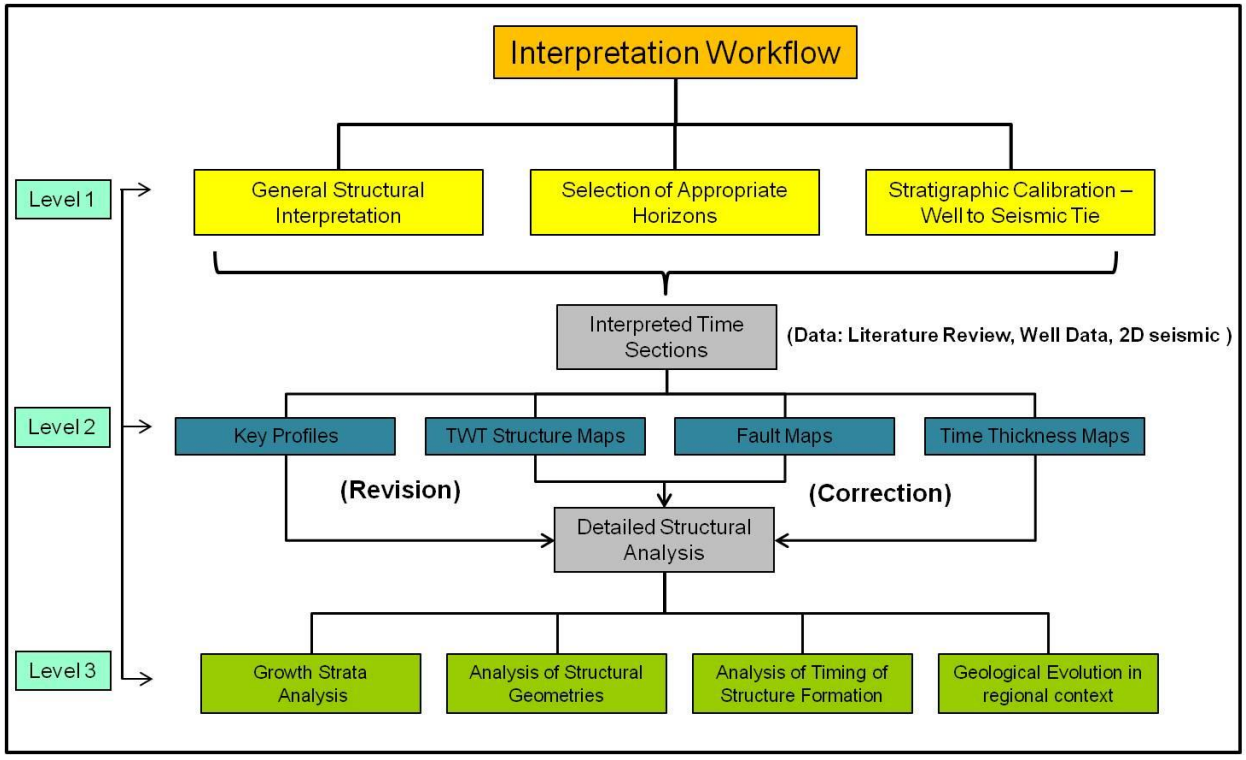

Figure 3.1: An outline of the interpretation workflow followed during the study. Detailed structural analysis is done under three levels of investigation (levels 1,2,3), see text for details.

The present work can be broadly divided into three (3) levels of investigation, all aimed at paving way in drawing conclusion about the structural configuration and evolution of the Troms-Finnmark Fault Complex in a coherent manner. Level 1 deals with data loading, QC, fault pattern analysis, well-to-seismic tie and pre-decided horizons' interpretation. Level 2 is driven by interpretation during level 1 and is mainly related to the generation of various time-structure maps, fault plane maps and time-thickness maps etc. Level 3 focuses on the subsets of the larger data-set, for instance, while describing a key profile observation regarding minute details such as growth strata identification, calculation of fault throws, presence of roll-over anticline etc is

handled during this stage of the study. These three levels of investigation represent a general approach in data handling to its description and presentation in this chapter. An overview of the generalized interpretation workflow that has been followed during present study is presented in the *Figure 3.1*. However, it is pertinent to note that each level of investigation discussed in this figure, diverges in to more complex sub-category and each sub-category then necessitate its own set of challenges. The descriptive part of the detailed structural analysis sorts under two levels in the present work i.e., level 1 & level 2 *(Fig 3.1).* Beginning with data loading and the quality check, seismic interpretation entails both structural and stratigraphic interpretation. Interpretation of pre-decided reflections *(Fig 3.3)* is carried out by making use of the available borehole data, present within the 2D seismic grid.

3.1 Data

Data set comprises of a grid of 2D seismic reflection lines and boreholes containing check-shot and well-tops information *(Fig. 3.2).*

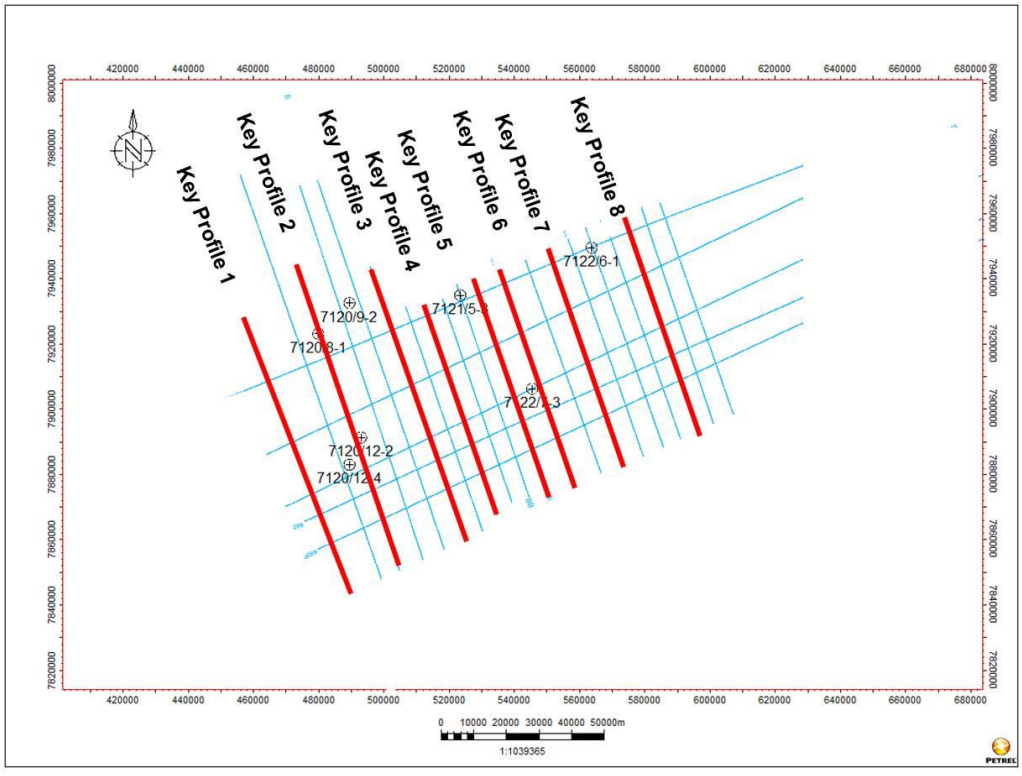

Figure 3.2: Base map of the study area showing location of seismic lines and boreholes used in the study. Red lines show the location of key profiles that are discussed later in this chapter.

The 2D seismic data contain both dip and strike lines with 8 x 9 km line spacing approximately. Dip lines are oriented NNW-SSE and strike lines show ENE-WSW orientation *(Fig. 3.2).* Borehole data from 7120/8-1, 7120/9-2, 7120/12-4 and 7121/5-3 were used to determine the tie between the seismic data and stratigraphy in the wells. Detailed information of these wells is taken from NPD (Table 3.1 & 3.2) *(Figs. 3.4; 3.5; 3.6 & 3.7).* The well 7120/8-1 is located within the Hammerfest Basin and the oldest penetrated formation is the upper Triassic Fruholmen Formation with the TD (total depth) of 2610m (RKB). Borehole 7120/9-2 is also located within the Hammerfest Basin and Røye Formation of Permian is the deepest penetrated formation with the TD of 5072 m (RKB). This is the only well within the study area that has penetrated Permian strata hence it proved valuable in making seismic-to-well tie at Permian level (Table 3.1).

Table 3.1: Additional information of boreholes used in study for stratigraphic calibration (NPD website).

Wellbore name	**7120/8-1**	**7120/9-2**
NS UTM [m]	7923384.58	7932809.5
EW UTM [m]	479897.51	489425.03
UTM zone	34	34
Drilling operator	Den Norske Stats Oljeselskap	Norsk Hydro Produksjon
Drilling days	75	186
Entry date	28.06.1981	18.04.1984
Completion date	10.09.1981	20.10.1984
Type	EXPLORATION	EXPLORATION
Status	P&A	P&A
Content	GAS/CONDENSATE	GAS
Discovery wellbore	YES	NO
KB [m]	25	23
Water depth [m]	270	293
TD (MD) [m RKB]	2610	5072
Oldest penetrated age	LATE TRIASSIC	LATE PERMIAN
Oldest formation	FRUHOLMEN FORMATION	RØYE FORMATION

The borehole 7120/12-4 is the only well present on the Finnmark Platform. It has penetrated the Ugle Formation of Carboniferous age and it is drilled down to 2199 m (RKB). However, the Jurassic to Cretaceous sequence is missing on the platform and the Triassic sequence is overlain by young sediments of the Late Tertiary and Quaternary age *(Fig. 3.4).* This well is used as a reference point for identifying intra-Triassic & intra-Jurassic reflections throughout the part of

Finnmark Platform included in this study. Well 7121/5-3 is present within the Hammerfest Basin and lies in the central part of the study area. It has penetrated the Upper Triassic, Snadd Formation as the oldest stratigraphic unit with the total depth of 2265m (RKB) (Table 3.2). Well data from the Hammerfest Basin and the Finnmark Platform were applied to obtain the best possible control of the correlations across the fault. Availability of borehole data for the purpose of reflection's correlation has made the interpretation reliable across the master faults. The key reflections have been interpreted using well tops from these wells *(Fig. 3.3).*

Table 3.2: Additional information of boreholes used in study for stratigraphic calibration (NPD website).

Wellbore name	**7120/12-4**	**7121/5-3**
NS UTM [m]	7883245.96	7935226.77
EW UTM [m]	489450.11	523420.77
UTM zone	34	34
Drilling operator	Norsk Hydro Produksjon	Den Norske Stats Oljeselskap
Drilling days	59	22
Entry date	18.02.1984	16.02.2001
Completion date	16.04.1984	09.03.2001
Type	EXPLORATION	EXPLORATION
Status	P&A	P&A
Content	DRY	OIL/GAS SHOWS
Discovery wellbore	NO	NO
KB[m]	23	24
Water depth [m]	152	345
TD (MD) [m RKB]	2199	2265
Oldest penetrated age	LATE CARBONIFEROUS	LATE TRIASSIC
Oldest formation	UGLE FORMATION	SNADD FORMATION

It is concluded that the study area contains sedimentary package from Quaternary to Carboniferous. Sedimentary sequence within the Hammerfest Basin is well preserved as witnessed by wellbore information; however, towards the Finnmark Platform, Triassic sediments are overlain by recent sedimentary deposits hence the complete Jurassic and Cretaceous package is missing (Table 3.3).

3.2 Interpretation Tool

Petrel 2011 is employed for seismic interpretation which is proprietary software of Schlumberger. It is a PC based application aimed to combine all data types ranging from 2D/3D

seismic, well logs and various types of reservoir data. It can perform 2D/3D interpretation, well log correlation, subsurface geological modeling as well as submit and visualize simulation results, calculate volumetrics and generate various types of digital maps (www.slb.com).

Table 3.3: Well Tops used in the study, highlighted formations have been interpreted on the 2D data.

Age	Group (Gp.) / Formation (Fm.)	7120/9-2	7120/12-4	7121/5-3	7120/8-1
		Top MD (m)	Top MD (m)	Top MD (m)	Top MD (m)
Cenozoic	Nordland Gp.	316	175	369	295
	Sotbakken Gp.	380	Missing	412	603
	Torsk Fm.	380		412	603
Cretaceous	Nygrunnen Gp.	1072		844	1056
	Kveite/Kviting Fm.	1072		844	1056
	Adventdalen Gp.	1097		865	1150
	Kolmule Fm.	1097		865	1150
	Kolje	1847		1625	1650
	Knurr FM	1871		1790	1942
Jurassic	Hekkingen FM	1906		1832	1990
	Fuglen Fm.	1965		-	2086
	Kapp Toscana Gp.	1971		1880	2092
	Stø Fm.	1971		1880	2092
	Nordmela Fm.	2048		1928	2190
	Tubåen Fm.	2156		1984	2330
Triassic	Fruholmen Fm.	2290		2034	2462
	Snadd Fm.	2552	435	2223	Not Penetrated
	Sassendalen Gp.	3962	485	Not Penetrated	
	Kobbe Fm.	3962	485		
	Klappmyss Fm.	4245	685		
	Havert Fm.	4806	992		
Permian	Tempelfjorden Gp.	4844	1366		
	Ørret Fm.	4844	1366		
	Røye Fm.	4956	1469		

Hence it provides the single platform to undertake the “seismic-to-simulation” workflow thereby greatly reducing the need for specialized tool for each new job (www.slb.com).

3.3 Interpretation Procedure

Petrel 2011 comes with easy-to-handle data loading procedure (www.slb.com). After data loading, a general overview of the data was made. Seismic data were displayed in a base map and it was realized that certain 2D lines present in the western part of the study area have greater areal extent than the lines present towards the east *(Fig. 3.2).*

In the seismic data set, five regional 2D seismic lines were found to be of regional extent covering the entire Hammerfest Basin in the middle and the Finnmark Platform towards SE while part of the Loppa High at their NW extremity. Such regional lines are utilized to build a general understanding of the type of structures, behavior of various reflections across the basin and other fault associated features *(Fig. 3.4).* Once a general familiarity with the main structural elements present in the area got established, the main workflow of seismic interpretation as described in *Figure 3.1* took its course.

Following data loading, general structural interpretation was carried out which then led way to the horizon interpretation. It was where, seismic-to-well tie at various well locations were made in order to calibrate the seismic data with the borehole data *(Fig. 3.5).* Check-shot survey data of four wells in the "*.txt format*" was loaded in to the software. The wells were displayed on the seismic lines and there tops made visible by loading another "*.txt file*" into the software. Once wells were loaded and displayed successfully, the next step was to interpret the pre-decided key reflections (*see section 3.4 for details*) around the wells and later over the entire data. Confidence level with which these reflections were interpreted and correlated over the entire data-set is very high, as well control was available both within the Hammerfest Basin and the Finnmark Platform.

Reflection	Formation	Age	Color Code
Base Tertiary	Top Kveite	70	
Early Cretaceous	Top Kolje	125	
Base Cretaceous	Hekkingen FM	145.5	
Intra Jurassic	Stø FM	169	
Intra Triassic	SNADD FM	210	
Intra Permian	Røye FM	265	

Figure 3.3: Color codes of the interpreted reflections in the study area.

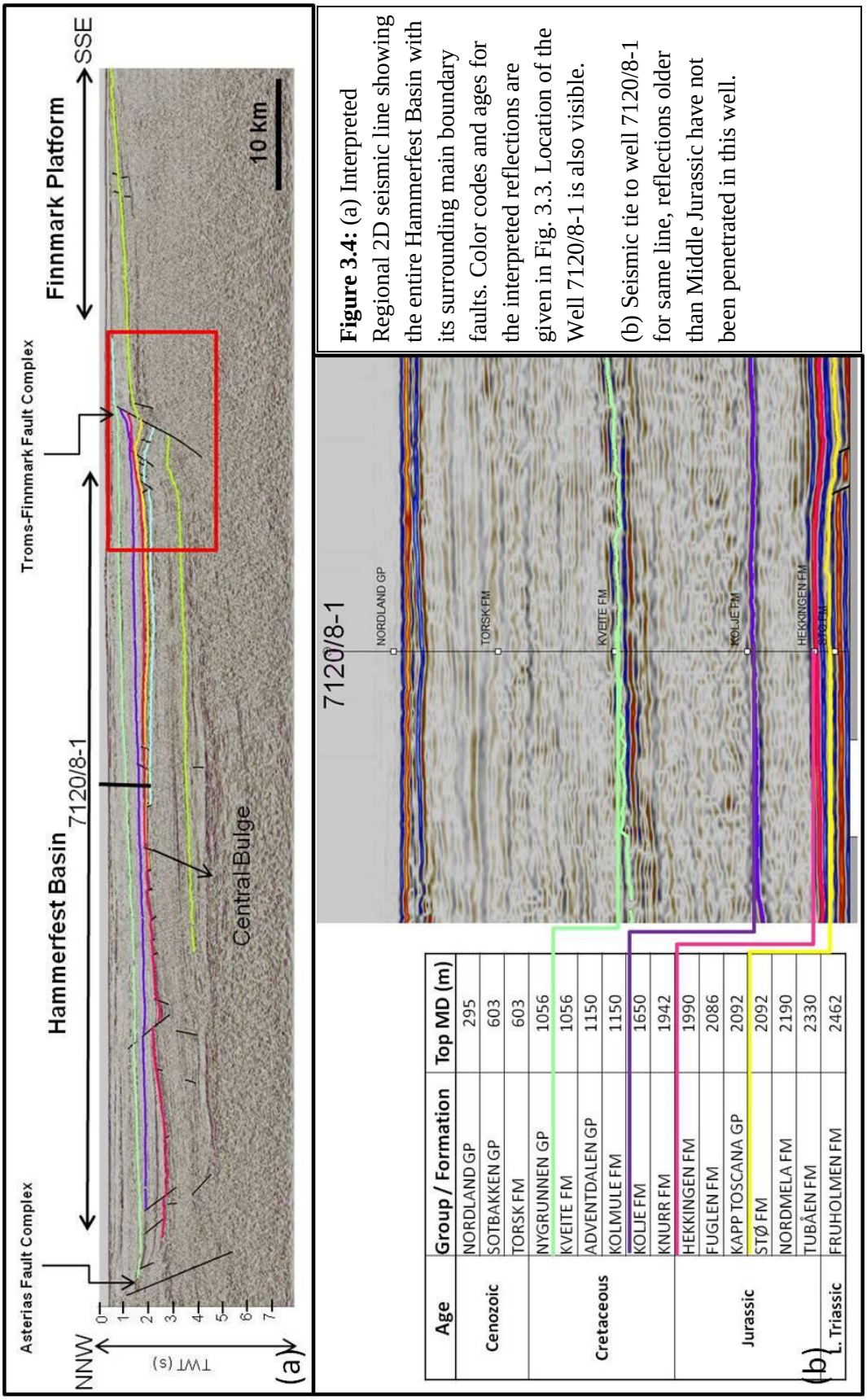

Age	Group / Formation	Top MD (m)
Cenozoic	NORDLAND GP	295
	SOTBAKKEN GP	603
	TORSK FM	603
Cretaceous	NYGRUNNEN GP	1056
	KVEITE FM	1056
	ADVENTDALEN GP	1150
	KOLMULE FM	1150
	KOLJE FM	1650
	KNURR FM	1942
Jurassic	HEKKINGEN FM	1990
	FUGLEN FM	2086
	KAPP TOSCANA GP	2092
	STØ FM	2092
	NORDMELA FM	2190
	TUBÅEN FM	2330
L. Triassic	FRUHOLMEN FM	2462

Figure 3.4: (a) Interpreted Regional 2D seismic line showing the entire Hammerfest Basin with its surrounding main boundary faults. Color codes and ages for the interpreted reflections are given in Fig. 3.3. Location of the Well 7120/8-1 is also visible.

(b) Seismic tie to well 7120/8-1 for same line, reflections older than Middle Jurassic have not been penetrated in this well.

3.4 Rationale for the selection of Interpreted Reflections

The Barents Shelf has experienced three phases of crustal stretching; oldest being the late Paleozoic followed by middle Mesozoic and the youngest during early Tertiary (Faleide et al., 2010). Therefore, reflections were chosen so as to reflect these critical ages *(Fig. 3.3).* Analysis of their behavior across the master faults and the associated features belonging to these ages must give clue about the activity of Troms-Finnmark Fault Complex. Interpretation and detailed investigation of these horizons will answer the most fundamental questions of the present study, "*Were the master faults active during the late Paleozoic? Do they show sign of activity in mid. Mesozoic? Are there any signs of sinistral strike-slip movement in Jurassic? Does the study area show any concrete evidence of structural inversion and if affirmative, what is the likely origin? Is it possible to constrain the Tertiary reactivation?"* Their answers in affirmative or otherwise will have different consequences on the interpretation of structural development of the study area.

Age	Group / Formation	Top MD (m)
Cenozoic	NORDLAND GP	316
	SOTBAKKEN GP	380
	TORSK FM	380
Cretaceous	Nygrunnen GP	1072
	Kveite FM	1072
	Adventdalen GP	1097
	Kolmule FM	1097
	Kolje	1847
	Knurr FM	1871
Jurassic	Hekkingen FM	1906
	Fuglen FM	1965
	Kapp Toscana GP	1971
	Stø FM	1971
	Nordmela FM	2048
	Tubåen Fm	2156
Triassic	FRUHOLMEN FM	2290
	SNADD FM	2552
	Sassendalen GP	3962
	Kobbe FM	3962
	Klappmyss FM	4245
	Havert FM	4806
Permian	Tempelfjorden GP	4844
	Ørret FM	4844
	Røye FM	4956

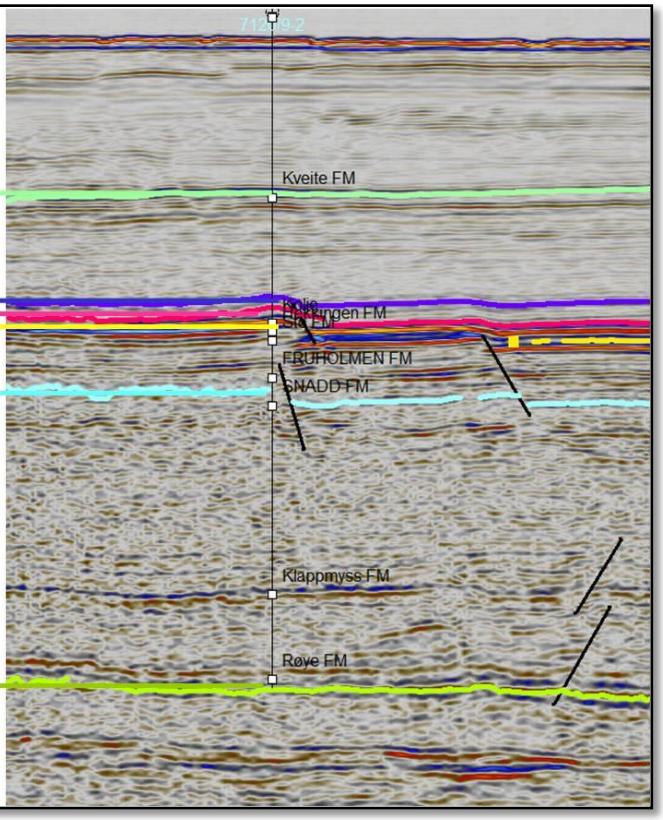

Figure 3.5: Seismic tie to well 7120/9-2, the only well within the Hammerfest Basin (study area) that penetrated the intra Permian reflection.

3.5 Comments on lithostratigraphy of the Interpreted Reflections

As discussed in the previous section, well data from four boreholes have been utilized for seismic-to-well calibration *(Figs. 3.5; 3.6; 3.7 & 3.8).* Three (7120/8-1, 7120/9-2, 7121/5-3) out of four wells are located within the Hammerfest Basin while only a single well (7120/12-4) is located on the Finnmark Platform *(Fig. 3.2).* Following paragraphs contain brief description of the formations representing the interpreted reflections in the study area which have been taken from the previously published data.

Intra Permian (IP) is the lowermost reflection interpreted in the study area. This reflection is represented by Røye Formation *(Fig. 3.3)* which is present both in the Hammerfest Basin and the Finnmark Platform (*Fig. 3.4a*). This formation is dominated by silicified sediments due to early silicification controlled by plenty of silica sponge spicules. Lithology varies from silicified calcareous claystone to silicified marls, silty carbonate mudstone and spiculitic cherts, while at places it converts into wackestone to grainstone facies (Larssen et al., 2002).

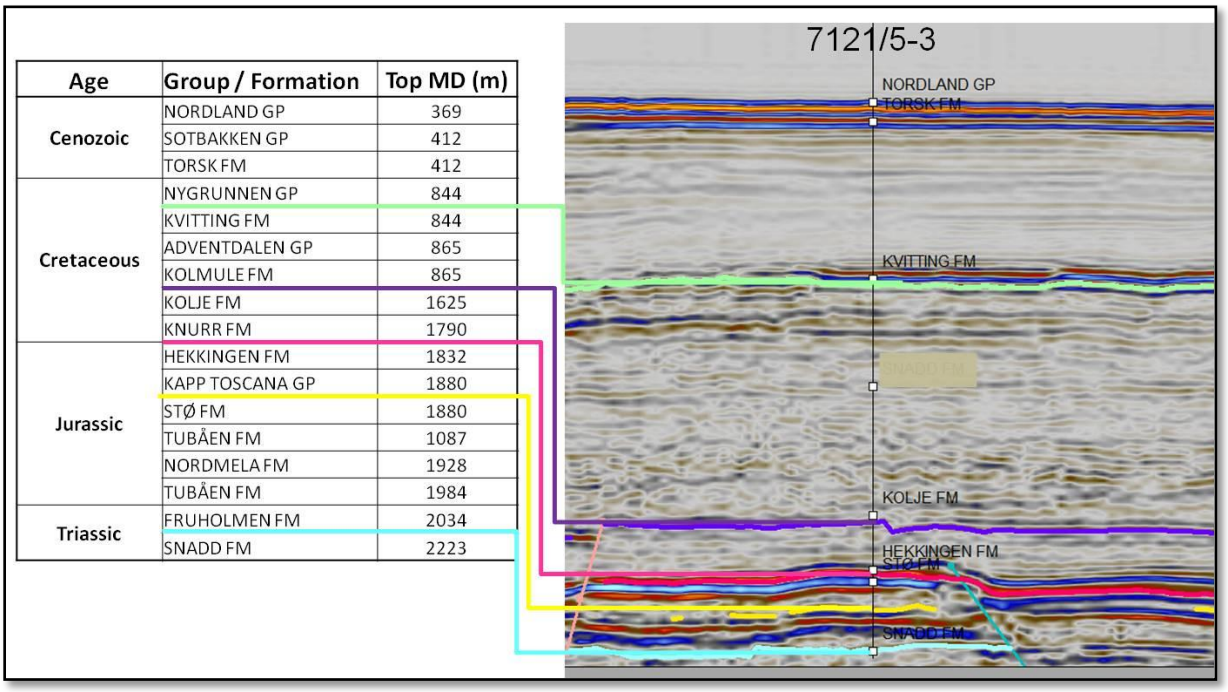

Age	Group / Formation	Top MD (m)
Cenozoic	NORDLAND GP	369
	SOTBAKKEN GP	412
	TORSK FM	412
Cretaceous	NYGRUNNEN GP	844
	KVITTING FM	844
	ADVENTDALEN GP	865
	KOLMULE FM	865
	KOLJE FM	1625
	KNURR FM	1790
Jurassic	HEKKINGEN FM	1832
	KAPP TOSCANA GP	1880
	STØ FM	1880
	TUBÅEN FM	1087
	NORDMELA FM	1928
	TUBÅEN FM	1984
Triassic	FRUHOLMEN FM	2034
	SNADD FM	2223

Figure 3.6: Seismic tie to well 7121/5-3, the oldest penetrated age/formation by this well is Triassic/Snadd. Well is present within the central part of the study area, for location refer to the Fig. 3.2.

In the present study, intra Permian reflection has been interpreted between 2300- 4000 ms (twt) approximately in the Hammerfest Basin while on the Finnmark Platform it has been interpreted

in the range of 700-2500 ms (twt) approximately (Table 3.4) *(Fig. 3.11, Fig. 3.12 & Fig. 3.17).* Owing to its lithostratigraphy, it is represented by strong reflection with medium-high amplitude.

Intra Triassic (IT) reflection is represented by Snadd Formation *(Fig. 3.3)* and it is present both in the Hammerfest Basin and the Finnmark Platform *(Fig. 3.4a).* This formation predominantly consists of grey shale that coarsens upward into shale with interbeds of siltstone and sandstone (Dalland et al., 1988). In the present study, it has been interpreted between 1300-3500 ms (twt) approximately in the Hammerfest Basin while on the Finnmark Platform this reflection has been in the range of 500-1500 ms (twt) approximately (Table 3.4) *(Fig. 3.10, Fig. 3.11, Fig. 3.14 & Fig. 3.17).* Towards the Finnmark Platform, the intra Triassic reflection is characterized by medium to low amplitude and good continuity which is cut by erosional unconformity in the study area *(Fig 3.12 c).* Particularly, its amplitude decreases considerably in the Hammerfest Basin and reflection pattern becomes discontinuous and chaotic at places within the Hammerfest Basin where it is considerably tricky to correlate.

Age	Group / Formation	Top MD (m)
Cenozoic	SEA BED	152
	NORDLAND GP	175
Triassic	KAPP TOSCANA GP	435
	SNADD FM	435
	SASSENDALEN GP	485
	KOBBE FM	485
	KLAPPMYSS FM	685
	HAVERT FM	992
Permian	TEMPELFJORDEN GP	1366
	ØRRET FM	1366
	RØYE FM	1469
	ØRRET FM	1502
	RØYE FM	1648
	ØRRET FM	1688
	RØYE FM	1700
	ØRRET FM	1728
	RØYE FM	2003
Carboniferous	GIPSDALEN GP	2118
	UGLE FM	2118

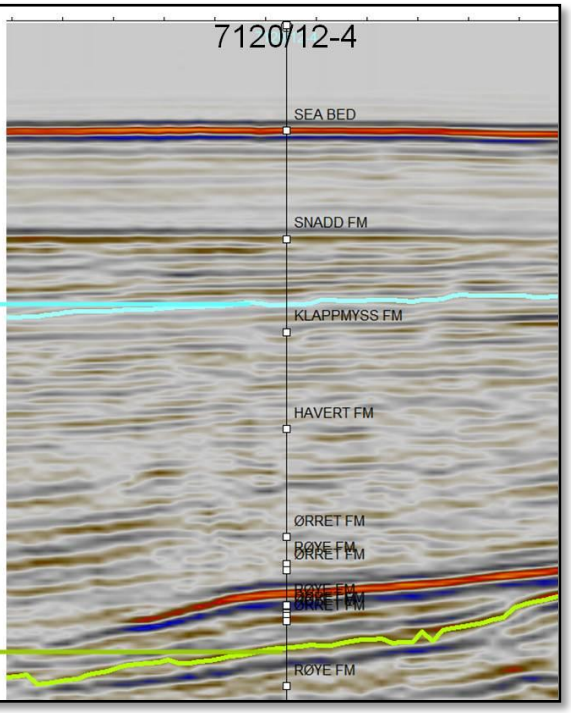

Figure 3.7: Seismic tie to well 7120/12-4, the oldest penetrated age/formation by this well is Carboniferous/Ugle. Well is present within the western part of the study area and is the only well located on the Finnmark Platform (within study area), for location refer to the Fig. 3.2.

Middle Jurassic (MJ) reflection is represented by Stø Formation *(Fig. 3.3)* which is present only within the Hammerfest Basin *(Fig.3.4a).* Lithologically, it comprises of mature sandstone, however, thin intervals of shale and siltstone are also present, while phosphatic lag conglomerate is also reported in the upper units of this formation from some wells (Dalland et al., 1988). In this study, this reflection has been interpreted between 1200-3400 ms (twt) approximately (Table 3.4) *(Fig.3.10 & Fig. 3.14).*

Table 3.4: Range of two-way-time (s) for the interpreted intra Permian, intra Triassic and middle Jurassic reflections in the study area.

Key Profile	Intra Permian - TWT (s)		Intra Triassic - TWT (s)		Middle Jurassic - TWT (s)	
	Hammerfest Basin	Finnmark Platform	Hammerfest Basin	Finnmark Platform	Hammerfest Basin	Finnmark Platform
1	2.5 - 3.5	1.4 - 1.8	2.1 - 3.5	0.7 - 1.2	1.8 - 3.4	**Absent**
2	2.8 - 4 .0	0.7 - 1.6	1.8 - 2.3	0.5 - 0.6	1.7 - 2.2	
3	3.3 - 4.0	1.0 - 1.6	2.1 - 2.4	0.6 - 0.8	1.9 - 2.3	
4	3.2 - 3.5	1.2 -1.8	2.0 - 2.3	0.7 - 1.2	1.8 - 2.2	
5	2.8 - 3.5	1.2 - 2.2	1.3 - 1.8	0.6 - 0.9	1.2 - 1.7	
6	2.3 - 3.5	1.0 - 1.8	1.8 - 2.1	0.7 - 1.2	1.7 - 1.9	
7	3.0 - 3.3	1.0 - 2.0	1.9 - 2.3	0.6 - 1.2	1.8 - 1.9	
8	2.7 - 3.3	1.0 - 2.5	1.8 - 2.3	0.6 - 1.5	1.7 - 2.1	

In the Hammerfest Basin, the mid Jurassic reflection is characterized by medium to high amplitude and good continuity but the amplitude decreases and it becomes discontinuous in the central part the Hammerfest Basin. In the central part of the Hammerfest Basin this reflection is hard to correlate across the rotated fault blocks due to the strong rotation of strata and erosion at the faulted-block shoulders *(Fig. 3.11 a).*

Base Cretaceous reflection in the present study is defined by Top Hekkingen Formation (*Fig. 3.3).* The formation comprises of brownish grey to very dark grey shale and claystone with less frequent thin intercalations of limestone, dolomite, siltstone and sandstone (Dalland et al., 1988). During current study, this formation has been interpreted as a strong positive reflection between 1200-3000 ms (twt) approximately (Table 3.5) *(Fig. 3.10).* It is present only within the

Hammerfest Basin and is characterized by the high amplitude and very good continuity which makes it considerably uncomplicated reflection to be correlated across the study area.

Early Tertiary reflection is characterized by Top Kolje Formation *(Fig. 3.3).* In the present study, it has been interpreted between 900-2800 ms (twt) approximately (Table 3.5) *(Fig.3.10 & Fig. 3.11).* Lithologically, Kolje Formation is represented by dark brown to dark grey shale and claystone as dominant constituents while minor interbeds of pale limestone and dolomite are also not uncommon (Dalland et al., 1988). Seismic character of this formation is represented by medium to high amplitude and it exhibits excellent lateral continuity.

Table 3.5: Range of two-way-time (s) for interpreted base Cretaceous, early Cretaceous and base Tertiary reflections in the study area.

Key Profile	Base Cretaceous - TWT (s)		Early Cretaceous - TWT (s)		Base Tertiary - TWT (s)	
	Hammerfest Basin	Finnmark Platform	Hammerfest Basin	Finnmark Platform	Hammerfest Basin	Finnmark Platform
1	1.2 - 3.0	**Absent**	1.1 - 2.8	**Absent**	0.7 - 2.3	**Absent**
2	1.3 - 2.5		0.9 - 2.2		0.7 - 1.9	
3	1.5 - 1.8		1.2 - 1.6		0.7 - 0.9	
4	1.6 - 1.8		1.4 - 1.6		0.8 - 1.1	
5	1.5 - 2.0		1.3 - 1.6		0.6 - 1.0	
6	1.5 - 1.8		1.3 - 1.7		0.7 - 0.9	
7	1.5 - 1.9		1.1 - 1.7		0.6 - 0.9	
8	1.7 - 1.9		1.5 - 1.6		0.9 - 1.0	

Base Tertiary is the shallowest horizon that has been interpreted between 500-2300 ms (twt) approximately during the present study (Table 3.5) *(Fig. 3.10 & Fig. 3.14).* This reflection corresponds to Top Kveite/Kviting formations. Lithologically, Kveite Formation is represented by greenish-grey to grey shales and claystones while thin interbeds of limestone and siltstone are also present. Kviting Formation is represented by calcareous sandstones with interbedded sandy and glauconitic mudstones (Dalland et al., 1988). Seismic signature of these chronostratigraphic equivalent formations is marked by low/medium - high amplitude and at places it shows poor lateral continuity but such instances are rare in the study area.

3.6 Description of Key Profiles – Structural Architecture & Fault Plane Geometries

The Troms-Finnmark Fault Complex runs parallel to the coastline of Troms and Finnmark counties *(Fig. 2.3)* between 69°20'N, 16°E and $71^0$40'N, $23^0$40'E. It serves as a structural division between Finnmark Platform in the south-southeast and northward basins such as Harstad Basin, Tromsø Basin and Hammerfest Basin (Gabrielsen et al., 1990). At its southern extremity, this fault complex shows a structural trend of NNE-SSW to NE-SW, while it changes its strike to more ENE-WSW at about $19^0$20E *(Fig. 2.3)* (Gabrielsen et al., 1990). On smaller scale however, this fault complex shows NE-SW to E-W and ESE-WNW trending segments that together constitute a dog-leg style (Berglund et al., 1986). Cumulative throw of more than 1.5s (twt) is estimated for this fault complex (Gabrielsen 1984). Towards northeast, it terminates along the offshore extension of Trollfjord-Komagelv Fault Zone exhibiting a WNW-ESE trend *(Fig 2.3)* (Gabrielsen 1984, Berglund et al., 1986, Ziegler et al., 1986, Gabrielsen & Færseth 1989, Gabrielsen et al., 1990). Present study encompasses part of Troms-Finnmark Fault Complex that serves to separate tectonically stable Finnmark Platform in the south from the more deformed Hammerfest Basin in the North.

This section is dedicated to document all structural elements and their sub-features present within the study area. Consequently, 2D seismic dip lines are selected as near-true representatives of the cross-sectional view of the study area which provide better visualization of structural forms and their control on sedimentation. Eight 2D seismic dip lines *(key profile 1-8, Fig. 3.2)* are termed as key profiles and discussed later in this section. These key profiles serve to best describe the change in geometry and structural trend of the Troms-Finnmark Fault Complex. During the present study, this fault complex has been divided into three segments, based on the following:

i) Variation in strike of the master faults within the study area
ii) MF1, MF2 & MF3 are segments of a large fault array exhibiting overlapping relationship, for all three segments *(Fig. 3.9).*

The fault segment MF3 shows NE-SW trend predominantly. Similarly, the segment MF2 is characterized by EW-ENE-WSW structural trend while the western-most fault segment MF1 exhibits a NE-SW trend *(Fig. 3.9).* The large array of the Troms-Finnmark Fault Complex with its constituent segments in the study area forms a case study of extensional relay structures

similar to the accommodation zone (Bosworth, 1985), fault bridge (Ramsay & Huber, 1987) strain transfer zone (Morley et al., 1990) or "step-overs" in strike-slip fault systems (Aydin & Nur, 1985). In such kind of structural configuration extension experienced by one fault is relayed across a ramp to the next fault segment (Trudgill & Cartwright, 1994). Fault linkage between two segments in such a case could be one of the following (Walsh & Watterson, 1991 as cited in Trudgill & Cartwright, 1994):

a. Unlinked Faults: Isolated Fault Segments showing no connectivity of any form between the adjacent segments.
b. Soft-linked Faults: Mechanical and geometric consistency is attained by ductile deformation between the overlapping fault segments, although they appear to be cut-off from one another.
c. Hard-linked Faults: Segment boundaries are linked on the scale of the map or cross-section.

This point forward, an integrated approach is adopted which involves description of key profiles, time-structure maps, fault maps and time-thickness maps. Hence, all data sets are presented and described in a coherent manner that supplement the observations made on one data-set to the observation on the next data-set and so on. This work plan helped to achieve the following:

- Classification of fault system by utilizing the time-structure maps , fault maps and profiles.
- Dating the age of fault activity and comparing the timing of fault activation in different master fault segments (MF1, MF2 & MF3).
- Comprehending the structural regime and the governing stress system at different stages of fault development.
- Comparison of the results obtained from the present study with the regional picture already known from the Barents Sea.

The first two points (a, b) described above are concluded within this chapter and their conclusions form foundation for the next two points (c, d). The latter two points (c, d) although connected with the previous points are addressed in the next chapter. All of the description follows a time line starting with the oldest part of the development i.e., the Permian, and ending

with the youngest events in the study area i.e., the Tertiary, hence a bottom- up approach is adopted as a scheme for the description of tectonic events in the study area.

The intra-Permian time-structure map at Finnmark Platform shows gradual increase in time values from south towards the main boundary fault in the North *(Fig. 3.8).* However, towards SE of the study area, abrupt change in time values indicate presence of a fault which is attested by the fault map at this level as well. Across the main boundary fault, a sudden increase in time values signifies the great vertical displacement experienced by Intra-Permian reflection which exceeds 1.5 s (twt) in places. In the Hammerfest Basin, higher time values towards the North indicate the deepening of intra-Permian reflection in this direction. However, the greatest time values are in the NW direction which shows that the basin is not symmetrical in configuration *(Fig. 3.8).* Key profiles shown on the map itself are discussed in detail, later in this chapter.

The MF1, MF2 & MF3 (master faults 1,2,3) constitute a large fault array with overlapping zones in between them *(Fig. 3.9).* Relay structure between these fault segments are connecting hanging-wall of the one segment with the footwall of another. The master faults MF3 & MF2 are overlapping with no hard-linkage established between them; however, they are not entirely isolated segments either. Presence of a fault between two overlapping segments qualifies this connectivity as "*soft-linked"* type *(Fig. 3.9).* In order to understand the geometry and structural configuration of the MF2 & MF3 segments in the large array of Troms-Finnmark Fault Complex, three key profiles for each segment are selected, which will be discussed later in this chapter *(Fig.3.9).* Key Profile 6 covers both MF1 & MF2 fault segments. The fault segment MF3 is represented by the only key profile 1 due to limitation of the data towards the extreme west of the study area *(Fig.3.9).*

At the Intra-Permian level both the Finnmark Platform and the Hammerfest Basin exhibit significant deformation. It is obvious from the predominantly NE-SW trending faults at the Finnmark Platform. Towards the south-east of the study area, a laterally continuous significant planar normal fault (PF) dips to the North and its throw diminishes from the East to the West *(Fig.3.9).* Small grabens are also present at this level on the Finnmark Platform. Similarly, presence of northward dipping faults is ubiquitous on the platform *(Fig.3.9).* In the Hammerfest Basin, a group of synthetic and antithetic faults in the proximity of the master faults is also present while further in the central parts of the basin small grabens at Intra-Permian level are also

found. Degree of faulting seems to be concentrated towards the southern margin of the Hammerfest Basin while towards its northern main boundary fault (the Asterias Fault Complex); faulting is less frequent *(Fig.3.9).* It is however pertinent to note at this stage that during the present study, only five regional lines covered the northern main boundary fault of the Hammerfest Basin *(Fig.3.2).*

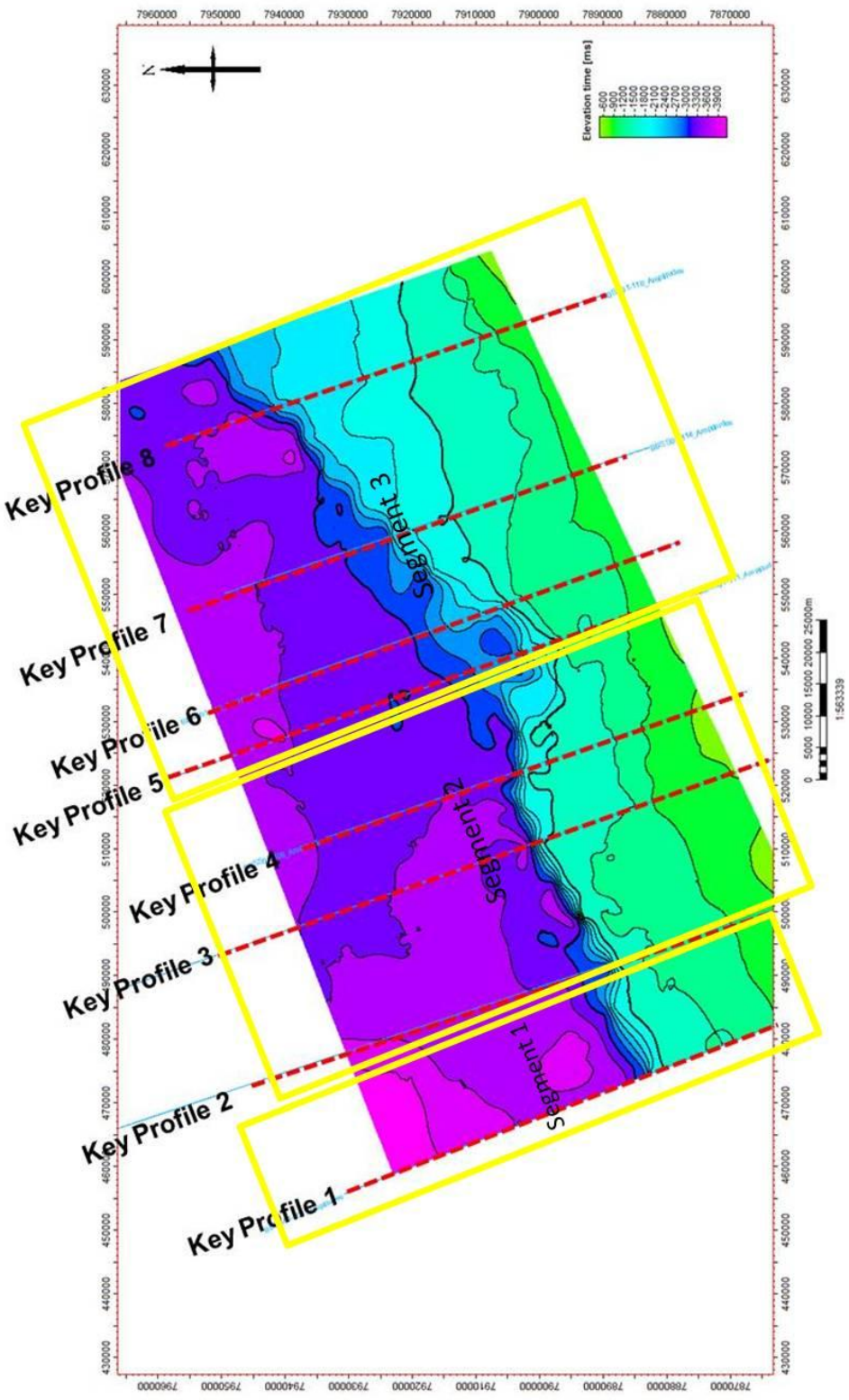

Figure 3.8: Time-structre map at intra Permian level showing structural segments of main study area. Contouring (twt) at the intra Permian level. Location of seismic lines further discussed as key profiles is also indicated.

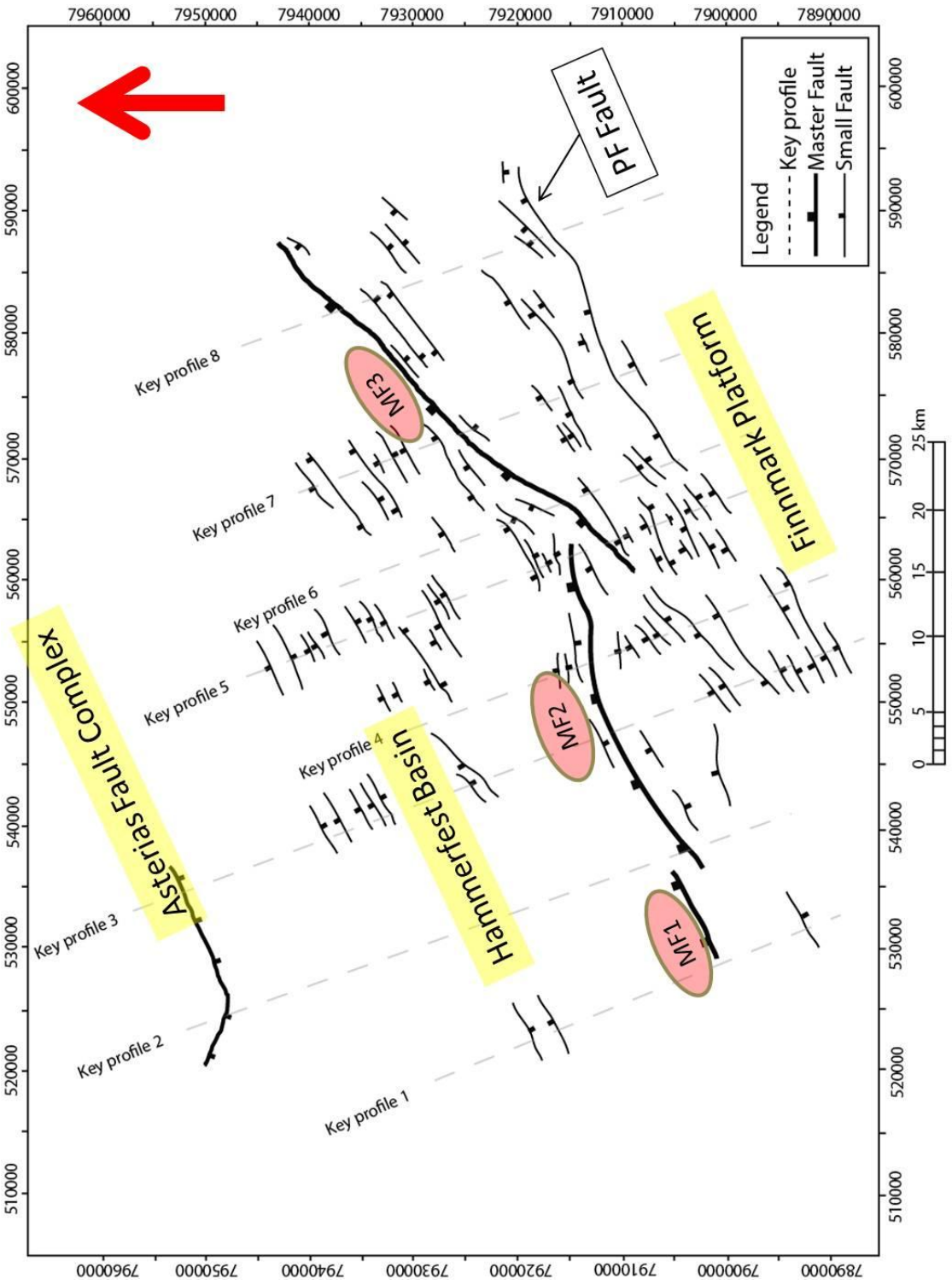

Figure 3.9: Fault Map at intra Permian level with different segments of the larger Troms-Finnmark Fault Complex.

3.6.1 Key Profile 1

This dip line belongs to the westernmost part of the available 2D seismic data and is oriented NW-SE. Hence, it images the NE-SW trending MF1 segment of the Troms-Finnmark Fault Complex very well *(Figs. 3.8 & 3.9).* The base Tertiary, the early Cretaceous, the base Cretaceous and the intra Jurassic reflections are interpreted only within the Hammerfest Basin while the intra Triassic and the intra Permian are the only two reflections interpreted both over the platform and the basin *(Fig. 3.10 a,b).* At the Finnmark Platform, the Quaternary sediments are overlying the Triassic succession, which implies that stratigraphic interval ranging from the lower Jurassic to the Tertiary is missing on the platform *(Fig 3.7).* All interpreted horizons are consistent in showing a general northward tilt which in turn points that the Hammerfest Basin is getting deeper from South to the North *(Fig 3.10 a).*

Master fault (MF1) is the main boundary fault which shows listric geometry and is concave downward to the North separating the Finnmark Platform in the south from the Hammerfest Basin towards the North *(Fig 3.10 a,b).* MF1 cuts stratigraphic succession of mid Cretaceous down to the basement? and is therefore termed as the ***First-Class*** fault (*sensu* Gabrielsen, 1984). Interpreted reflections at the intra Permian and the intra Triassic levels show varying amounts of vertical separation across MF1. At intra Permian level the vertical separation is approximately 0.7 s (twt) while it reduces to 0.5 s (twt) at intra-Triassic level *(Fig. 3.10b).*

A general scheme adopted for nomenclature of faults interpreted on the platform and in the basin is such that faults of the Hammerfest Basin are represented by the capital alphabet “F” with numeric “1,2,3…n” representing their numbers while faults of the Finnmark Platform are shown with small “f” and a numeral “1,2,3…n”. This nomenclature has been consistent throughout the description of the key profiles *(Fig. 3.10 a, b).*

Within Hammerfest Basin, frequency of faulting varies from bottom to the top interpreted reflections. The intra Permian reflection is showing a northward dip and is relatively undisturbed by faulting whereas the interpreted intra-Triassic, the intra Jurassic and the base Cretaceous reflections are affected by the planar normal faults showing a northward dip-slip component predominantly *(Fig. 3.10 a,b).* The base Tertiary and the early Cretaceous reflections are relatively unperturbed in this part of the study area *(Fig. 3.10 a,b).* Majority of faults (F1 to F4 & F8 to F11) in this area are synthetic to the master fault MF1 i.e., show a northward displacement

along dip while some faults (F5, F6, F7) also demonstrate a southward dip-slip component, hence are termed antithetic to the master fault MF1 *(Fig. 3.10 a).* Fault pattern within the basin constitute stair-case geometry with the normal faults occurring at regular intervals. As a consequence, basin gets deeper towards the NW. The fault F4 along with the faults F5 & F6 forms a broad graben which is the deepest part of the basin in the area under discussion *(Fig. 3.10 a).* Rotation of the intra Triassic and the intra Jurassic reflections is apparent along the fault F9, giving rise to classical sedimentary wedge between the intra Jurassic and base Cretaceous reflections *(Fig. 3.10 a)*

The Finnmark Platform in this profile is representing the least disturbance by faulting, the only fault f1 is cutting the intra Permian reflection down to the south and it shows planar geometry. Hence, the fault f1 is termed as antithetic to the master fault MF1 *(Fig. 3.10 a,b).*

A noteworthy feature in the close vicinity of the master fault MF1 is the presence of a domal feature *(Fig. 3.10b).* This feature is quite consistent in geometry from the intra Permian to the intra Triassic whereas, its effect diminishes upward in the younger interpreted intervals. Identification of the growth strata between the intra Jurassic and the base Cretaceous reflections sets evidence for this feature to be identified as a roll-over anticline. This anticlinal feature is affected by the fault F1 at its crestal level *(Fig. 3.10 b).* Interpreted reflections lying above the intra Jurassic show normal drag with the master fault MF1 while the base Tertiary in this part of the study is not affected by the master fault MF1 *(Fig. 3.10b).*

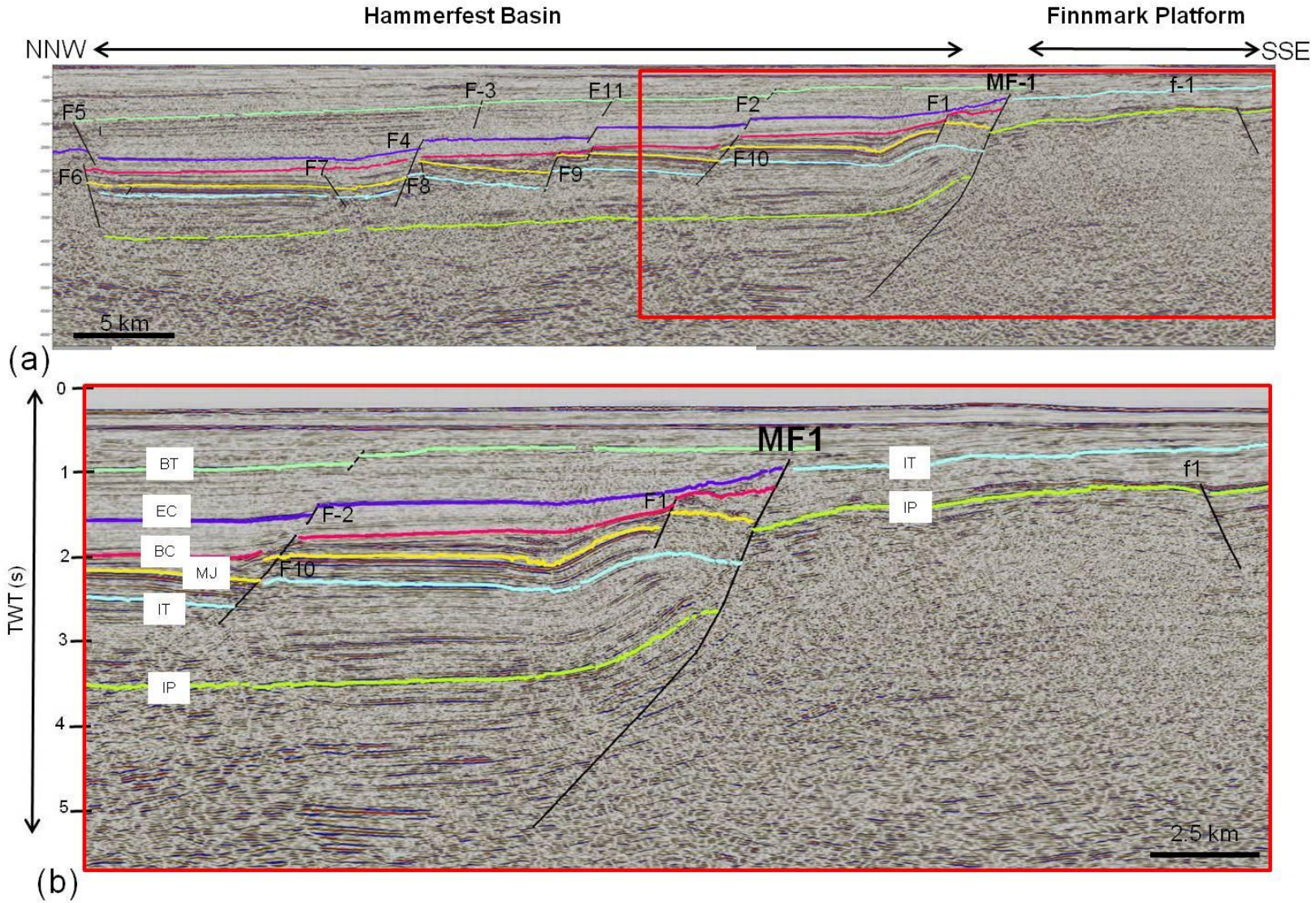

Figure 3.10 a: Key Profile 1 along fault segment MF1. **(b)** Zoomed-in part of (a) represented by red square. See Figs. 3.8 & 3.9 for location of the line. BT: Base Tertiary, EC: Early Cretaceous, BC: Base Cretaceous, MJ: Middle Jurassic, IT: Intra Triassic, IP: Intra Permian.

3.6.2 Key Profile 2

This dip line also belongs to the western part of the available 2D seismic data and is oriented NW-SE and therefore, it images the ENE-WSW & EW trending MF2 segment of the Troms-Finnmark Fault Complex quite well *(Figs. 3.8 & 3.9).* This is a regional transect covering the entire Hammerfest Basin bounded at northern and southern margins by the Asterias and Troms-Finnmark fault complexes. The base Tertiary, the early Cretaceous, the base Cretaceous and the intra Jurassic reflections are interpreted within the Hammerfest Basin while the intra Triassic and the intra Permian reflections are interpreted both over the platform and in the basin *(Fig.3.10 a,b).* At the Finnmark Platform, Quaternary sediments are overlying the Triassic sequence, which implies that the stratigraphic interval ranging from lower Jurassic to Tertiary is missing on the platform *(Fig. 3.7).* All interpreted reflections are consistent in showing a general northward tilt which in turn points that the Hammerfest Basin is getting deeper from the South to the North. This observation is supplemented by observing the base Cretaceous reflection in the South (near Troms-Finnmark Fault Complex) and following the same toward the North (towards the Asterias Fault Complex), there seems a time shift of 1s (twt) for this reflection as it gets deeper towards the North *(Fig. 3.11a).*

This transect is significant to understand the structural configuration of the entire Hammerfest Basin with its northern and southern main boundary faults. Development of broad low amplitude roll-over anticlines is associated with both the main boundary faults *(Fig. 3.11a).* A central bulge of the basin is readily observed which also has developed several North and South-dipping normal faults cutting the stratigraphic succession between the base Cretaceous and the intra Triassic reflections *(Fig. 3.11a).* Development of this central bulge can be attributed to the movements along the two boundary faults which resulted in the formation of reverse drag in the proximity of the faults and relatively uplifted flatter horizons in the middle of the basin *(Fig. 3.11a).*

Master fault (MF2) is the main boundary fault which shows listric geometry and is concave downward to the North separating the Finnmark Platform in the south from the Hammerfest Basin towards the North *(Fig. 3.11b).* The fault segment MF1 cuts the stratigraphic succession from the base Tertiary down to the basement? and is therefore termed as the ***First-Class*** fault (*sensu* Gabrielsen, 1984). At the intra Permian level the vertical separation is approximately 1.4 s (twt) while it becomes 1.8 s (twt) at the intra Triassic level *(Fig. 3.11b).*

In the Hammerfest Basin, frequency of faulting varies from bottom to the top interpreted reflections. The intra Permian reflection is showing a northward dip and is relatively less disturbed by faulting as compared to the interpreted reflections above it *(Fig. 3.11 a,b).* The intra Triassic, the intra Jurassic and the base Cretaceous reflections are affected by the planar normal faults showing a northward dip-slip component. Majority of the faulting (F1 to F8) is focused within these interpreted reflections *(Fig. 3.11b).* The early Tertiary and the base Tertiary reflections are relatively unperturbed in this part of the study area *(Fig. 3.11 a,b).* Majority of the faults *(F3 to F7)* are synthetic to the master fault MF1 i.e., show a northward displacement along dip while some faults *(F1, F2, F8)* show a southward dip component as well, hence, they are termed as antithetic *(Fig. 3.11b).* Faulting dominates in the proximity of the boundary faults of the Hammerfest Basin while considerable deformation due to faulting is also experienced by the central bulge lying in middle of the basin *(Fig. 3.1a).* Towards the master fault MF2, faulting has occurred on the roll-over anticline where both the synthetic and the antithetic faults are present *(Fig 3.11b).*

Like the Key Profile 1, the Finnmark Platform in this profile is also representing the least disturbed and tectonically stable area. However, few minor planar normal faults affecting the intra Permian reflection are observed that show a northern dip. Among them is the fault f1 which is proximal to the master fault MF2 and show a north dip-slip component and hence, termed as the synthetic fault *(Fig. 3.11b).* The intra Permian and the intra Triassic reflections are making erosional contacts with the overlying younger sedimentary sequence of the Quaternary, on the platform. The intra Triassic reflection is cut by the angular unconformity in the North long before the intra Permian reflection which is cut by this unconformity towards the South. Both the reflections show a northward tilt which makes an angular relationship with the near-horizontal erosional surface at the top *(Fig. 3.11a).*

A roll-over anticline is found to be associated with the fault MF2 *(Fig. 3.11 b). This* feature is quite consistent in geometry from the intra Permian to the intra Triassic reflections, whereas, it is overlain by a prominent syn-sedimentary wedge *(Fig. 3.11b)* between the intra Jurassic and the base Cretaceous reflections providing a mechanism to define the underlying anticline as the "roll-over" feature. Approximately, all faults occurring towards the hanging-wall of the MF2 are concentrated on this roll-over anticline. Development of faulting on this anticline implies that these faults were formed as a result of continued stretching once the roll-over anticline was formed. As a consequence, the synthetic and the antithetic (F1…F8) faults developed to accommodate any additional stretch *(Fig. 3.11b).*

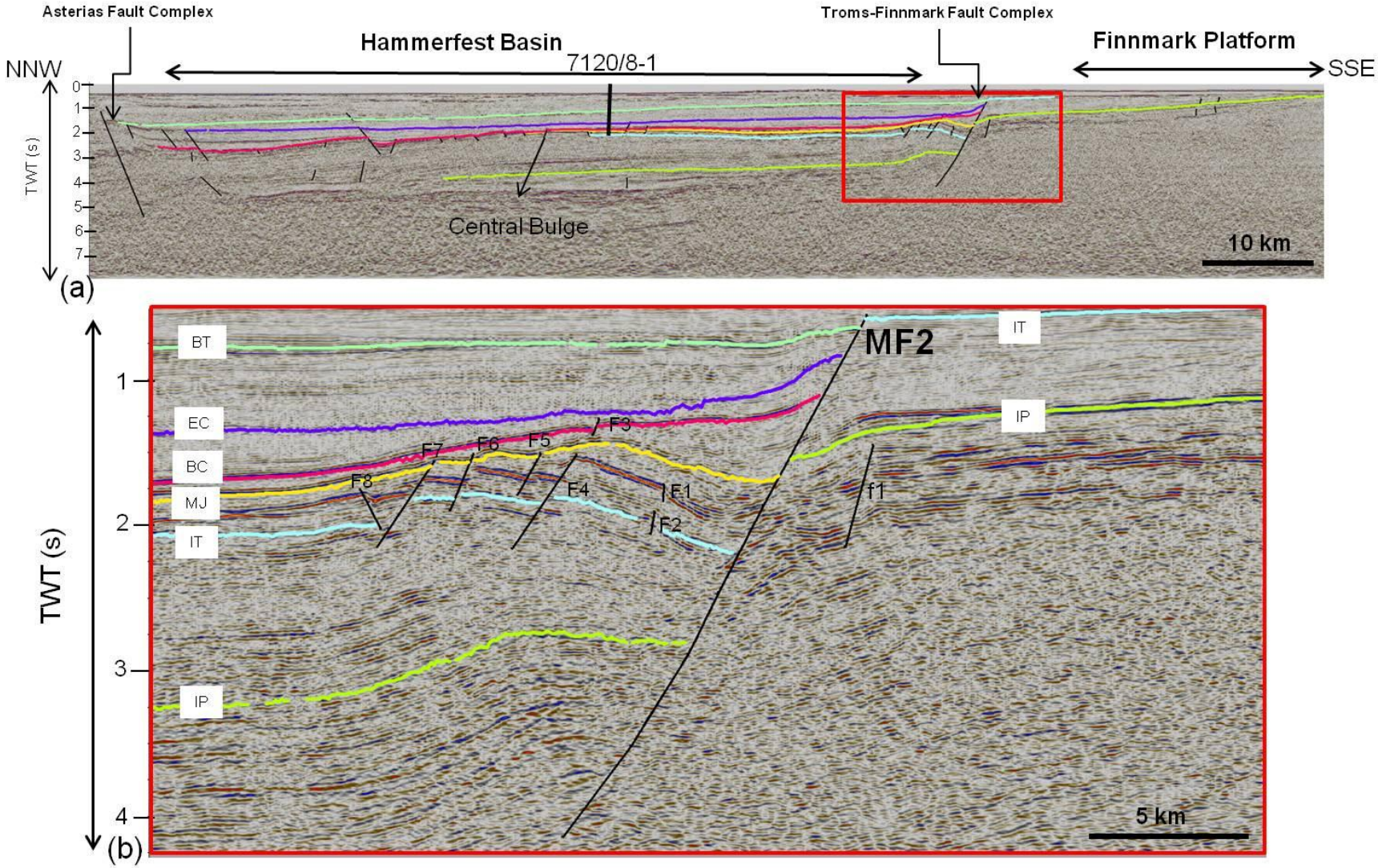

Figure 3.11a: Key Profile 2 along the fault segment MF2. **(b)** Zoomed-in part of (a) represented by red square. See Figs. 3.8 & 3.9 for location of the line. BT: Base Tertiary, EC: Early Cretaceous, BC: Base Cretaceous, MJ: Middle Jurassic, IT: Intra Triassic, IP: Intra Permian.

3.6.3 Key Profile 3

This dip line belongs to the central part of the fault segment MF2 and is oriented NW-SE such that it images the ENE-WSW trending part of the fault very well *(Figs 3.8 & 3.9).* This is also a regional transect covering the entire Hammerfest Basin bounded by the main boundary faults at its southern and the northern margins. The base Tertiary, the early Cretaceous, the base Cretaceous and the intra Jurassic reflections are interpreted within the Hammerfest Basin only while the intra Triassic and the intra Permian reflections are interpreted both over the platform and in the basin *(Fig.3.12 a, b).* At the Finnmark Platform, the Quaternary sediments are overlying the Triassic succession reflecting the absence of stratigraphy from the lower Jurassic to the Tertiary *(Fig. 3.7).* The interpreted reflections on the platform are consistent in showing a general northward tilt towards the master fault MF2. In the basin, however, this trend is reversed i.e., reflections are tilted southward towards the master fault MF2 *(Fig.3.12a).*

The master fault (MF2) is the main boundary fault with listric geometry and is concave downward to the North separating the Finnmark Platform in the south from the Hammerfest Basin towards the North *(Fig. 3.12b).* This fault cuts stratigraphic succession from the base Tertiary down to the basement? and is therefore termed as the ***First-Class*** fault *(sensu* Gabrielsen, 1984*).* Vertical separation across the master fault MF2 can only be assessed at the intra Permian and the intra Triassic levels which are approximately 1.6 s (twt) and 1.5s (twt) respectively *(Fig 3.12b).*

Frequency of faulting within the Hammerfest Basin varies from bottom to the top interpreted reflections. The intra Permian reflection is disturbed by a number of synthetic and antithetic faults with minor stratigraphic throws. Antithetic faults at the intra Permian level includes faults such as F3 & F4 *(Fig 3.12b)* in the proximal part of the main boundary fault MF2 while others mainly oppositely verging normal faults F13 & F14 form a graben at this level and are located in the more distal part of the basin *(Fig.3.12a).* Similarly, the intra Triassic reflection is disturbed near the central bulge but frequency of faulting displacing this reflection is less, such faults include F8, F10, F11 & F12 *(Fig. 3.12a).* The intra Jurassic, the base Cretaceous and the early Cretaceous reflections are faulted down to the North near the central bulge of the basin and are represented by the faults F5 to F12 in this profile. Majority of these faults are dipping towards the North hence, termed as synthetic, however, exception to this trend is represented by the fault F12, which shows a southward dip-slip component, hence termed as

an antithetic fault. The interpreted base Tertiary reflection shows the least disturbance and is dipping gently towards the North in this part of the study area *(Fig.3.12a).*

Frequency of faulting on the Finnmark Platform is less as compared to the Hammerfest Basin *(Fig. 3.12a).* Intra Triassic reflection is less disturbed by faults as compared to the Intra Permian level. All faults present over the platform are showing a general northward dip-slip, these faults include f1, f2 and f3 and are present in the extreme SSE part of the profile *(Fig. 3.12a).* A close-up view is presented in the *Figure 3.12c*, which also shows presence of minor normal faults at sub-Permian level. The intra Triassic reflection makes an erosional contact with the overlying Quaternary deposits, represented by an angular unconformity *(Fig. 3.12c).*

The "roll-over anticline" associated with the fault MF2 in the previous profile is absent here. Drag associated with the master fault MF2 in this profile is normal in nature which can easily be seen at the interpreted intra Triassic, intra Jurassic and the base Cretaceous levels *(Fig. 3.12b).* A part of the central bulge present in the Key Profile 2 is observed which has its crest near the faults F9 and F10 *(Fig. 3.12a),* both of these faults are planar normal faults dipping towards the North. Immediately, after the fault F10, two opposite verging faults F11 and F12 together with their downward extensions of the faults F13 and F14, makes a graben which is the deepest part of basin seen on this profile *(Fig. 3.12 a).* Instead of reverse drag, normal drag is associated with the main fault MF2 *(Fig. 3.12b).* Identification of growth strata, however, between the interpreted middle Jurassic and the base Cretaceous reflections is quite straightforward *(Fig. 3.12a)* giving clue to the activity along the main boundary fault MF2 during this time.

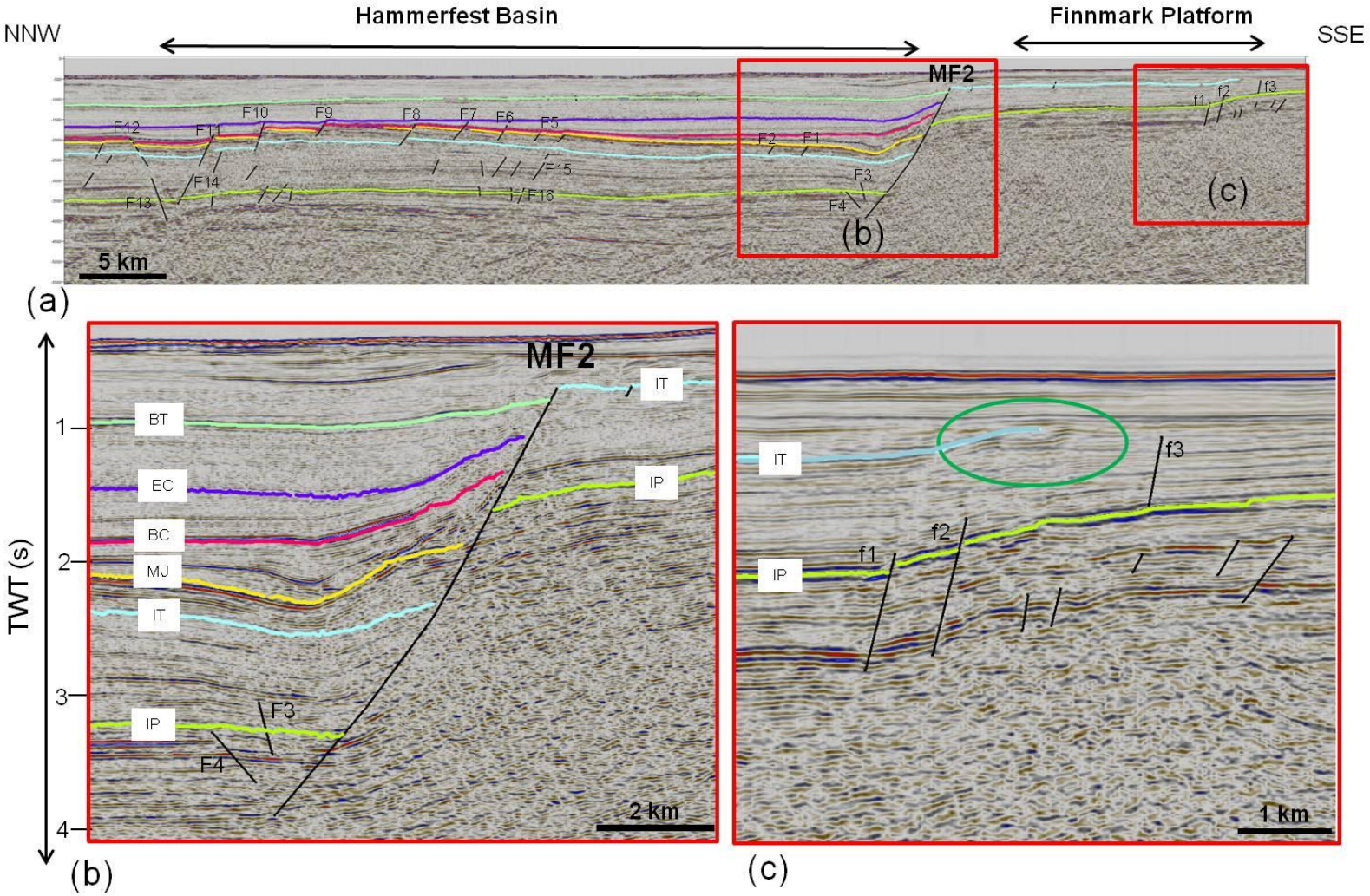

Figure 3.12 a: Key Profile 3 along fault segment MF2. **(b)** Zoomed-in part of (a) represented by red square, focusing on the fault MF2. **(c)** Zoomed-in part of (a) representing angular unconformity at Intra Triassic level. See Figs. 3.8 & 3.9 for location of the line and Fig. 3.3 for reflection codes, refer to Fig. 3.11 for the abbreviations of reflections.

3.6.4 Key Profile 4

This dip line also belongs to the central part of the fault segment MF2 and is oriented NW-SE *(Fig. 3.8).* The main boundary fault MF2 at this location is showing an E-W trend *(Fig. 3.9),* for this reason it was deemed necessary to describe the structural features found along this cross-section. This profile is restricted to the central part of the Hammerfest Basin in the NW and covers a significant part of the Finnmark Platform towards SE, with the master fault MF2 separating the two provinces *(Fig. 3.9).* The base Tertiary, the early Cretaceous, the base Cretaceous and the middle Jurassic reflections are absent on the Finnmark Platform, hence they are interpreted within the Hammerfest Basin only while the intra Triassic and the intra Permian reflections are interpreted both over the platform and in the basin *(Fig. 3.13 a, b).* At the Finnmark Platform, stratigraphic interval from the early Jurassic to the late Tertiary is missing and Quaternary deposits directly overlie the Triassic succession *(Fig. 3.7).* The interpreted reflections on the platform show a gentle northward tilt towards the master fault MF2. In the basin base tertiary and early Cretaceous reflections show a northward tilt too, however, base Cretaceous and middle Jurassic reflections are tilted towards the North in the proximal part of the master fault MF2, whereas, in the distal part they show a gentle southward dip towards the MF2 *(Fig. 3.13a).* Similarly, the intra Triassic reflection is represented by a general dip towards the master fault MF2 while the intra Permian reflection shows the opposite trend *(Fig. 3.13 a,b).*

The master fault MF2 is a downward concave normal fault separating the Finnmark Platform in the South from the Hammerfest Basin towards the North *(Fig. 3.13 a, b).* The master fault MF2 cuts the stratigraphic succession from the base Tertiary down to the basement? and is therefore, termed as the ***First-Class*** fault (*sensu* Gabrielsen,1984). Vertical separation across the fault MF2 can only be assessed at interpreted the intra Permian and intra Triassic reflections, which are approximately 1.5 s (twt) and 1.3 s (twt) respectively *(Fig. 3.13b).* The master fault MF2 is associated with the normal drag, clearly visible at the intra Jurassic, the base Cretaceous and the base Tertiary reflections, however, there is slight development of reverse drag at the intra Triassic reflection as well *(Fig. 3.13 a,b).*

Frequency of faulting within the Hammerfest Basin varies from bottom to top at the interpreted stratigraphic intervals. The intra Permian reflection is affected by minor planar normal faults. Faulting is concentrated in the close vicinity of the master fault MF2, with faults F16 & F18 showing northward and southward dips respectively making a small horst

between them which also is affected by another southward dipping minor normal fault F17. Another fault F14 at the intra Permian level is present in the distal part of the basin and shows a north dip *(Fig. 3.13 a, b).* The intra Triassic reflection is relatively less affected by faulting in comparison with the middle Jurassic and the base Cretaceous reflections. All the faults are displacing this reflection towards the North, hence are termed as synthetic faults. Such faults are represented by the faults F1, F11 & F12 in this profile *(Fig. 3.13 a,b).* Majority of the faults ranging from the faults F2 – F12 are present at the intra Jurassic and the base Cretaceous reflections *(Fig. 3.13a).* Faults present in the proximity of the master fault MF2, such as F2, F3, F4 & F5 are dipping towards the North, hence, termed as the synthetic faults. Farther into the basin, faults at the intra Jurassic and the base Cretaceous reflections are both synthetic and antithetic in nature, with faults F8, F9 & F10 representing the later type *(Fig. 3.13a).* The early Cretaceous reflection is the least disturbed among all the interpreted reflections present in the Hammerfest Basin while the base Tertiary reflection shows minor planar normal faults dipping towards the North *(Fig. 3.13a).*

Unlike the previously described cross-sections, frequency of faulting on the Finnmark Platform is substantially amplified *(Fig. 3.13 a).* Both the intra Permian and the intra Triassic reflections are disturbed by planar normal faults. Majority of these faults represent the northern dip-slip such as the faults f1, f2, f3, f5 & f6, hence, they are termed as the synthetic faults *(Fig. 3.13a,b).* However, fault f4 is an exception with southward dip (antithetic fault) and together with the fault f5; it constitutes a graben feature in the SSE part of this profile *(Fig. 3.13a).*

Recognition of the growth strata between the middle Jurassic and the base Cretaceous reflections is quite unambiguous. The wedge shaped geometry of the strata between these interpreted reflections gives clue about the activity along the main boundary fault MF2 during this period *(Fig. 3.13a,b).*

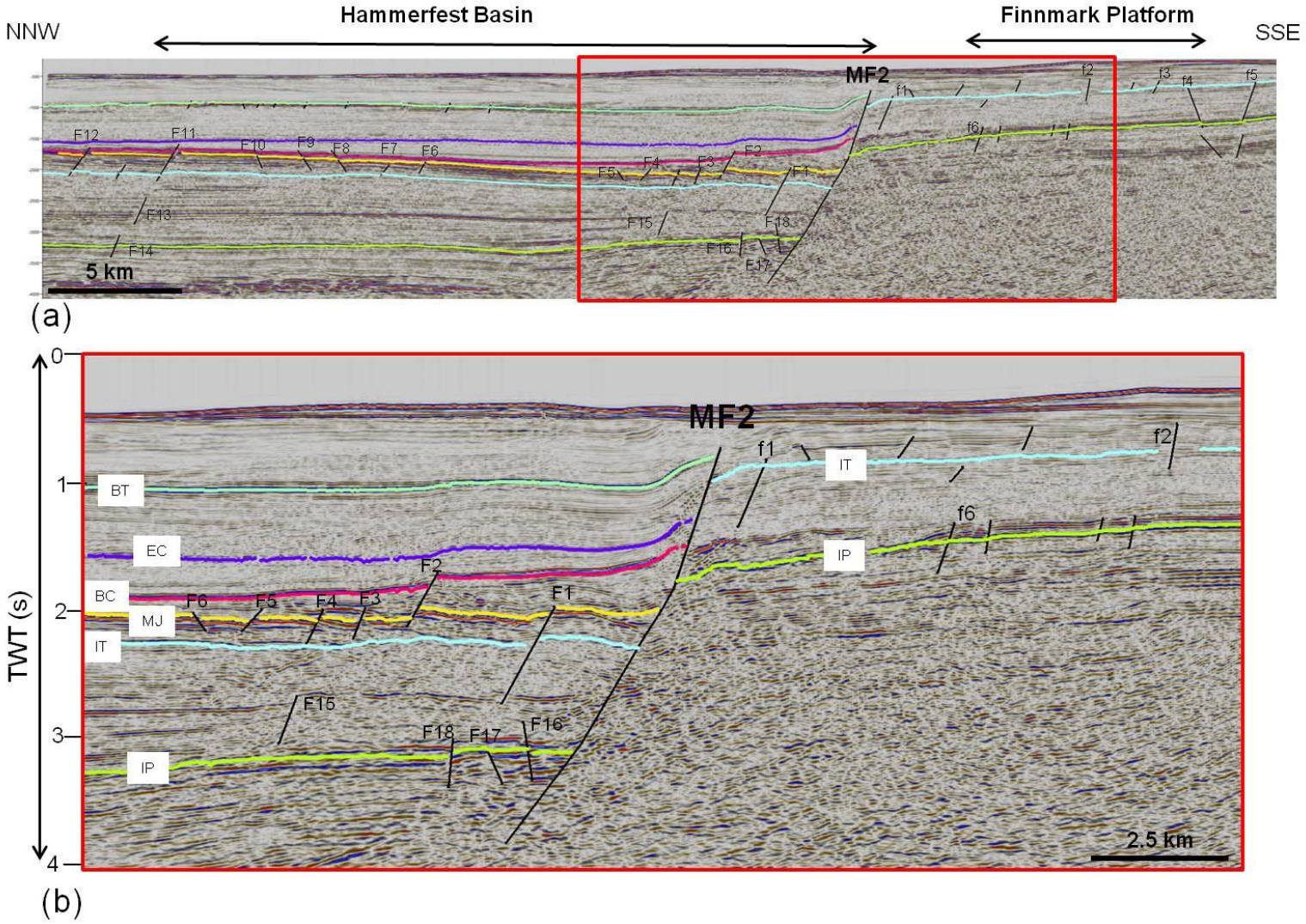

Figure 3.13 a: Key Profile 4 along fault segment MF2. **(b)** Zoomed-in part of (a) shown by red square. See Figs. 3.8 & 3.9 for location of the line. BT: Base Tertirary, EC: Early Cretaceous, BC: Base Cretaceous, MJ: Middle Jurassic, IT: Intra Triassic, IP: Intra Permian.

3.6.5 Key Profile 5

This dip line belongs to the eastern margin of the fault segment MF2 and is oriented NW-SE *(Fig. 3.8).* The master fault MF2 at this location is showing an ENE-WNW trend and the master fault MF3 is trending in NE-SW direction *(Fig. 3.9).*This profile is covering considerable part of the Finnmark Platform in the SE and it expands to the central part of the Hammerfest Basin in the NW *(Fig. 3.8)* while the master faults MF2 and MF3 are separating the two areas *(Fig. 3.9).* The middle Jurassic, the base Cretaceous, the early Cretaceous and the base Tertiary reflections are interpreted within the Hammerfest Basin only while the intra Permian and the intra Triassic reflections are interpreted both over the platform and in the basin *(Fig. 3.14 a,b).* At the Finnmark Platform, stratigraphic sequences from the lower Jurassic to the Tertiary are missing and the Quaternary sedimentation directly overlies the Triassic sequence *(Fig. 3.7).* Interpreted reflections on the platform show a northward tilt towards the master fault MF3 which is displaced at places by faulting. Similarly, in the basin all interpreted reflections show a gentle northward tilt away from the master faults MF3 & MF2 *(Fig. 3.14 a,b).*

The master fault MF2 is a planar normal fault separating the footwall block of the master fault MF3 from the Hammerfest Basin *(Fig. 3.14 a, b).* It cuts the stratigraphic succession between the intra Triassic up to the early Cretaceous *(Fig 3.14 b),* with no ample evidence of this master fault cutting the intra Permian reflection and hence not a basement involved fault therefore it is termed as the ***Third-Class*** fault (*sensu* Gabrielsen, 1984). Vertical separation across the fault MF2 can only be assessed at the interpreted intra Triassic and the middle Jurassic reflections, which are approximately 0.5 s (twt) and 0.4 s (twt) respectively *(Fig. 3.14b).* The master fault MF3 cuts the stratigraphic interval from the base Tertiary to the sub-Permian level and is probably rooted in the basement, therefore, it is termed as the ***First-Class*** fault (*sensu* Gabrielsen, 1984). Vertical separation across this fault can be calculated at the intra Permian and the intra Triassic reflections which are approximately 0.6 s (twt) and 0.4 s (twt) respectively *(Fig. 3.14b).* A relay ramp between the two master faults MF2 & MF3 can be observed which has developed northward dipping planar normal faults F23, F24 & F25 *(Fig. 3.14b).* Presence of the faults within this relay zone reflects that the master fault segments MF2 & MF3 are the soft-linked faults of a larger fault array *(Fig. 3.9 & Fig. 3.14 a, b).* In the Hammerfest Basin, frequency of faulting varies from bottom to the top interpreted stratigraphic intervals. Although faulting within the basin is ubiquitous however, upon closer

observation it can be seen that faults are predominantly focused in two zones of the basin i.e., in the close vicinity of the master fault MF2 and farther into the basin where a broad symmetrical graben is observed *(Fig. 3.14 a, b).* The intra Permian reflection is affected by planar normal faults in the same way as the younger interpreted reflections. Faulting is concentrated in the close vicinity of the master fault MF2, with synthetic faults F22, F23 & F24 showing a northward dip, while further towards the NW into the basin, opposite verging faults F19 & F24 make a broad graben at the intra Permian level *(Fig. 3.14 a).* Majority of faults ranging from the faults F1 – F13 are present at the interpreted intra Triassic, the intra Jurassic and the base Cretaceous reflections *(Fig. 3.14 a, b).* All of the faults present at these intervals are planar normal faults dipping towards the North, hence are termed as synthetic faults with the exception of faults F7 & F9 which dip towards south, hence they are termed as the antithetic faults *(Fig. 3.14 a).* The faults F6 & F9 constitute a broad symmetrical graben at the level of the intra Triassic to the base Cretaceous reflections which becomes narrower to the deeper interpreted stratigraphic interval. This broad graben is internally deformed with the presence of both synthetic and the antithetic planar normal faults such as the faults F10, F11, F12, F13 & F20 *(Fig. 3.14 a).* The early Cretaceous reflection is also less disturbed; however, its thickness is controlled by the older faults that have evolved prior to deposition of this interval *(Fig. 3.14 a, b).* The base Tertiary reflection shows minor planar normal faults dipping towards the North *(Fig. 3.14 a).* Similar to the key profile 4, frequency of faulting on the Finnmark Platform is considerably enhanced *(Fig. 3.14 a, b).* Both the intra Permian and the intra Triassic reflections are disturbed by the planar normal faults which include both synthetic and antithetic faults. Synthetic faults on the platform include the faults f1- f3, f7, f9 - f10 while antithetic faults displacing intra Triassic and intra Permian reflections down to the south include the faults f4, f5 & f6 *(Fig. 3.14 a,b).*

A rollover anticline associated with the master fault MF2 is recognized with the faulted crest *(Fig. 3.14 a,b).* The signature of roll-over anticline is clear on the interpreted reflections ranging from the base Cretaceous down to the intra Permian. Faults at the crest of this anticline might have generated to accommodate the effect of continued stretching even after the development of the roll-over geometry *(Fig. 3.14 a, b).* Recognition of the growth strata between the middle Jurassic and the early Cretaceous reflections is quite distinctive. The wedge shaped geometry of the strata between these interpreted reflections gives hint about the activity along the main boundary fault MF2 during this period *(Fig. 3.13a, b).*

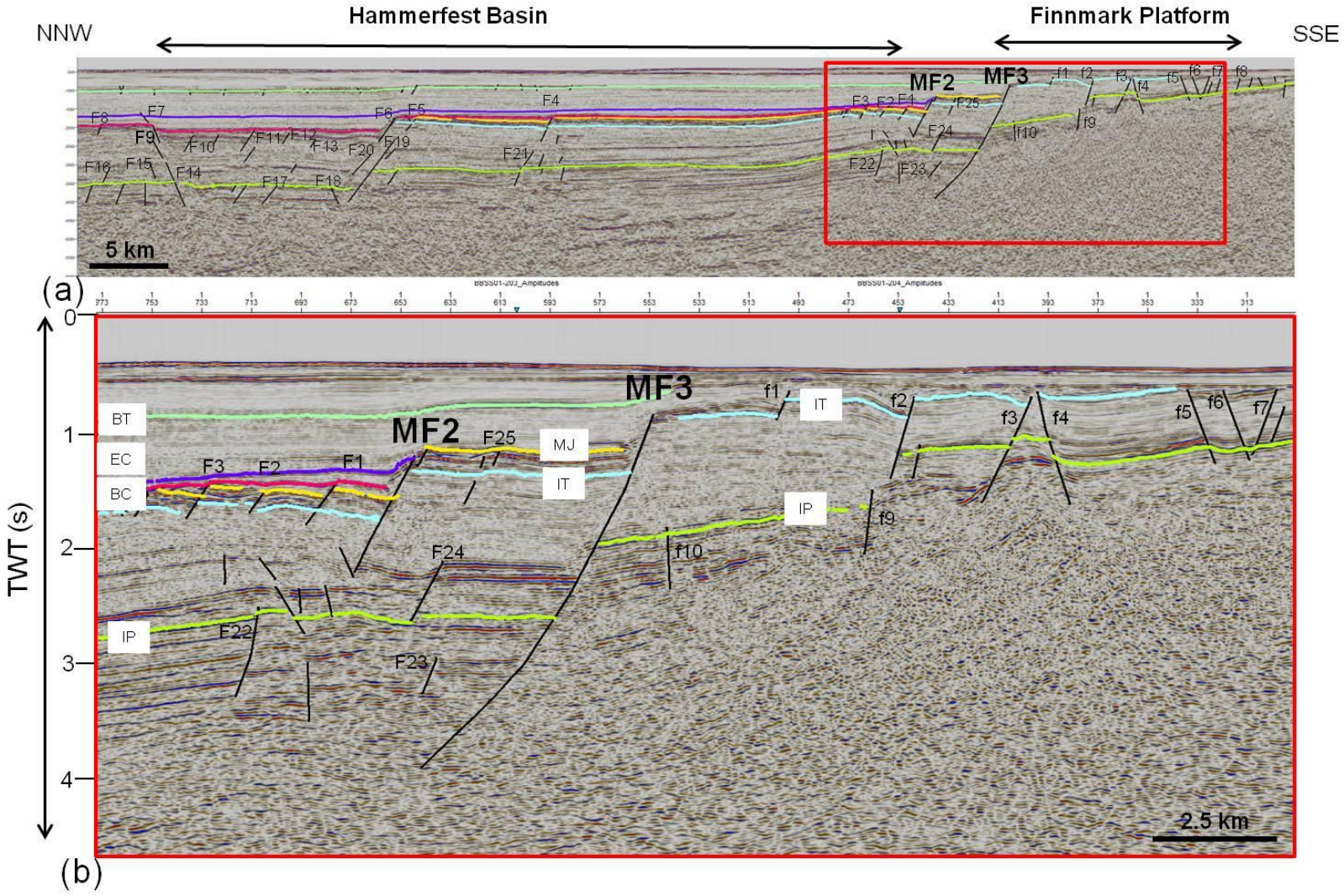

Figure 3.14 a: Key Profile 5 along the fault segments MF2 & MF3. **(b)** Zoomed-in part of (a) shown by red square. See Figs. 3.8 & 3.9 for location of the line. BT: Base Tertiary, EC: Early Cretaceous, BC: Base Cretaceous, MJ: Middle Jurassic, IT: Intra Triassic, IP: Intra Permian.

3.6.6 Key Profile 6

This dip line belongs to the southwestern part of the fault segment MF3 and is oriented NW-SE *(Fig. 3.8 & Fig. 3.9).* The master fault MF3 at this location is showing a NE-SW trend *(Fig. 3.9)*. This profile covers approximately equal areas of the Finnmark Platform in the SE and the Hammerfest Basin towards NW across the master fault MF3 *(Fig. 3.9).* The interpreted reflections ranging from the base Tertiary down to the middle Jurassic reflections are absent on the Finnmark Platform, hence they are interpreted within the Hammerfest Basin only while the intra-Permian and the intra Triassic reflections are interpreted both over the platform and in the basin *(Fig. 3.15).* At the Finnmark Platform, stratigraphic sequences from the early Jurassic to the Tertiary are missing and the Quaternary deposits directly overlie the Triassic succession *(Fig. 3.7).* The interpreted reflections on the platform show a northward tilt towards the master fault MF3 which is displaced at places by faulting. Similarly, in the basin all interpreted reflections show a gentle northward tilt away from master fault MF3 *(Fig. 3.15).*

The master fault MF3 is a listric normal fault dipping towards the North which cuts interpreted reflections from the base Tertiary down to the intra Permian and continues further down-section into the basement (?) therefore it is termed as the ***First-Class*** Fault (*sensu* Gabrielsen, 1984). Vertical separation across this fault can be calculated at the intra Permian and the intra Triassic reflections which are approximately 0.5 s (twt) and 0.6 s (twt) respectively (*Fig. 3.15).* Master fault MF3 is associated with the reverse drag, clearly visible at base Cretaceous, intra Jurassic and intra Triassic reflections; however drag associated with deeper stratigraphic intervals than the intra Triassic show development of normal drag *(Fig. 3.15).*

In the Hammerfest Basin, majority of the faults are concentrated upon the crest of the roll-over anticline *(Fig.3.1).* The interpreted intra Permian reflection is less affected by faulting however, the planar normal faults F7 & F8 show southward and northward dip respectively at this level, hence, they are termed as antithetic and synthetic normal faults accordingly *(Fig. 3.15).* The interpreted reflections that have been involved in the folding process due to fault activation have developed extensive faulting and they include the intra Triassic, the middle Jurassic and the base Cretaceous reflections. Normal synthetic and antithetic faults to the master fault MF3 are observed with moderate throws at the level of these interpreted reflections, where faults F1 & F2 are dipping towards south while faults F3– F6 show a

northward dip *(Fig. 3.15).* The faults F2 & F3 are opposite verging normal faults which together make a small horst block between them *(Fig. 3.15).* The middle Jurassic and the base Cretaceous reflections are rotated along the faults F3 & F5 *(Fig. 3.15).* Similarly, the early Cretaceous and the base Tertiary reflections are less disturbed by faulting however, thickness of the early Cretaceous reflection is controlled by the underlying faults *(Fig. 3.15).*

Frequency of faulting on the Finnmark Platform increases towards SSE of this cross-section *(Fig. 3.15).* Both the intra Permian and intra Triassic reflections are disturbed by the synthetic and antithetic planar normal faults. A synthetic fault f1 on the platform shows a moderate throw and has displaced the intra Permian reflection down towards the North *(Fig. 3.15).* A roll-over anticline associated with the master fault MF3 is recognized with intensely faulted crestal portion *(Fig. 3.15).* The signature of the roll-over feature is clear on the interpreted reflections ranging from the base Cretaceous down to the intra Triassic level. Synthetic and antithetic faults at the crest of this anticline have developed to accommodate the effect of continued stretching even after the development of the roll-over anticline, besides, antithetic faults F1 & F2 tend to decrease the impact of the reverse drag by balancing the movement in the opposite direction as that of the master fault MF3 *(Fig. 3.15).*

Recognition of the growth strata between the base Cretaceous and the early Cretaceous reflections is quite distinctive. This wedge-shaped geometry of strata grows in thickness towards the master fault MF3. Its thickness decreases above the crest of the roll-over anticline and increases again towards NNW. Fault-dating is carried out using this method and it is interpreted that the master fault MF3 experienced activity during late Jurassic to early Cretaceous period *(Fig. 3.15).*

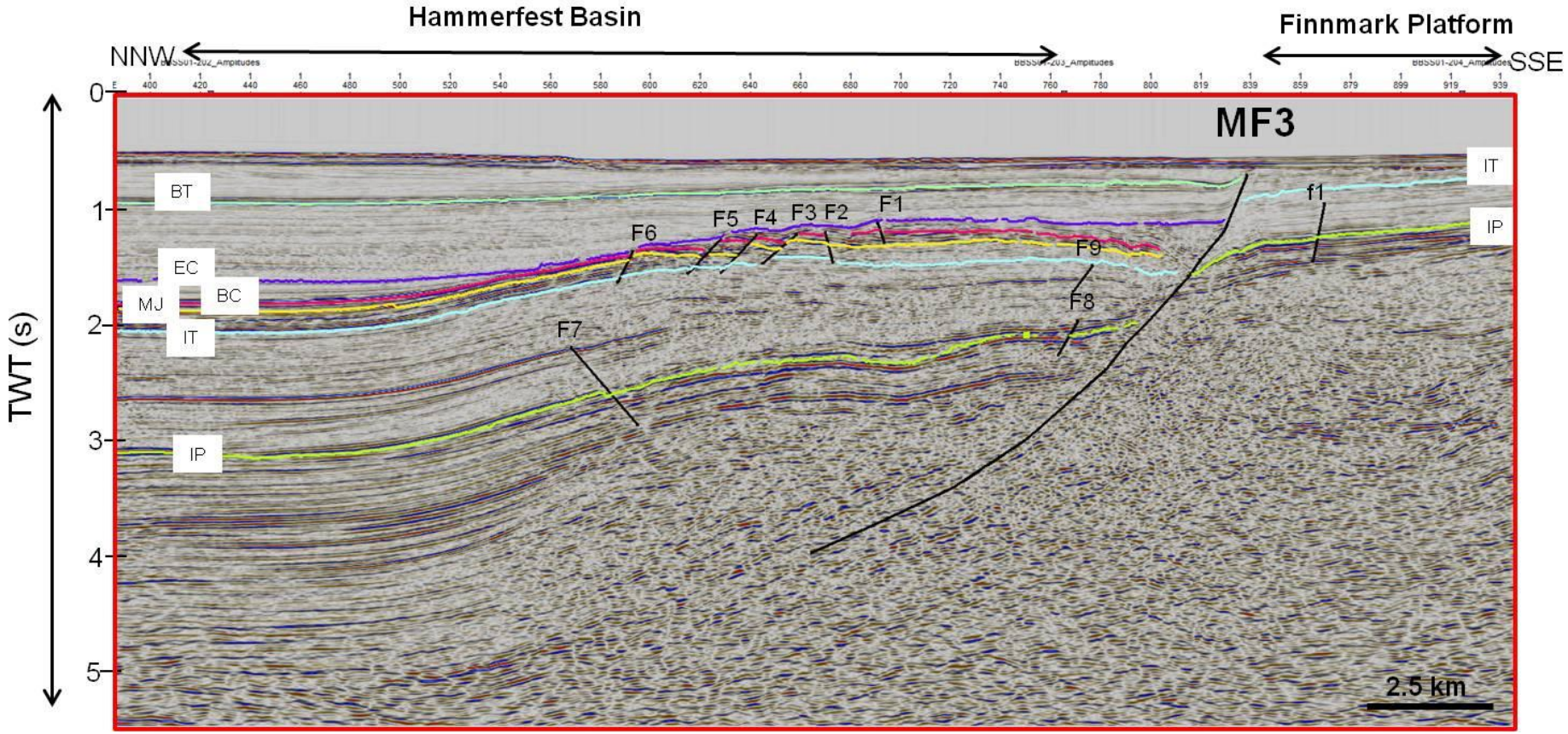

Figure 3.15: Key Profile 6 along fault segment MF3. See Fig 3.8 & 3.9 for location of the line. BT: Base Tertiary, EC: Early Cretaceous, BC: Base Cretaceous, MJ: Middle Jurassic, IT: Intra Triassic, IP: Intra Permian.

3.6.7 Key Profile 7

This dip line belongs to the central part of the fault segment MF3 and is oriented NW-SE *(Figs. 3.8 & Fig. 3.9).* The main boundary fault MF3 at this location is showing a NE-SW trend *(Fig. 3.9).* This cross-section covers parts of the Finnmark Platform in the SE and the Hammerfest Basin towards NW across the master fault MF3 *(Fig. 3.9).* Interpreted reflections from the middle Jurassic up to the base Tertiary are absent on the Finnmark Platform, hence they are interpreted within the Hammerfest Basin only while the intra Permian and the intra Triassic reflections are interpreted both over the platform and in the basin *(Fig. 3.16 a, b).* At the Finnmark Platform, stratigraphic sequences from the lower Jurassic to the Tertiary are missing and the Quaternary sequence directly overlies the Triassic stratigraphy *(Fig. 3.7).* Interpreted reflections on the platform show a northward tilt towards the master fault MF3 which is displaced at places by faulting. Similarly, in the basin all interpreted reflections show a gentle northward tilt away from master fault MF3 *(Fig. 3.16 a).*

Master fault MF3 is a listric normal fault dipping towards the North which cuts interpreted reflections from the early Cretaceous to the intra Permian and continues further downward into the basement (?); therefore it is termed as the ***First-Class*** fault (*sensu* Gabrielsen, 1984). Vertical separation across this fault can be calculated at the intra Permian and the intra Triassic reflections alone as these are the only reflections present in both the areas. At the intra Permian level vertical throw of the master fault MF3 is approximately 1.2 s (twt) while at the intra Triassic level it is calculated to be approximately 0.8 s (twt) *(Fig. 3.16 a,b).*

The Hammerfest Basin in this profile is intensely deformed by a variety of North & South dipping planar normal faults. The interpreted intra Permian to the base Cretaceous reflections show a concentration of faults between them while most of the deformation is focused at the intra Triassic to the base Cretaceous levels strictly *(Fig. 3.16 a,b).* The intra Permian reflection is affected by planar normal faults but the intensity of faulting at this level is less as compared to the interval between the intra Triassic and the base Cretaceous reflections. The effect of reverse drag is quite obvious at the intra Permian level and the broad graben present at the younger interpreted reflections become narrower down to this reflection which is represented by the faults F10 & F11. An antithetic fault F12 is present at the crest of roll-over at the intra Permian level while another synthetic fault F11 is found farther into the basin *(Fig. 3.16 b).* The strata between the intra Permian and the intra Triassic reflections is also affected by synthetic and antithetic normal faults, represented by the faults F9, F13, F14 &

F15 *(Fig. 3.16 b).* Additionally, these planar normal faults are characterized by minor throws as compared to the faults at the younger interpreted reflections in this cross-section *(Fig. 3.16 a).* Majority of deformation associated with faulting in the Hammerfest Basin is centered in the interpreted reflections between the intra Triassic at the bottom through the middle Jurassic and the base Cretaceous at the top. Crest of the roll-over anticline is the most deformed sub-area in this cross-section *(Fig. 3.16 a).* This intensely faulted sub-area exhibits both northward and southward dipping planar normal faults with moderate throws. The faults F1, F2, F3 show dip-slip towards the North and hence are termed as synthetic faults with reference to the master fault MF3. Similarly, the faults F4 & F5 represent the dip-slip component towards the South and are called the antithetic faults in relation to the MF3 *(Fig. 3.16 b).* Towards the NW away from the roll-over anticline, a series of down-to-the-North faults, followed by down-to-the-South faults are interpreted, which together constitute a large graben. This large graben itself, however, is internally deformed by northward dipping planar normal faults *(Fig. 3.16 a).* A part of another broad graben is present at the extreme NW of this level where faults are dipping towards the North. The two grabens are separated by relatively stable horst sub-area between them showing no evidence of deformation *(Fig. 3.16 a).* The early Cretaceous reflection is least disturbed by faulting however its thickness is controlled by the underlying faults i.e., thicker above the down-faulted blocks and vice versa *(Fig. 3.16 a,b).* Similarly, the base Tertiary reflection is affected by minor North and South dipping normal faults *(Fig. 3.16 b).*

Frequency of faulting on the Finnmark Platform is focused on upper stratigraphic intervals including the intra Triassic reflection, however, the intra Permian reflection is also considerably faulted by North / South dipping normal faults *(Fig. 3.16 a).* A prominent fault on the Finnmark Platform with significant throw is represented by the interpreted fault PF, shown in the green circle. It is showing northward dip-slip component and hence termed as synthetic fault with reference to main boundary fault MF3 *(Fig. 3.16 a).* This fault is laterally correlatable towards the East and its throw increases eastward as well *(Fig. 3.9).* Combination of opposite verging normal faults at the intra Triassic and the intra Permian levels make small grabens on the platform which are represented by the faults f4, f5 and f6 respectively *(Fig. 3.16 b).*

A roll-over anticline associated with the master fault MF3 is recognized with intensely faulted crestal part *(Fig. 3.16 b).* The signature of roll-over anticline is clear on the interpreted reflections ranging from the base Cretaceous down to the intra Permian level.

Synthetic (faults F1, F2 & F3) and antithetic faults at the crest of this anticline have developed to accommodate the effect of continued stretching even after the development of roll-over geometry, besides, antithetic faults F4 & F5 tend to counter the impact of roll-over by balancing the movement in the opposite direction as that of the master fault MF3 *(Fig. 3.16 b).* An interesting observation regarding the drag is about the reversal of drag from the reverse at the intra Permian level to normal at the base Cretaceous and the intra Triassic levels. This could be attributed to the effect positive structural inversion as the roll-over anticline at the base Cretaceous to the intra Jurassic level is still recognizable but upon proximity of the master fault MF3, it changes into the normal drag which is thought to be associated with the reactivation of the master fault MF3 as an inverted feature *(Fig. 3.16 b).* This observation is in accordance with that of *(*Gabrielsen & Færseth, 1989*)* who proposed the effect of structural inversion in the northeastern segment of the Troms-Finnmark Fault Complex. The discussion regarding development of positive structural inversion in this area is dealt with in the next chapter.

Recognition of the growth strata between the base Cretaceous and the middle Jurassic reflections is quite distinctive. This wedge-shaped geometry of strata grows in thickness towards the master fault MF3 while its thickness decreases above the crest of the roll-over anticline *(Fig. 3.16 b).* Hence, fault-dating is possible using this technique and it is interpreted that the master fault MF3 experienced activity during the mid Jurassic to the early Cretaceous period, shortly followed by positive structural inversion *(Fig. 3.16 b).*

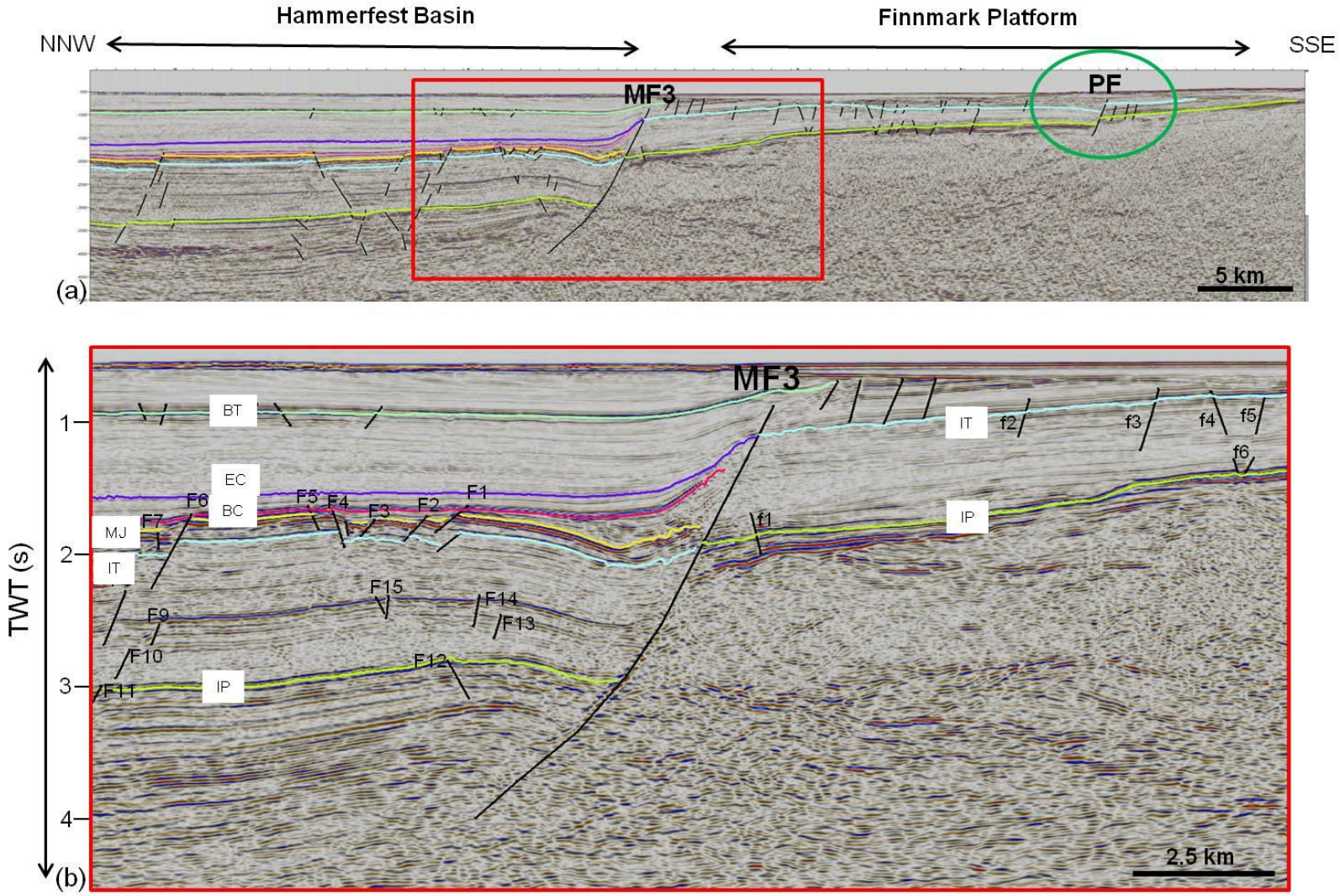

Figure 3.16 a: Key Profile 7 along fault segment MF2. **(b)** Zoomed-in part of (a) shown by red square. See Figs. 3.8 & 3.9 for location of the line. BT: Base Tertiary, EC: Early Cretaceous, BC: Base Cretaceous, MJ: Middle Jurassic, IT: Intra Triassic, IP: Intra Permian.

3.6.8 Key Profile 8

This dip line belongs to the north-eastern part of the fault segment MF3 and is oriented NW-SE *(Figs. 3.8 & Fig. 3.9).* The main boundary fault MF3 at this location is showing a NE-SW trend *(Fig. 3.9).* This profile covers parts of the Finnmark Platform in the SE and the Hammerfest Basin towards NW across the master fault MF3 *(Fig. 3.9).* The intra Permian and the intra Triassic reflections are interpreted both over the platform and in the basin while the middle Jurassic, the base Cretaceous, the early Cretaceous and the base Tertiary reflections are absent on the Finnmark Platform, hence they are interpreted within the Hammerfest Basin only *(Fig. 3.17 a,b).* At the Finnmark Platform, stratigraphic sequences from the lower Jurassic to the Tertiary are missing and the Quaternary sequence directly overlies the Triassic stratigraphy *(Fig. 3.7).* The interpreted reflections on the platform show a northward tilt towards the master fault MF3 which is displaced at places by faulting. Similarly, in the basin all interpreted reflections show a gentle northward tilt away from the master fault MF3 *(Fig. 3.17a).*

The master fault MF3 is a downward concave normal fault dipping towards the North which cuts interpreted reflections from the early Cretaceous to the intra Permian and continues further downward into the basement (?); therefore it is termed as ***First-Class*** fault (*sensu* Gabrielsen, 1984). Vertical separation across this fault calculated at the intra Permian and the intra Triassic reflections is approximately 0.6 s (twt) and 0.3 s (twt) respectively *(Fig. 3.17 b).*

Frequency of faulting in the Hammerfest Basin varies from bottom to top interpreted reflections. Basinal side is intensely deformed by a variety of north and south dipping planar normal faults *(Fig. 3.17 a).* The interpreted intra Permian reflection shows minimum disturbance due to faulting *(Fig. 3.17 a,b).* Most of the faulting is concentrated above the intra Permian reflection to as young as the base Cretaceous reflection *(Fig. 3.17 a,b).* The faults F7 – F14 are present below the interpreted intra Triassic reflection and they show both the northward and southward dips. The faults F7, F8, F9, F10 and F13 show a north dip and hence termed as synthetic while the faults F11, F12 show south dip and are called as antithetic faults *(Fig. 3.17 b).* The faults F1- F6 are present within the intra Triassic to the base Cretaceous reflections and demonstrate a northward dip, hence termed as synthetic faults with reference to the master fault MF3 *(Fig. 3.17 b).* Towards the NW away from the reactivated roll-over anticline, a series of down-to-the-North faults (F4, F5, F6, F7, F8 & F9)

are present, which altogether constitute a large half-graben that shows internal rotation of the interpreted intra Triassic to the base Cretaceous reflections. At the extreme NW part of this cross-section, planar normal faults with north dip are also present *(Fig. 3.17 a,b).* The early Cretaceous and the base Tertiary reflections are undisturbed by faulting in this profile. An important observation in this part of the study area is that all the reflections between the base Cretaceous and the intra Triassic are gently dipping towards the master fault MF3, however, younger than the base Cretaceous reflections are nearly horizontal or slightly tilted to the North *(Fig. 3.17 a, b).*

Frequency of faulting on the Finnmark Platform is focused on upper stratigraphic intervals including the intra Triassic reflection, however, the intra Permian reflection is also disturbed by the North & South dipping normal faults *(Fig. 3.17 a).* A prominent planar normal fault on the Finnmark Platform with significant throw is represented by the interpreted fault PF, shown in the green circle. It is showing north dip and hence termed as synthetic fault with reference to main boundary fault MF3 *(Fig. 3.17 a).* This fault is laterally correlatable towards the East and its throw increases eastward as well *(Fig. 3.9).* Majority of the faults found on the platform are synthetic to the master fault MF3 however south dipping planar normal faults represented by faults F2, F3, F4 are exception to this trend and are termed as antithetic faults *(Fig. 3.17 b).*

A reactivated roll-over anticline (drag-reversal) associated with the master fault MF3 is recognized with intensely faulted crest *(Fig. 3.17 b).* It is termed as reactivated roll-over feature because after development of the roll-over geometry associated with movement along the master fault MF3, reactivation of the master fault MF3 as positive inversion feature occurred, which transformed the apparent reverse drag to the normal drag. The possible mechanism for such an outcome is dealt with in the next chapter. Synthetic (faults F1, F2, F3 & F13) and antithetic faults (F11, F12 & F14) at the crest of this anticline have also been documented that are influencing the strata from the intra Triassic to the base Cretaceous reflections *(Fig. 3.17 b).*

Fault dating at this profile is not possible because of absence of any visible growth strata, however, based on the experience derived from description of the previous profiles, the master fault MF3 is assigned an age of the middle Jurassic to the early Cretaceous.

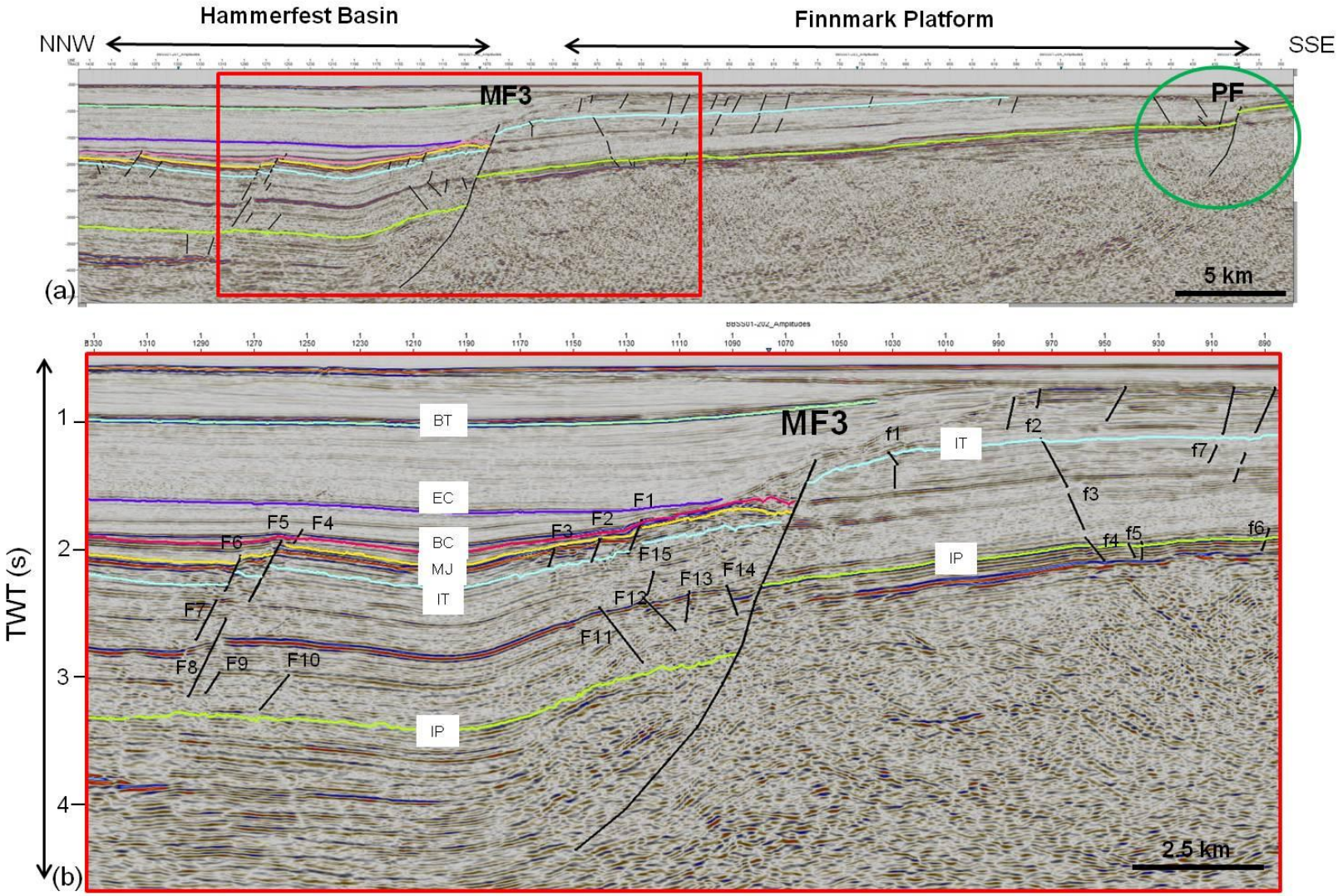

Figure 3.17 a: Key Profile 8 along the master fault segment MF3. **(b)** Zoomed-in part of (a) shown by red square. See Figs. 3.8 & 3.9 for location of the line. BT: Base Tertiary, EC: Early Cretaceous, BC: Base Cretaceous, MJ: Middle Jurassic, IT: Intra Triassic, IP: Intra Permian.

3.7 Time-Structure (twt) Maps and Fault Maps

This section primarily focuses on presenting and describing the time-structure maps and the fault maps, which together with the already described key cross-sections will enable to comprehend the fault segments MF1, MF2 & MF3 with progressively younger interpreted reflections. Change in structural architecture of the fault segments together with its associated features both within the Hammerfest Basin and the Finnmark Platform is described by making frequent cross-references to the already offered key profiles. Intra Permian time-structure map and fault plane maps have already been described in order to demarcate the structural segmentation of the study area *(Fig. 3.8 & Fig 3.9).* In this section, time-structure and fault maps derived at the intra Triassic, the middle Jurassic, the base Cretaceous, the early Cretaceous and the base Tertiary are described in a bottom-up approach.

3.7.1 Intra Triassic

The intra Triassic reflection is interpreted both on the Finnmark Platform and within the Hammerfest Basin hence this reflection is one of the two reflections that have been interpreted across the main boundary fault. The time-structure map on the Finnmark Platform shows general westward deepening of the reflection represented by color variation from shallow to the deep *(Fig. 3.18).* In the Hammerfest Basin, however, it shows a complex pattern of structural trends, central part of the basin is relatively shallow as compared to the areas immediately eastward and westward of the centre *(Fig. 3.18).* Displacement of the intra Triassic reflection across the master faults MF1, MF2 & MF3 is also not uniform, central parts of the master faults MF2 & MF3 show great vertical displacements as compared to their edges *(Fig. 3.18).*

The greatest vertical separation for this reflection is recorded by central part of the master fault MF2 shown by the key profile 3*(Fig. 3.12 a,b)* and the map shows huge contrast in color between the platform and the adjacent basinal area due to variation in time values *(Fig. 3.18).* Shape of the array of master faults MF1, MF2 & MF3 can precisely be viewed on this structure (twt) map and bears accordance with the trends of the master faults MF1, MF2 & MF3 as seen on the fault map of the same level *(Figs. 3.18 & Fig. 3.19).*

The fault map at the intra Triassic level shows fault interpretation both within the Hammerfest Basin and across the main boundary fault on to the Finnmark Platform *(Fig. 3.19).*

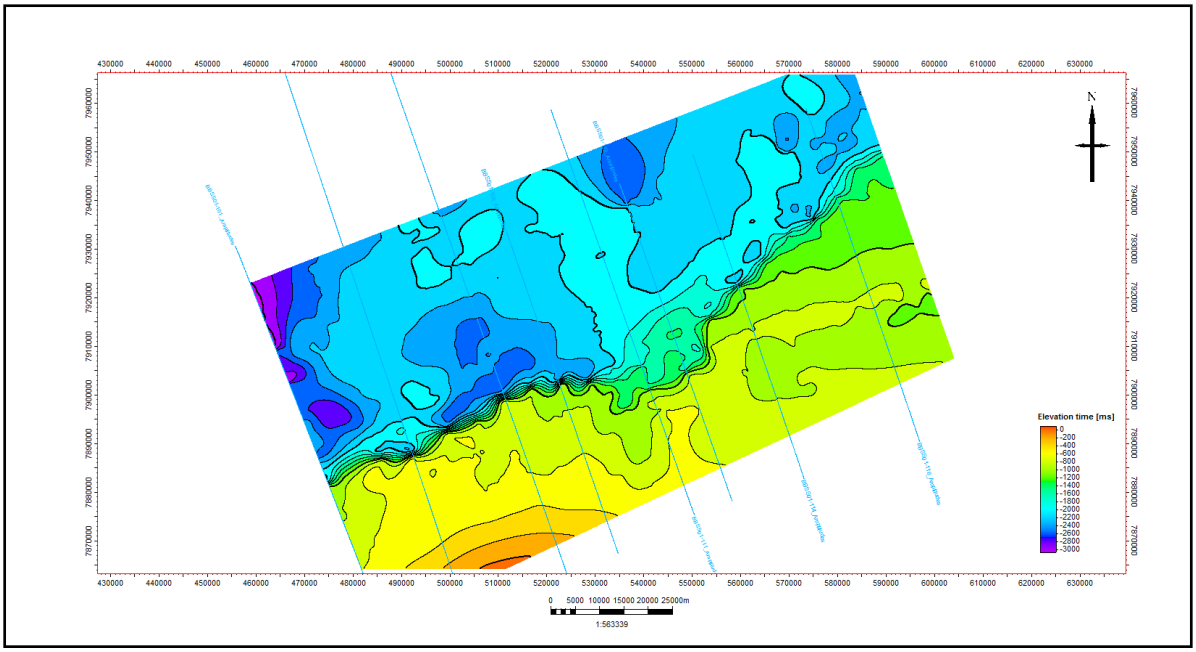

Figure 3.18: Time-structure map at the intra Triassic level. Location of the seismic lines already discussed as key profiles is also indicated.

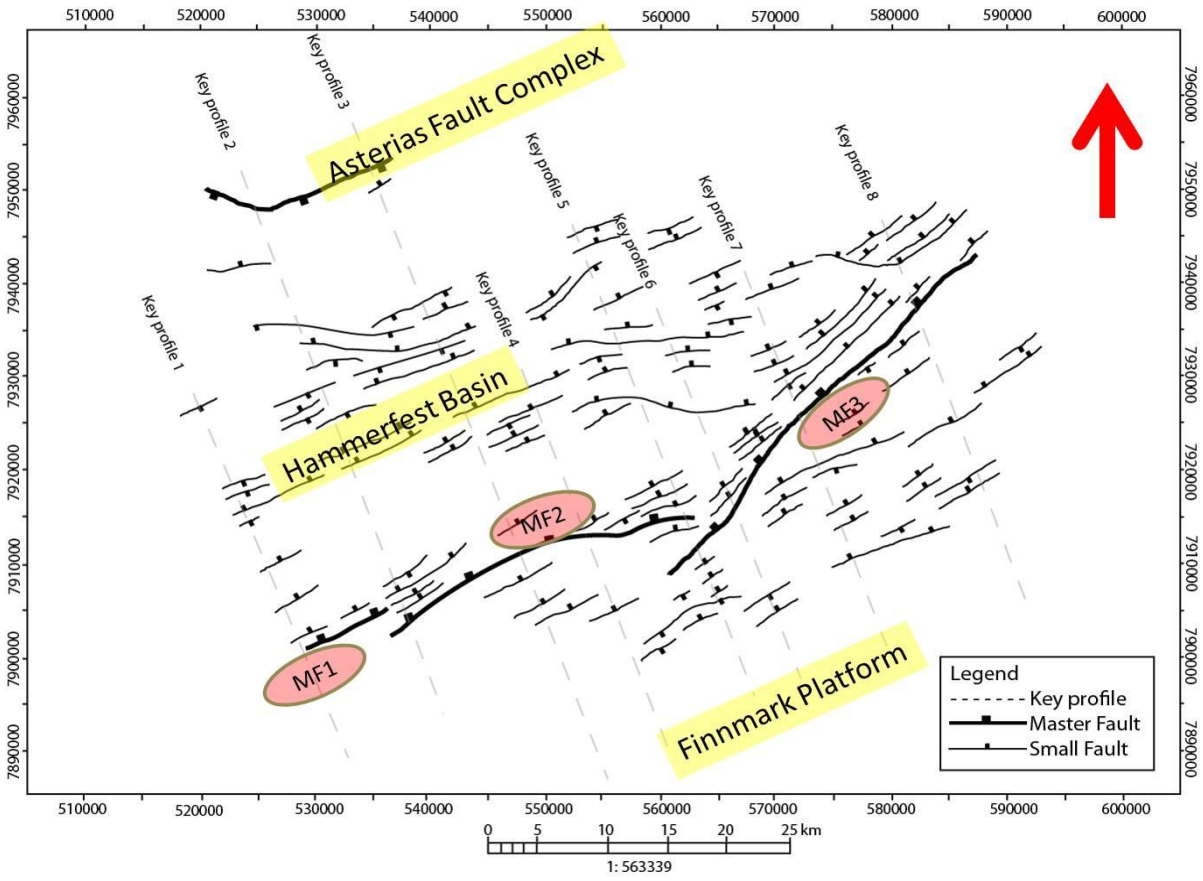

Figure 3.19: Fault map at the intra Triassic level with different segments of the master fault, grey dotted lines show location of the already discussed key profiles

An array of the master fault trending from NE-ENE-EW-NNE is present at this level as well. These isolated segments of master faults are termed as MF1, MF2 & MF3 *(Fig. 3.19).* These step-over faults are defined as softly-linked faults (following Trugdill & Cartwright, 1994), displacements along which are relayed across the next segment by means of ductile deformation, however, a small North-dipping normal fault is also interpreted between the fault segments MF2 & MF3 at key profile 5, which brings them together in communication. The master faults (MF1, MF2 & MF3) are dipping to the North while the small normal faults interpreted within the Hammerfest Basin show dip both towards the North and the South, hence are termed as the synthetic and the antithetic respectively, with reference to the northward dipping master faults *(Fig. 3.19).* Area of the Hammerfest Basin adjacent to the master fault MF3 is more deformed by the synthetic and antithetic normal faults, as compared to the basinal area adjacent to the master fault MF2 *(Fig. 3.19).* Normal faults within the Hammerfest basin predominantly show NE-SW trend however, faults with NW-SE trend are also found, such as two (2) laterally continuous faults at the key profile 6 and one (1) fault at the key profile 8 show north-westerly trend *(Fig. 3.19).* They are the same faults found at the middle Jurassic and the base Cretaceous levels as well. Small as well as large broad graben structures are found at the intra Triassic level (large features are those correlated on more than two seismic dip profiles) i.e., grabens found on key profiles 1, 2, 3, 5, 6 & 7 located in the middle part of the study area. The northern main boundary fault of the Hammerfest Basin, the Asterias Fault Complex, is also interpreted on the regional profiles that belong to North-Western part of the study area *(Fig. 3.19).* Small normal faults with northern and southern dip are associated with the Asterias Fault Complex and a large graben can also be seen which is trending in NW-SE direction close to the northern main boundary fault of the Hammerfest Basin *(Fig. 3.19).*

3.7.2 Middle Jurassic

The middle Jurassic reflection is interpreted only within the Hammerfest Basin due to its absence over the Finnmark Platform *(Fig. 3.7).* Hence, the map represents part of the study area where this stratigraphic interval is present *(Fig. 3.20).* The time-structure map shows bi-directional deepening of this reflection from the central part towards the East and the West respectively, which is evident by color coding i.e., green in the central part leads to shades of blue in both directions laterally away from the centre *(Fig. 3.20).*

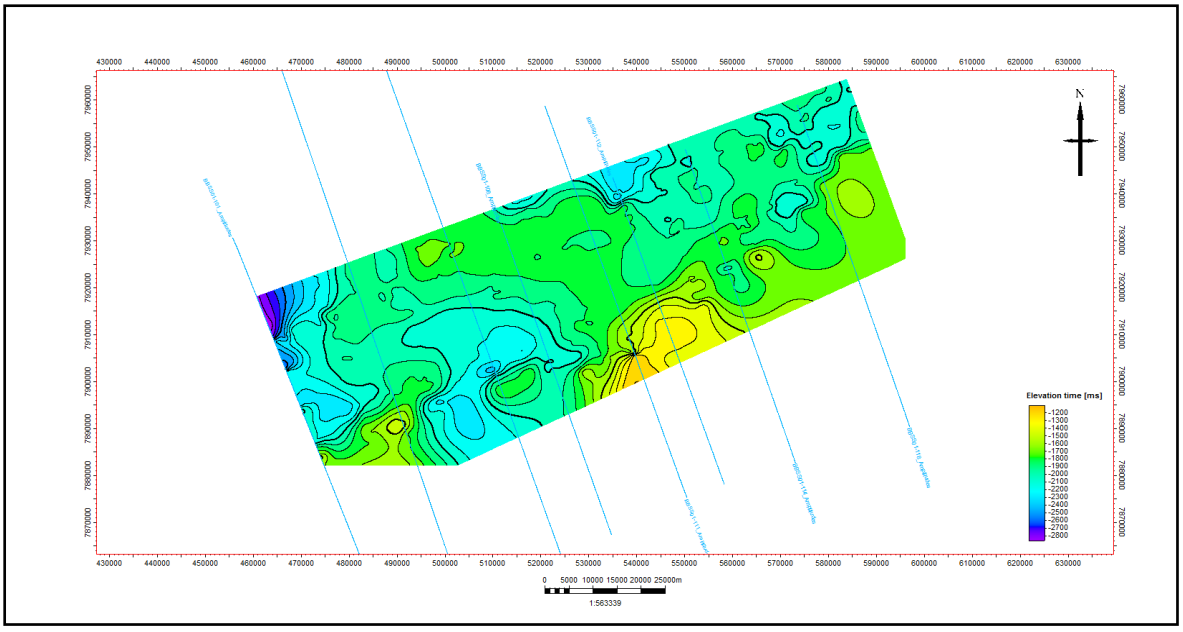

Figure 3.20: Time-structure map at the middle Jurassic level. Location of seismic lines already discussed as key profiles is also indicated.

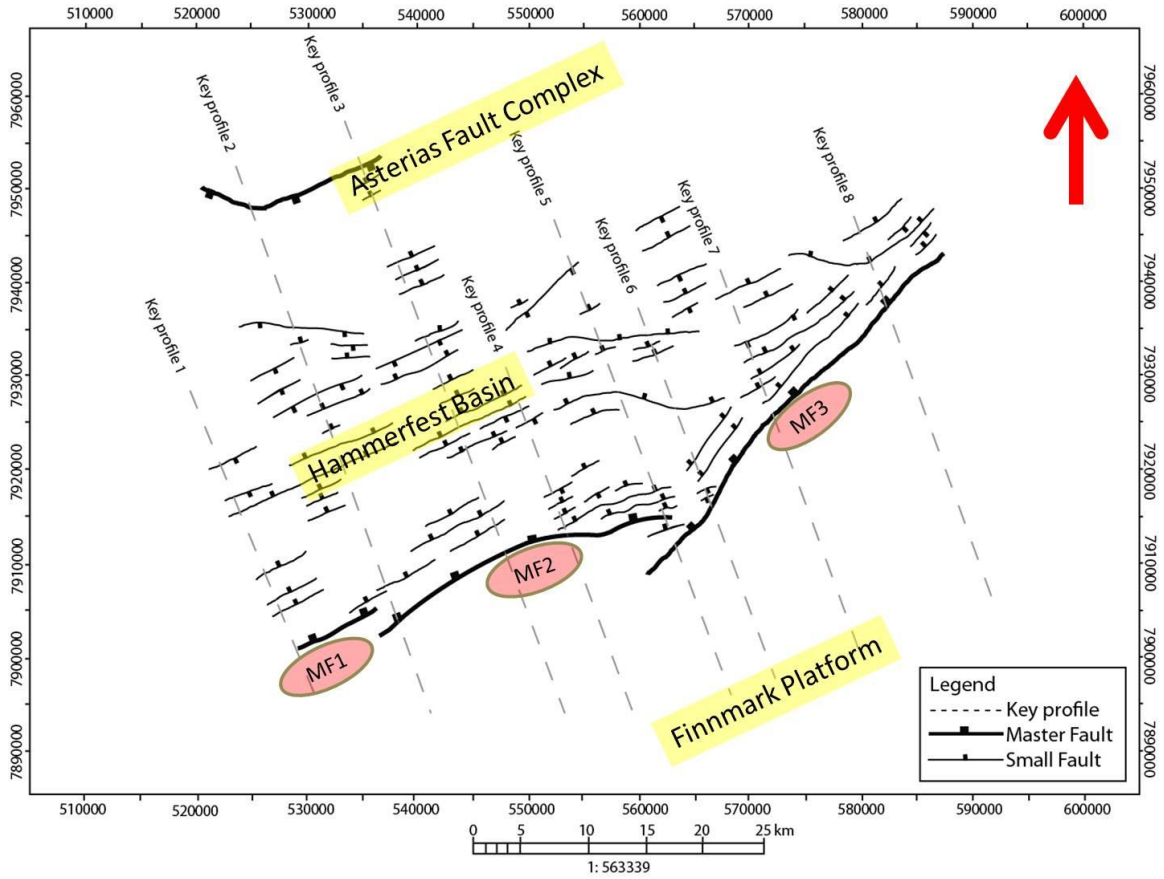

Figure 3.21: Fault Plane Map at the middle Jurassic level with different segments of master fault, grey dotted lines show location of already discussed key profiles.

Shape of the array of master faults MF1, MF2 & MF3 can loosely be traced on this map as well; however, segment MF2 is masked towards the SE *(Fig. 3.20).* Although, the middle Jurassic reflection is completely absent on the Finnmark Platform *(Fig. 3.7),* however the contouring algorithm of "Petrel 2011" does not assume zero value abruptly and in the process to make smooth contours, it extrapolated certain time value on the platform which makes it appear as if this reflection is present over the platform *(Fig. 3.20).* This is a software glitch which ought to be taken under consideration while looking at these maps.

The middle Jurassic fault map shows that the intensity of faulting increases in the Hammerfest Basin as compared to the intra Triassic fault map *(Fig. 3.19 & Fig. 3.21).* Increase in the faulting activity is supplemented by the presence of syn-sedimentary strata over this reflection in the cross-sections already discussed *(Fig. 3.11, Fig. 3.12 & Fig. 3.13 etc).* This implies that the study area was an active tectonic region during this time period *(Fig. 3.21).* An array of the master faults trending in NE-ENE-EW-NNE is seen, and the each isolated segments is termed as a separate master fault segment such as MF1, MF2 & MF3 *(Fig. 3.21).* These master faults separate the Hammerfest Basin in the North from the Finnmark Platform towards the South. They form a step-over geometry and are defined here as soft-linked faults (following Trugdill & Cartwright, 1994). Displacements along which are relayed across the next segment by means of ductile deformation; however, a small north-dipping normal fault can also be seen between MF2 & MF3 at key profile 5, which brings the two together in communication *(Fig. 3.21).* Master faults (MF1, MF2 & MF3) are dipping to the North while the small normal faults interpreted within the Hammerfest Basin show dip both towards the North and the South, hence are termed as synthetic and antithetic respectively, with reference to the northward dipping master faults *(Fig. 3.21).* Normal faults within the Hammerfest basin predominantly show NE-SW trend, however, faults with NW-SE trend are also not uncommon, such as two (2) laterally continuous faults at the location of key profile 6 and one (1) fault each at the location of key profiles 2 & 8 show north-westerly trend *(Fig. 3.21).*

Large graben structures are found to be associated at the mid Jurassic level (large features are those identified on more than two seismic dip profiles) i.e., grabens found on key profiles 1, 2, 3, 5, 6 & 7 in the middle part of the study area. The northern main boundary fault of the Hammerfest Basin, the Asterias Fault Complex is also interpreted on the regional profiles that belong to the north-western part of the study area *(Fig. 3.21).*

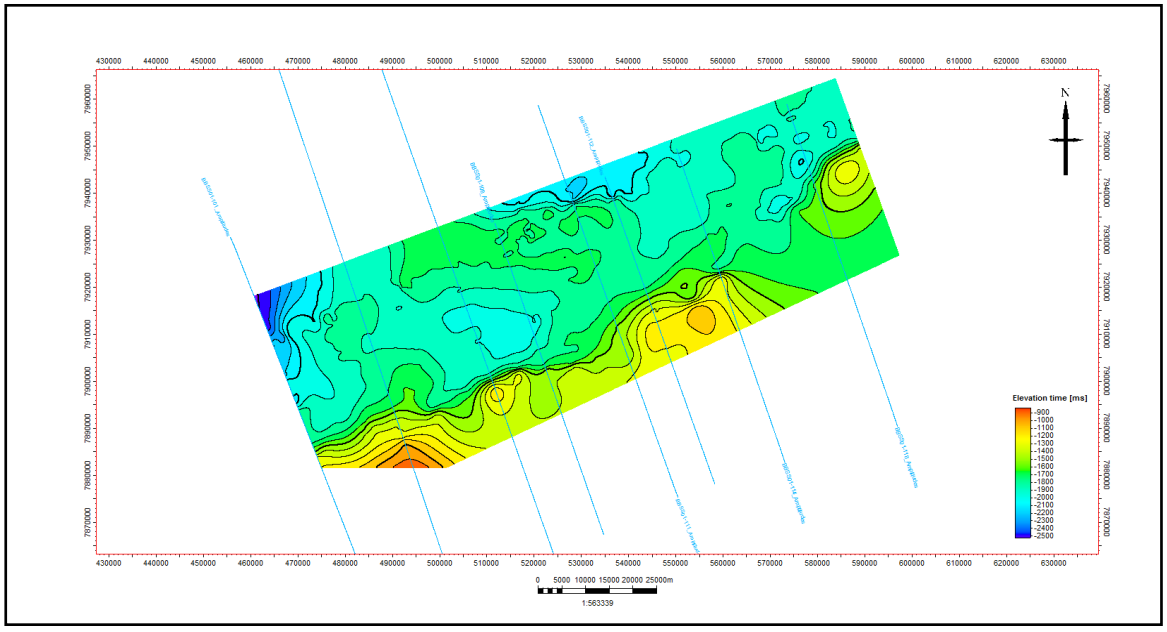

Figure 3.22: Time-structure map at the base Cretaceous level. Location of seismic lines already discussed as key profiles is also indicated.

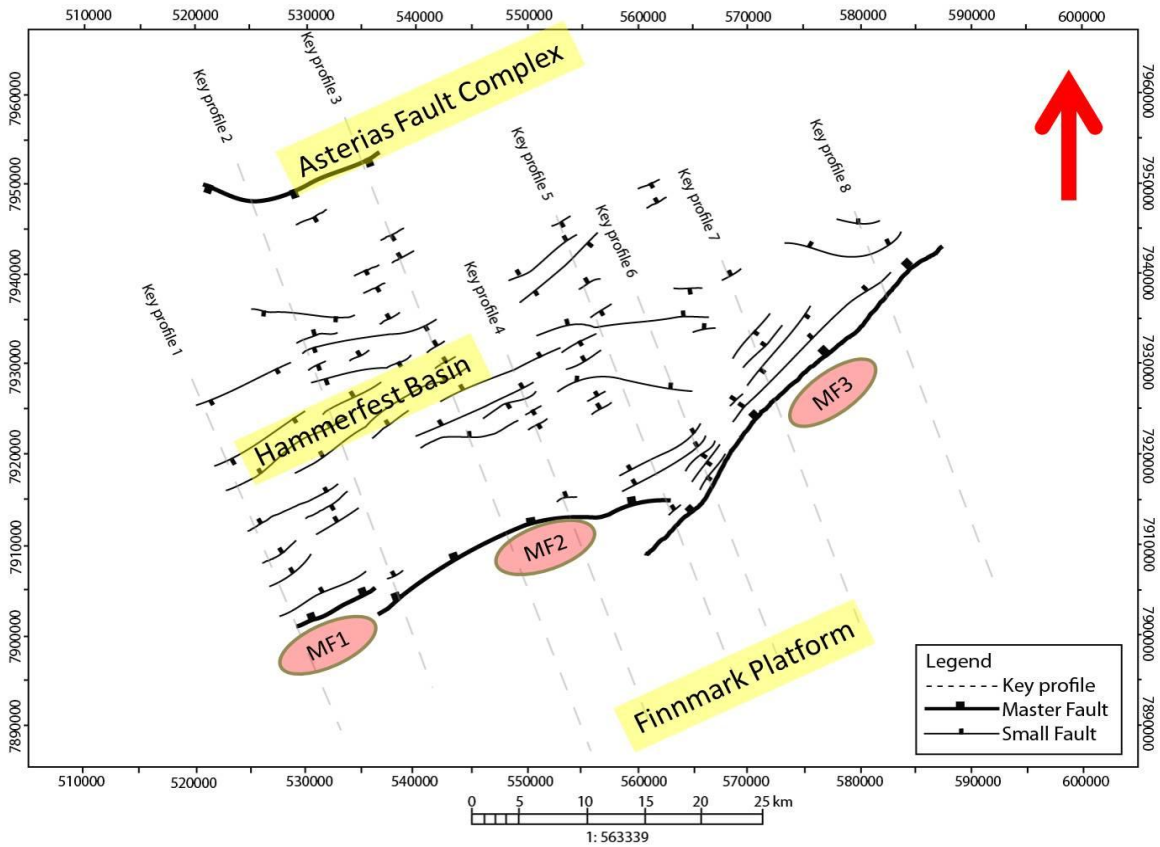

Figure 3.23: Fault Plane Map at the base Cretaceous level with different segments of the master fault, grey dotted lines show location of already discussed key profiles.

Small normal faults with northern and southern dip are associated with the Asterias Fault Complex and small normal faults in its proximity usually follow the same structural trend as those of other faults of the Hammerfest Basin i.e., NE-SW trend *(Fig. 3.21).*

3.7.3 Base Cretaceous

The interpreted base Cretaceous reflection is present only within the Hammerfest Basin as it is absent on the Finnmark Platform *(Fig. 3.7).* Hence, the generated time-structure map shows the structural architecture of only the basinal part of the study area at the base Cretaceous level *(Fig. 3.22).* The time-structure map shows deepening of this reflection on both sides of the central part of the basin i.e., central part of the study area represents the uplifted region (shown in green color in centre) for this reflection while it deepens towards the East and the West (shown in blue color) of this area *(Fig. 3.22).* The shape of the array of master faults MF1, MF2 & MF3 against which this reflection abuts in the seismic profiles can also be loosely traced in the time map *(Fig. 3.13, Fig. 3.14 etc).* The deepest area is located towards NW of the study area shown by dark blue to purple color indicating greater time values *(Fig. 3.22).*

The fault map at the base Cretaceous level reveals that intensity of faulting is less as compared to the similar maps at the intra Triassic and the intra Jurassic levels *(Fig. 3.19, Fig. 3.21 & Fig. 3.23).* This reflection marks the top of growth strata in the cross-sections thereby revealing that it is the time of tectonic activity in the study area *(Fig. 3.11, Fig. 3.12 etc).* An array of the master faults trending from NE-ENE-EW-NNE is present at this level as well. These isolated segments of the master fault are termed as MF1, MF2 & MF3 *(Fig. 3.23).* They together constitute a step-over geometry in which isolated segments are defined as softly-linked faults (following Trugdill & Cartwright, 1994) *(Fig. 3.23).* The displacement along such softly-linked faults is relayed across the next segment by means of ductile deformation, however, a small north-dipping normal fault can also be seen between MF2 & MF3 at the location of key profile 6 (shown as dotted line), which brings them together in communication. The master faults (MF1, MF2 & MF3) are dipping to the North while the small normal faults interpreted within the Hammerfest Basin show dip both towards the North and the South, hence are termed as the synthetic and the antithetic respectively, with reference to the northward dipping master faults *(Fig. 3.23).* Part of the Hammerfest Basin located in proximity of master fault MF3 shows plenty of synthetic and antithetic faults

whereas, such fault activity is uncommon in the close proximity of the master fault MF2 *(Fig. 3.23).*

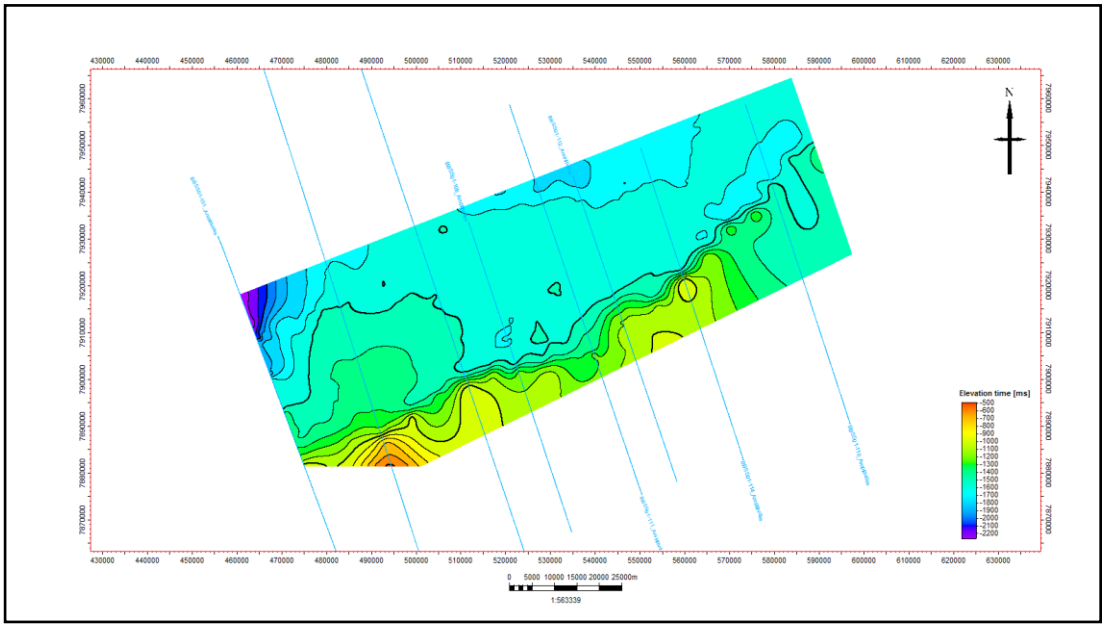

Figure 3.24: Time-structure map at the early Cretaceous level. Location of seismic lines already discussed as key profiles is also indicated.

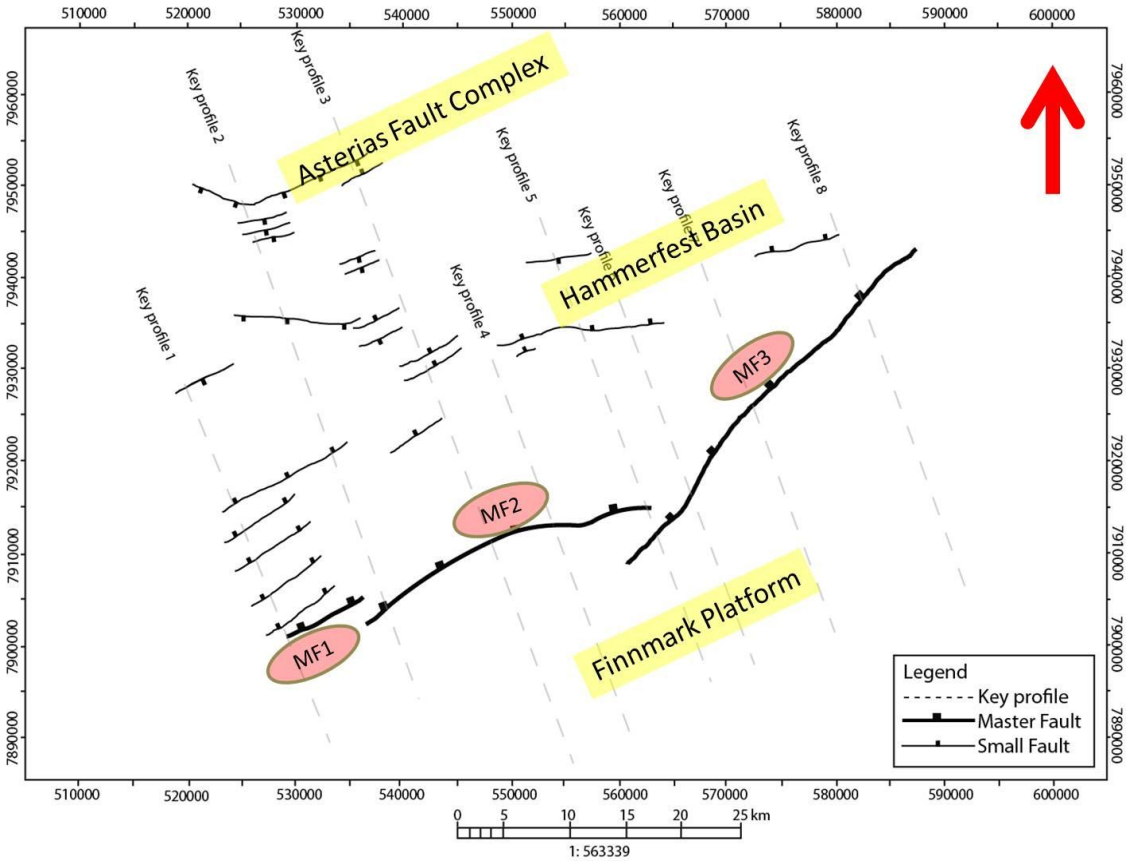

Figure 3.25: Fault Plane Map at the early Cretaceous level with different segments of master fault, grey dotted lines show location of already discussed key profiles.

The normal faults within the Hammerfest basin predominantly show NE-SW trend, however, faults with NW-SE trend are also not uncommon, for instance, the two (2) laterally continuous faults at the location of the key profile 6 and one (1) fault at the location of key profile 8 show north-westerly trend *(Fig. 3.23) *(key profiles are shown on the fault map with grey dotted lines)*. Small as well as large broad graben structures are found at this interpreted level as well (large features are those identified on more than two cross-sectoins) i.e., grabens found on key profiles 1, 2, 3, 5 & 7 in the middle part of the study area *(Fig. 3.23).* As already described in the explanation of the key profiles, most of the deformation in the basinal side is concentrated within the interpreted base Cretaceous down to the intra Triassic levels. Therefore, the base Cretaceous marks the upper boundary of that deformed package from which the structure (horst, graben, single planar fault) narrows downward to the underlying interpreted reflections *(Fig. 3.14 a & Fig. 3.15 a etc).* The northern main boundary fault of the Hammerfest Basin, the Asterias Fault Complex is also interpreted on the regional profiles that belong to north-western part of the study area *(Fig. 3.11 & Fig. 3.23).* Small normal faults with northern and southern dip are associated with the Asterias Fault Complex and a small graben at the location of the key profile 3 is also present in its proximity *(Fig. 3.23).*

3.7.4 Early Cretaceous

The early Cretaceous reflection is also interpreted only within the Hammerfest Basin as it is absent over the Finnmark Platform *(Fig. 3.7).* The time-structure map shows general northward deepening of the early Cretaceous reflection as time values gradually shift colors from shallower to deeper towards the North *(Fig. 3.24).* An array of the masters faults MF1, MF2 & MF3 against which this reflection abuts in the seismic profiles *(Fig. 3.15 & Fig. 3.16 etc)* is also traceable on this time map. The deepest part is located in the north-western corner of the mapped area shown by blue color indicating greater time values *(Fig. 3.24).*

The fault map at this level shows a marked decrease in the intensity of faulting as it can be observed on the cross-sections *(Fig. 3.11 & Fig. 3.12 etc).* This reflection masks the intensely deformed intra Triassic to the base Cretaceous package at the top; hence it marks the time of tectonic quiescence in the study area *(Fig. 3.13 & Fig. 3.25).* However, some minor faulting does appear in this interval as well within the Hammerfest Basin *(Fig. 3.25).* An array of the master faults trending from NE-ENE-EW-NNE is mapped at this level as well. These isolated segments of the master fault are termed as MF1, MF2 & MF3 *(Fig. 3.25).* These step-over

faults are defined as softly-linked faults (following Trugdill & Cartwright, 1994) *(Fig. 3.25),* displacements along which are relayed across the next segment by means of ductile deformation. The master faults are dipping to the North and majority of the small faults interpreted within the Hammerfest Basin show a northern dip-slip component as well. These small normal faults show NE-SW trend generally, however some faults also trend in NW-SE direction, two such faults identified are present between the location of key profiles 2 & 3 and at the location of key profiles 4 & 6 *(Fig. 3.25).* The northern main boundary fault of the Hammerfest Basin, the Asterias Fault Complex is also interpreted on the regional profiles that belong to the north-western part of the study area. Small southward dipping and approximately E-W trending normal faults are present in the proximity of the Asterias Fault Complex at the location of key profile 2 *(Fig. 3.11 & Fig. 3.25).*

3.7.5 Base Tertiary

The base Tertiary reflection is interpreted only within the Hammerfest Basin because of its absence over the Finnmark Platform *(Fig 3.7).* The time-structure map shows a general N-NE deepening of the base-Tertiary reflection *(Fig. 3.26).* It also reflects the shape of the array of masters faults MF1, MF2 & MF3 against which this reflection abuts in the seismic cross-sections. The deepest area is located towards NW of the study area shown by blue color indicating greater time values *(Fig. 3.26).*

Seismic cross-sections, previously described as key profiles 1-8 *(Figs 3.10 – Fig 3.17)* reveals absence of any pronounced faulting at this interval. This observation when integrated and viewed on the 2D fault map shows that study area underwent tectonic quiescence during this time period *(Fig. 3.27).* An array of the master faults trending from NE-ENE-EW-NNE can be subdivided into the two segments based on their trends, which are termed as MF2 & MF3 fault segments (*Fig. 3.27).* It is important to note at this stage that the base Tertiary reflection is not influenced by the master fault segments throughout the study area. The master fault segment MF1 that appears on the already discussed key profile 1 *(Fig. 3.10)* is not displacing this interval. However, this interval abuts against the master fault segment MF2 in the key profiles 2, 3 and 4 *(Fig. 3.11, Fig. 3.12, Fig. 3.13 & Fig. 3.27).* The base Tertiary reflection appears to terminate against the Master fault MF3 in the key profile 6 *(Fig. 3.15)* after which there is no such evidence of the master fault MF3 cutting this reflection *(Fig. 3.27).* The master faults MF2 & MF3 are dipping to the North and majority of the small faults interpreted within the Hammerfest Basin show a similar dip.

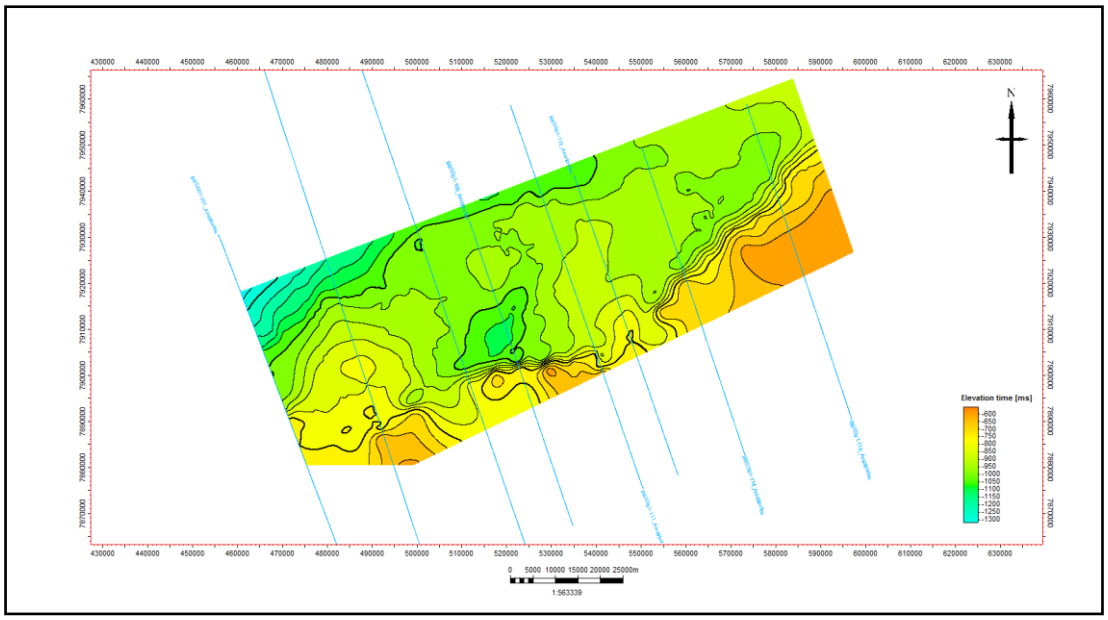

Figure 3.26: Time-structure map at the base Tertiary level. Location of seismic lines already discussed as key profiles is also indicated.

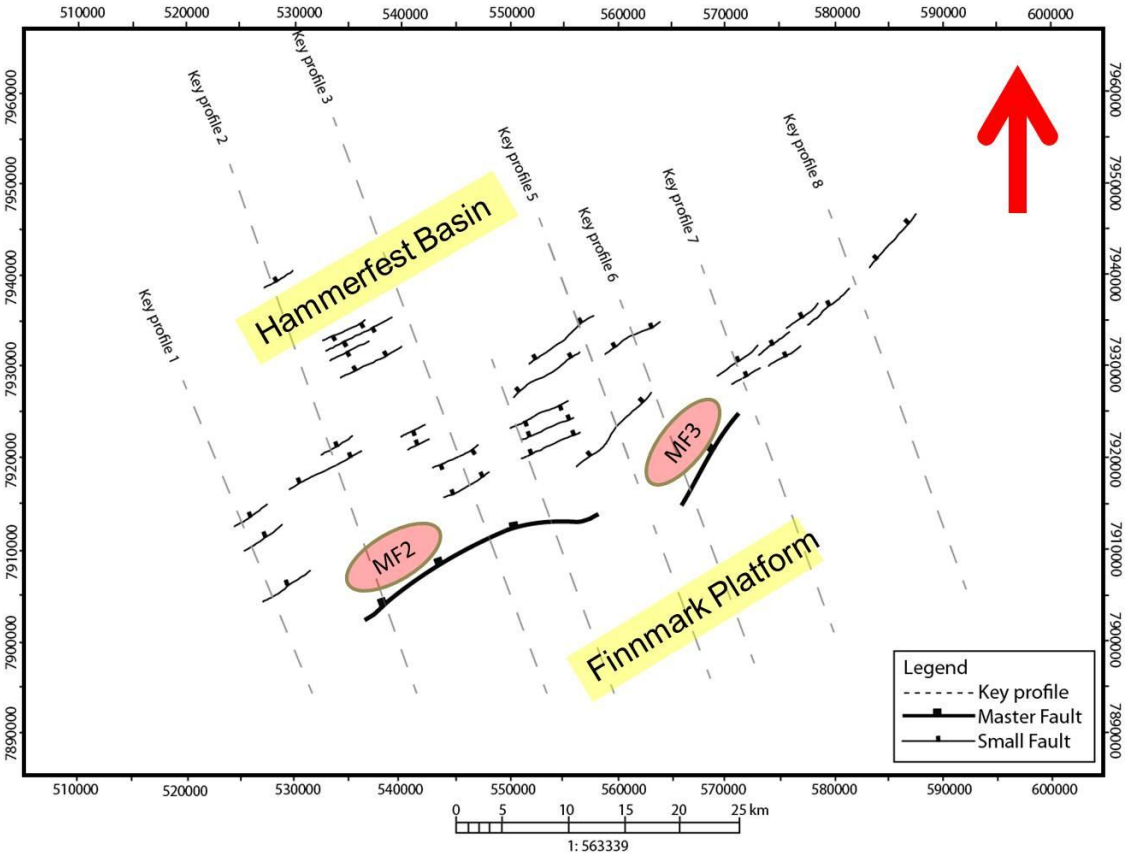

Figure 3.27: Fault Plane Map at the base Tertiary level with only two segments of the master fault, grey dotted lines show location of already discussed key profiles.

These small normal faults show NE-SW trend generally, however, some faults also trend in ENE-WSW fashion. Minor grabens are also found between location of the key profiles 3 & 4 and the key profiles 4 & 5 which are internally deformed by northward dipping small normal faults *(Fig 3.13 & Fig 3.27).*

3.8 Time-Thickness Maps

In order to get insight into the thickness variation trend of the interpreted reflections across the study area, four time-thickness maps are constructed by combining the two interpreted reflections for each map. These thickness maps together with the previously described cross-sections *(key profiles 1-8)* have enabled to extract information regarding the activity along the fault, therefore, instrumental in fault dating. Similarly, a comparison of the fault-related thickness variation within the different fault strands i.e., the master faults MF1, MF2 & MF3 is also carried out which further helps in understanding the fault system.

3.8.1 Intra Triassic – Intra Permian

The time-thickness map of this interval show gradual variation in thickness across the main boundary fault (segments MF1, MF2 & MF3) which is easily traceable on this map as well. Over the platform, a general thickening trend for this package is towards the main boundary fault i.e., northward deepening trend *(Fig. 3.28).* This information is supplemented by the observation previously made on the key profiles 3, 4 and 5 etc *(Fig. 3.12, Fig. 3.13 & Fig. 3.14).* On the platform, this interval shows thickness increase towards the west, an important feature in this part of the Finnmark Platform is the presence of a laterally correlatable down-to-the North normal fault at the Permian and the Triassic level *(Fig. 3.9, Fig. 3.16 a & Fig. 3.16 a).* An abrupt increase in thickness of the intra Triassic to the intra Permian is controlled by this northward dipping normal fault *(Fig. 3.28).* This increase in thickness is indicated by the change in color from the greenish to the bluish shade in the south-eastern part of the Finnmark Platform *(Fig. 3.28).* The greatest variation in thickness across the master fault can be observed in the north-eastern part of the study area between the key profiles 7 and 8 *(both belong to the master fault segment MF3, Fig. 3.16),* an additional place indicating the maximum thickness variation across the fault lies along the key profile 5 *(this profile belongs to the master fault segments MF2 & MF3, Fig. 3.14).* Along the master fault MF1, thickness change seems to be gradual i.e., it is fault controlled but differs considerably from the already discussed instances from the master fault segments MF2 and MF3. Similarly, a general northward thickening trend within the Hammerfest Basin is also observed while thickness in

some parts of the basin is controlled by local faulting *(Fig. 3.9, Fig. 3.12, Fig. 3.15 & Fig. 3.28).* Fault controlled thickness in the proximity of master faults is marked by mounds of severely rounded contours *(Fig. 3.28).*

Thickness variation for this package across the master fault segments MF1, MF2 & MF3 is noticeable but whether it is related to fault activity itself or not is the matter of debate, which will be dealt with in the next chapter. However, this is imperative to point out that no syn-sedimentary strata has been interpreted within the interpreted intra Triassic and the intra Permian levels *(Figs 3.11 a, b & Fig 3.14 a, b).*

3.8.2 Middle Jurassic – Intra Triassic

Thickness of this package shows great variation across the main boundary fault *(Fig. 3.29).* It is due largely to the fact that only one reflection (intra Triassic) is present across the master faults (MF1, MF2 & MF3) on the Finnmark Platform *(Fig. 3.7),* while, towards the Hammerfest Basin, both the reflections are present *(Fig. 3.10).* Therefore, this map shows a cumulative thickness of this package in the basinal area and hence a great thickness contrast across the fault is recorded *(Fig. 3.29).* Shape of the master faults MF1, MF2 and MF3 can be traced on this thickness map as well. The master fault MF1 together with the central portion of the master fault MF2 exhibits great thickness variation across them which are supplemented by the information obtained from the key profiles 1 and 2 respectively *(Fig. 3.10 a & Fig. 3.11 a).* The thickness variation across the fault segment MF2 shows maximum contrast in the centre represented by the key profile 2, while it gradually diminishes away from the centre towards the edges of this fault segment *(Fig. 3.29).* The thickness variation across the master fault segment MF3 remains uniform from the centre represented by the key profile 7 towards SE, represented by the key profile 5, while it decreases significantly further to the NE *(Fig. 3.29).* In the basin, the greatest thickness lies toward the western part of the study area and the change in thickness is gradual except at few places where it is fault controlled locally *(Fig. 3.19, Fig. 3.21 & Fig. 3.29).*

The strong indication of thickness variation across the fault is associated with the fact that the middle Jurassic reflection is present only within the Hammerfest Basin *(Fig. 3.12, Fig. 3.13 etc).* Similarly, lack of syn-sedimentary strata in the cross-sections for this package does not qualify it for the tectonically active period *(Fig. 3.14, Fig. 3.15 etc).*

3.8.3 Base Cretaceous – Middle Jurassic

Both the interpreted reflections are present only within the Hammerfest Basin *(Fig. 3.16).* Thickness of this interval gradually increases from the central part of the study area towards both the NE and the NW *(Fig 3.30).* Trends are gradual and gentle, showing less influence of fault controlled sedimentation except in the areas near the main boundary fault which shows sudden change in thickness because of fault activity *(Fig. 3.30).* The key profiles 1-7 reveal the presence of growth strata with the exception of the key profile 8 for this package *(Fig. 3.10 to Fig. 3.17).* This growth sequence is quite distinctive on the thickness map as well which shows an increase in thickness for the package near the boundary fault, beyond which the map is chopped *(Fig. 3.30).* Maximum thickness of the growth strata is found to be related with the south-eastern part of the fault segment MF2 in the vicinity of key profiles 2 and 3 *(Fig. 3.11, Fig. 3.12 & Fig. 3.30).* The thickness map also shows a decrease in thickness in the center of the basin located in the NW of the key profiles 5 and 6, which is associated with the central bulge of the Hammerfest Basin identified on several key profiles, for instance, key profile 2 *(Fig 3.11).*

3.8.4 Base Tertiary – Base Cretaceous

The time-thickness map of this interval demonstrates that the area between the key profiles 4 & 5 shows less sediment thickness than the areas immediately towards its East and West *(Fig. 3.31).* General thickening of this interval occurs towards NE & NW of the study area. The greatest thickness for this package is present at the location of key profile 1, related to the stair-case geometry of the normal faults dipping to the North *(Fig. 3.10 & Fig. 3.31).* This observation is also supplemented by the observation of fault maps at the base Cretaceous and the base Tertiary levels *(Fig. 3.23 & Fig. 3.27).* Area of the map showing very small thicknesses towards the South are actually extrapolated values of the software contouring algorithm by including some part of the Finnmark Platform, therefore, these must be ignored while viewing thickness variation of the study area at this interval (*Fig. 3.31).*

Similarly, lack of syn-sedimentary strata in the cross-sections for this package does not qualify this period as tectonically active (*Fig. 3.34*, *Fig. 3.15* etc).

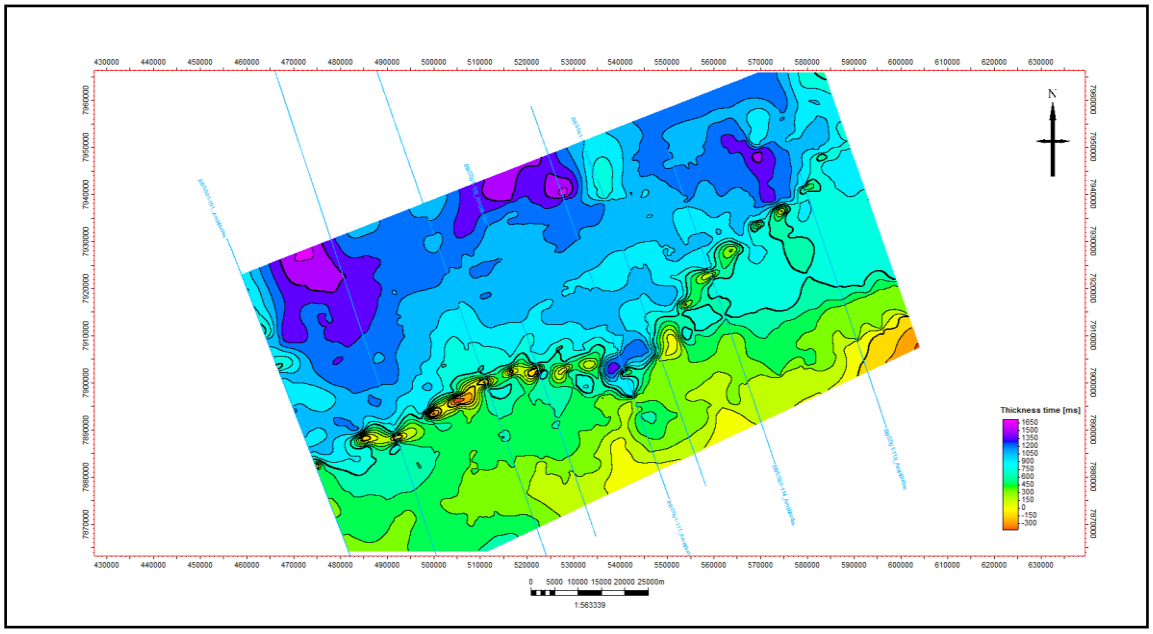

Figure 3.28: Time-thickness map between the interpreted intra Permian and the intra Triassic reflections. Location of the key profiles is also indicated. Great thickness of the package is present in the central and the north-western part of the study area while the fault segments MF1, MF2 & MF3 are also traceable.

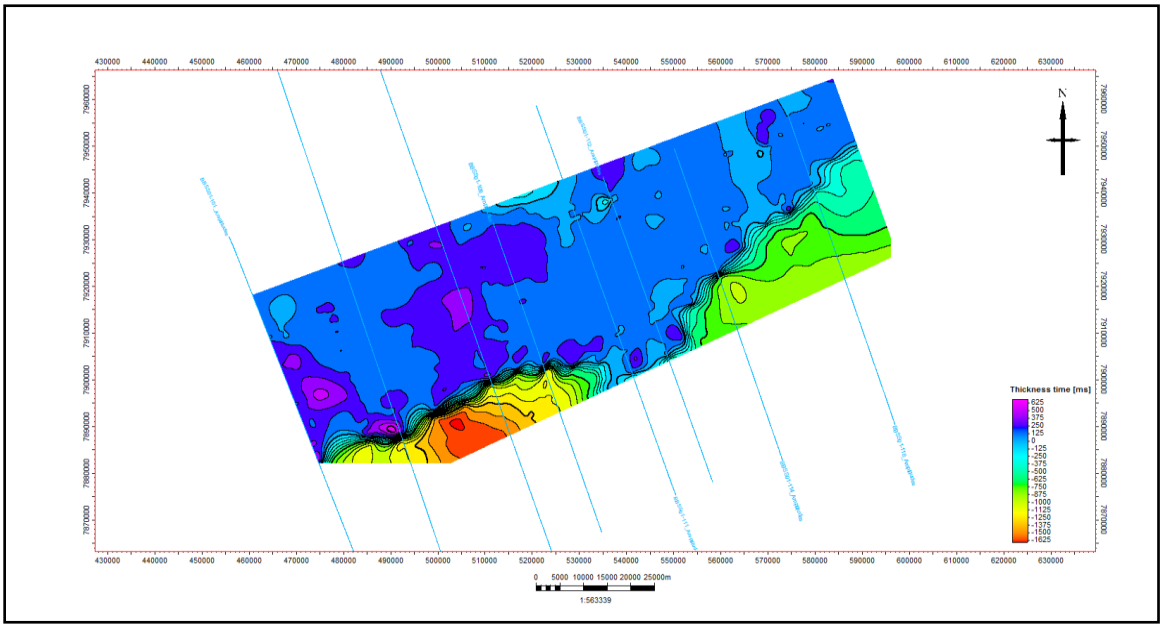

Figure 3.29: Time-thickness map between the interpreted intra Triassic and the middle Jurassic reflections. Location of the key profiles is also indicated. Maximum thickness of this package lies in the north-western part of the study area while the fault segments MF1, MF2 & MF3 are still recognizable at this interval.

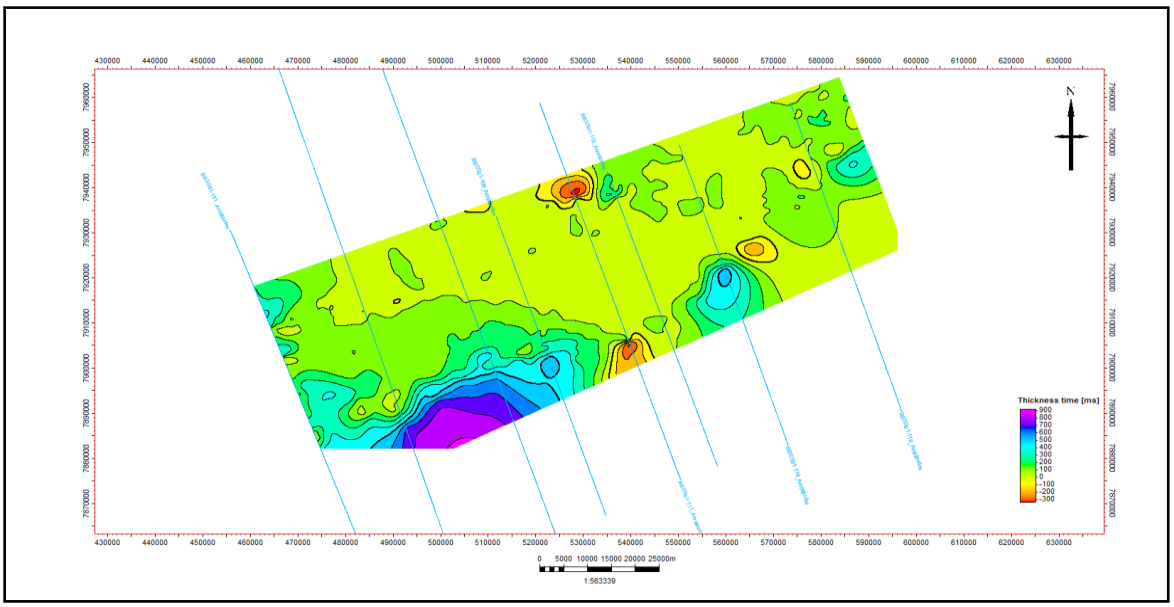

Figure 3.30: Time-thickness map between the interpreted middle Jurassic and the base Cretaceous reflections. Location of the key profiles is also indicated. A marked decrease in thickness at key profile 5 (central part) can be seen while increase in thickness related to the fault growth is identifiable on all key profiles (1-7) except the key profile 8.

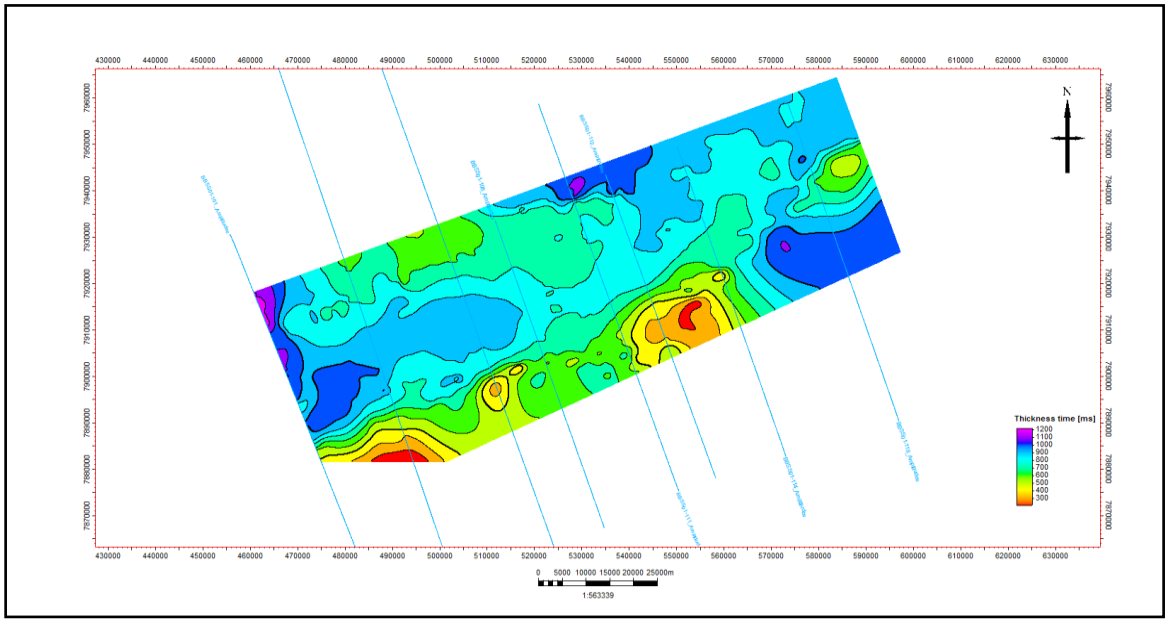

Figure 3.31: Time-thickness map between the interpreted base Cretaceous and the base Tertiary reflections. Location of the seismic lines already discussed as key profiles is also indicated. Increase in thickness can be observed towards the NE and NW of the study area, especially along the key profiles 1 & 8.

Chapter 4
Kinematic & Dynamic Analysis

As discussed earlier in the first chapter, detailed structural analysis entails three mutually connected sub-disciplines of structural geology which includes *descriptive*, *kinematic* and *dynamic* analyses. The descriptive part of such an analysis is presented in the previous chapter *(chapter 3)* while the kinematic and dynamic analyses are the prime focus of the current chapter. ***Kinematic analysis*** focuses on understanding the deformational movements that result in the formation of structures while ***dynamic analysis*** primarily deals with the deformational movements in the terminology of stresses and forces that make and shape the structural architecture of an area (Davis, 1984). This chapter particularly is related to the "level 3" of the study in which detailed analysis of structural geometries, fault growth sequences, paleo-stress analysis and finally evolution of the Troms-Finnmark Fault Complex in a regional context is discussed *(Fig. 3.1).*

Hence, this chapter is arranged in a way to elaborate the classification of the fault system prevalent in the area under consideration. Furthermore, in order to constrain the age of faulting a few established fault-dating techniques are worked with, to determine or at least, bracket the age of different fault strands (MF1, MF2 & MF3) of the larger Troms-Finnmark Fault Complex. Finally, an attempt on deciphering the governing stress system that lead to the present structural development is made along with a comparison of the present study with that of already known structural set-up of the Barents Shelf. Therefore, this chapter is closely connected with the observations and descriptions already presented in the previous chapters *(chapters 2 & 3).*

4.1 Fault Classification

The Troms-Finnmark Fault Complex in the study area comprises of three fault segments MF1, MF2 and MF3, which constitute together a linked fault system *(Fig. 4.1).* A linked fault system is described as a group of branching faults that are largely contemporaneous and their linkage forms a much large array than that of the individual fault segments. An important feature of such a linked fault system is that the constituent fault segments branch rather than cross-cut each other *(Fig. 3.9)* (Davison, 1994). Several map view patterns of the extensional linked fault system are possible which range from anastamosing with little change in orientation, through anastamosing with highly variable orientation to a reticulate style with highly oblique transfer fault *(Fig. 4.2)* (Davison, 1994). The map view pattern interpreted

during the present study shows both the synthetic and the antithetic faults to the main boundary faults (MF1, MF2 & MF3) trending predominantly in NE-SW direction and are clearly unlinked *(Fig. 4.3).* Three basic types of transfer zones between unlinked and linked faults have been proposed by Morley et al. (1990) which include following main types:

i) Conjugate Convergent
ii) Conjugate Divergent
iii) Synthetic

Each of these types can further be elaborated on the basis of their geometrical relationship with the adjacent segment such as approaching, overlapping, collateral and collinear *(Table 4.2).* Therefore, the relationship demonstrated by the three softly-linked fault segments (MF1, MF2 & MF3) of the Troms-Finnmark Fault Complex qualifies them to be placed in the category of "Approaching-Synthetic" fault segments *(Fig. 3.9 & Table 4.2).*

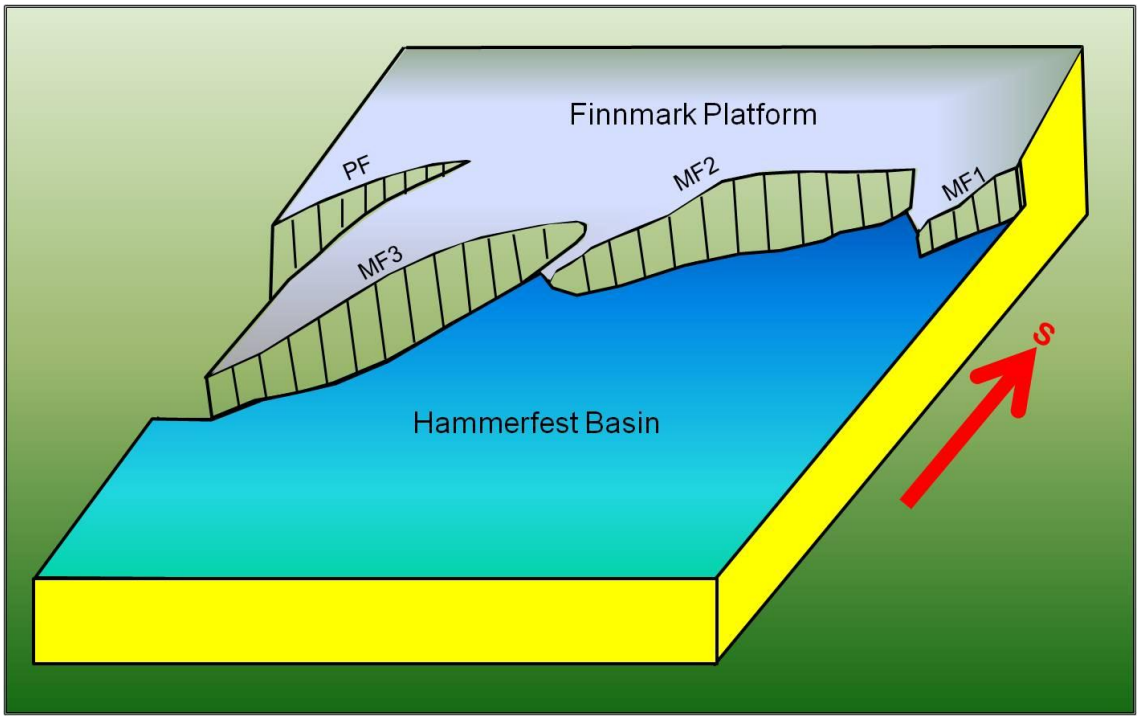

Figure 4.1: A schematic block diagram of the study area. A part of the Troms-Finnmark Fault Complex separating the Finnmark Platform in the South from the Hammerfest Basin in the North with its constituent segments MF1, MF2 & MF3 is shown. Towards SE the PF fault is also shown.

In the cross-section, extensional faults are represented by two main styles, the domino-style faults which are often sub-parallel planar faults along which the fault planes and bedding rotate concurrently *(Fig. 3.12 a)* and the listric faults where dip of the fault plane gradually decreases with depth until it becomes very low in a detachment horizon which could be a

mechanically weak lithology such as over-pressured shale or salt as well as the mid/lower crustal level *(Fig. 3.15)* (Davison, 1994). The cross-sections along the fault segments (MF1, MF2 & MF3) of the Troms-Finnmark Fault Complex display a wide spectrum of the master fault geometries which range from the planar normal fault through the slightly curved normal fault to the typical listric normal fault, which all show a down-to-the-North displacement *(Fig. 3.10 to Fig. 3.17).*

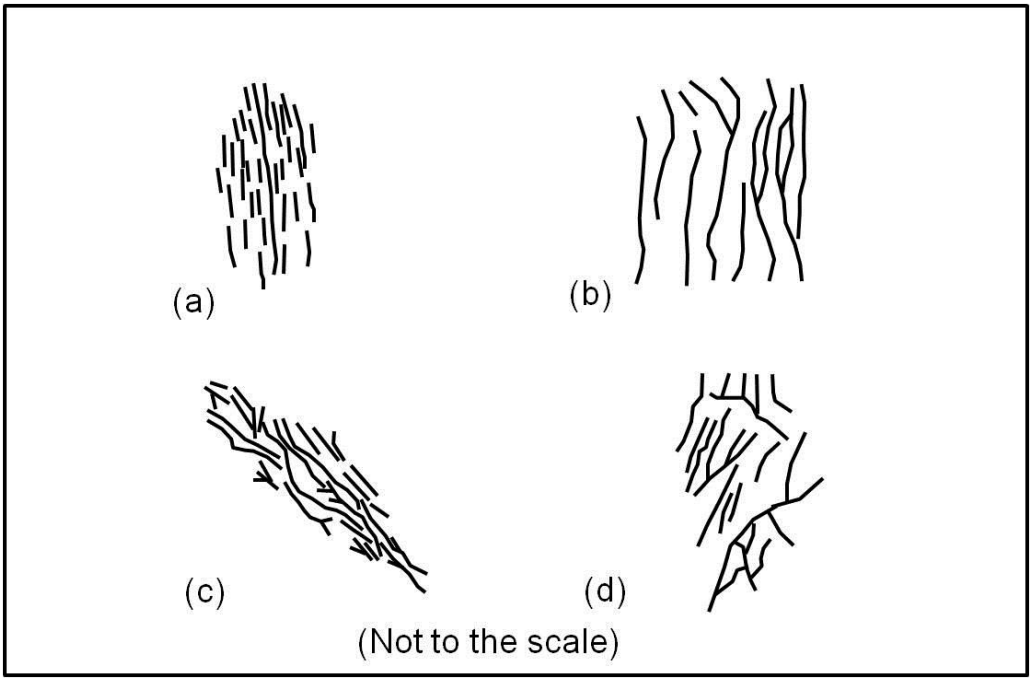

Figure 4.2: Pattern of the extensional fault systems in map view **(a)** Unlinked parallel fault system **(b)** sandbox model showing linked extensional faults **(c)** oblique partially linked fault system **(d)** Reticulate pattern with highly oblique transfer faults showing linkage to main fault (modified from Milani & Davison, 1988; in Davison, 1994) .

The structural fabric of the southwestern Barents Sea shows great variation in geometry, appearance and age, fundamentally, derived from the different basement blocks and different extent of the various rift episodes (Gabrielsen, 1984). Diversity in structural architecture has different tectonic implications which led Gabrielsen (1984) to propose an intuitive fault classification of the southwestern Barents Sea, based on the fault stature, which principally focuses on the faults' relationship with the basement (basement involved or detached) and their regional / tectonic significance, instead of relying primarily on the fault geometries *(Table 4.1).* These fault classes include the following main types:

a) First-Class
b) Second-Class
c) Third-Class

Table 4.1) Classification of fault systems of the southwest Barents Sea, devised by Gabrielsen (1984).

First Class	Basement involved	Regional Significance	Reactivated	Separate areas of different tectonic outline
Second Class	Basement involved	Semi-Regional	Reactivated / not reactivated	Separate areas of different tectonic outline
Third Class	Basement detached	Local Significance	Not reactivated	Does not separate areas of different tectonic outline

This classification led Gabrielsen (1984) to classify the Troms-Finnmark Fault Complex as the ***First-Class*** fault system with normal displacement initiating as early as the Permian and it experienced reactivation during later tectonic activity. During the present study, the three interpreted fault segments MF1, MF2 & MF3 of the Troms-Finnmark Fault Complex augments the observation of Gabrielsen (1984). These fault segments serve to delineate the platform area (Finnmark Platform) in the south from the basinal area (Hammerfest Basin) in the North, showing regional significance of these fault strands *(Figs 3.10 – Fig 3.17).* Additionally, in the cross-sectional view, these fault segments (MF1, MF2 & MF3) clearly cuts the pre-Permian strata and continues down-section thereby, most likely involving the basement *(Fig. 3.10 – Fig. 3.17, Fig. 4.4).* Therefore, the basement-involvement and regional significance of the three fault segments (MF1, MF2 & MF3) qualifies them to be placed in the category of the ***"First-Class"*** faults (*sensu* Gabrielsen, 1984).

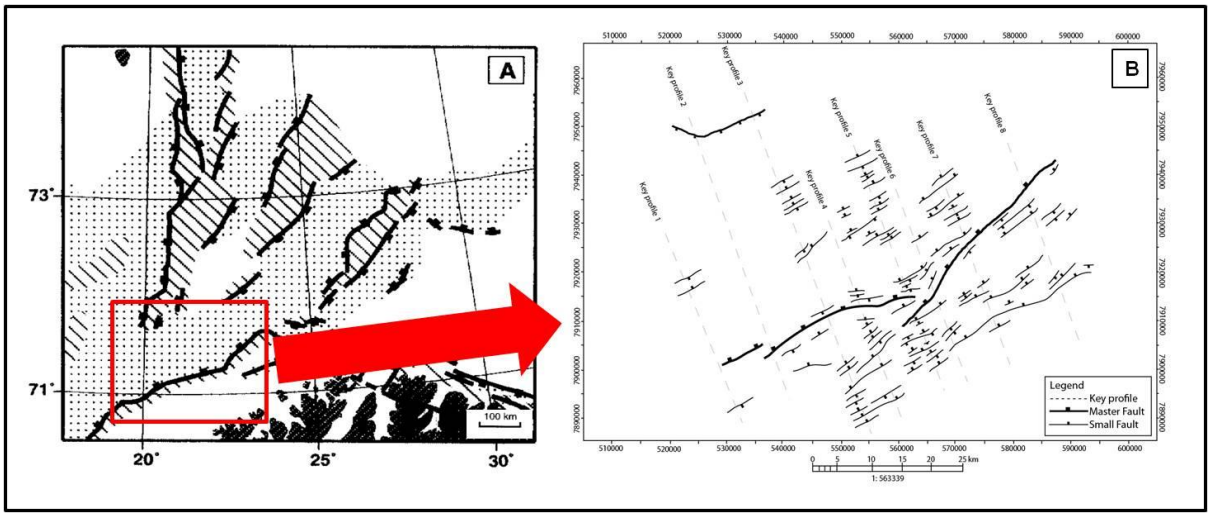

Figure 4.3: Comparison of the fault pattern in the map view, **(A)** Structure of the late Paleozoic rift system mapped by Gudlaugusson et al (1998) **(B)** Fault map of the interpreted intra Permian reflection predominantly showing NE-SW orientation.

Similarly, classification of the Troms-Finnmark Fault Complex presented by Berglund et al. (1986) proposes that this fault system involves one or two major listric normal faults that are

usually associated with the reverse drag/roll-over folds and the counter faults. The present study supplements the observation of Berglund et al. (1986) to the extent that the faults are predominantly listric in geometry and the presence of one major listric fault (MF1, MF2 & MF3) serves to separate the Finnmark Platform from the Hammerfest Basin *(Fig. 3.10 – Fig. 3.17).* However, there is no evidence of two major listric faults as proposed by Berglund et al. (1986), in their schematic model of the Troms-Finnmark Fault Complex *(Fig. 2.6).* The only evidence that could vouch for such a structural arrangement lies where the two master fault segments (MF2 & MF3) overlap each other *(Fig. 3.9),* however, the closer look at the geometries of the master faults MF2 and MF3 in the key profile 5 *(Fig. 3.14)* taken from the overlapping zone, provides a different perspective. In this profile *(Fig. 3.14),* both the master faults are present, but the fault segment MF2 shows planar geometry and is termed as the ***Third-Class*** fault (*sensu* Gabrielsen, 1984), since the oldest penetrated reflector by this fault belongs to the intra Triassic age, while the fault segment MF3 is the ***First-Class*** fault (*sensu* Gabrielsen, 1984) which shows listric geometry *(Fig. 3.14).* Therefore, the study area, with available 2D reflection data, clearly lacks the presence of two adjacent listric normal faults and rather supports the idea of a single master fault separating the Finnmark Platform in the South from the Hammerfest Basin in the North *(Fig. 3.10 to Fig. 3.17).*

Table 4.2: Classification of transfer zones between the unlinked and linked faults following Morley et al., (1990) (modified from Davison, 1996). Following this classification, the linkage between master fault segments of the Troms-Finnmark Fault Complex is termed as "Approaching-Synthetic Fault Segments".

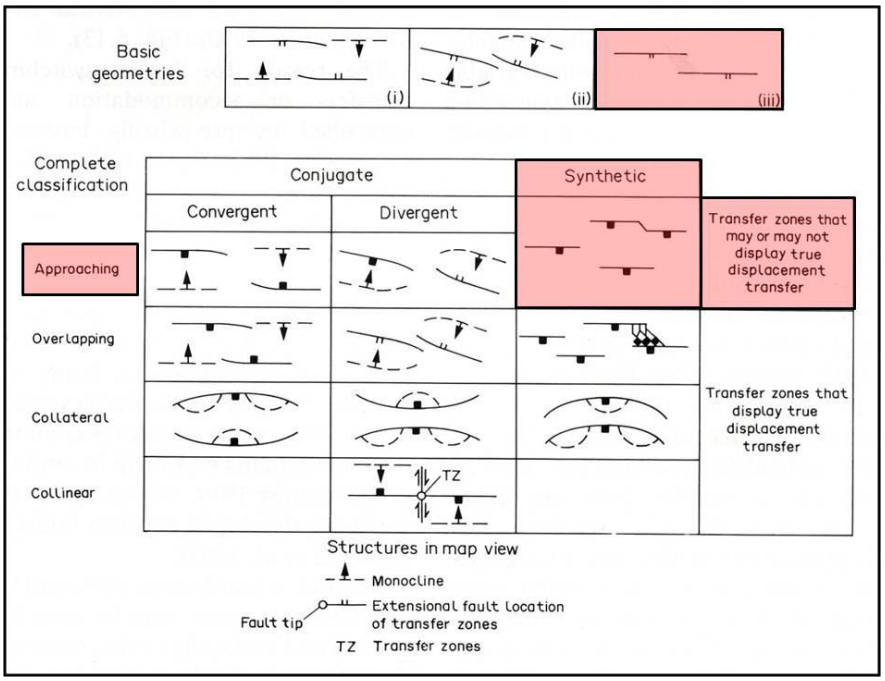

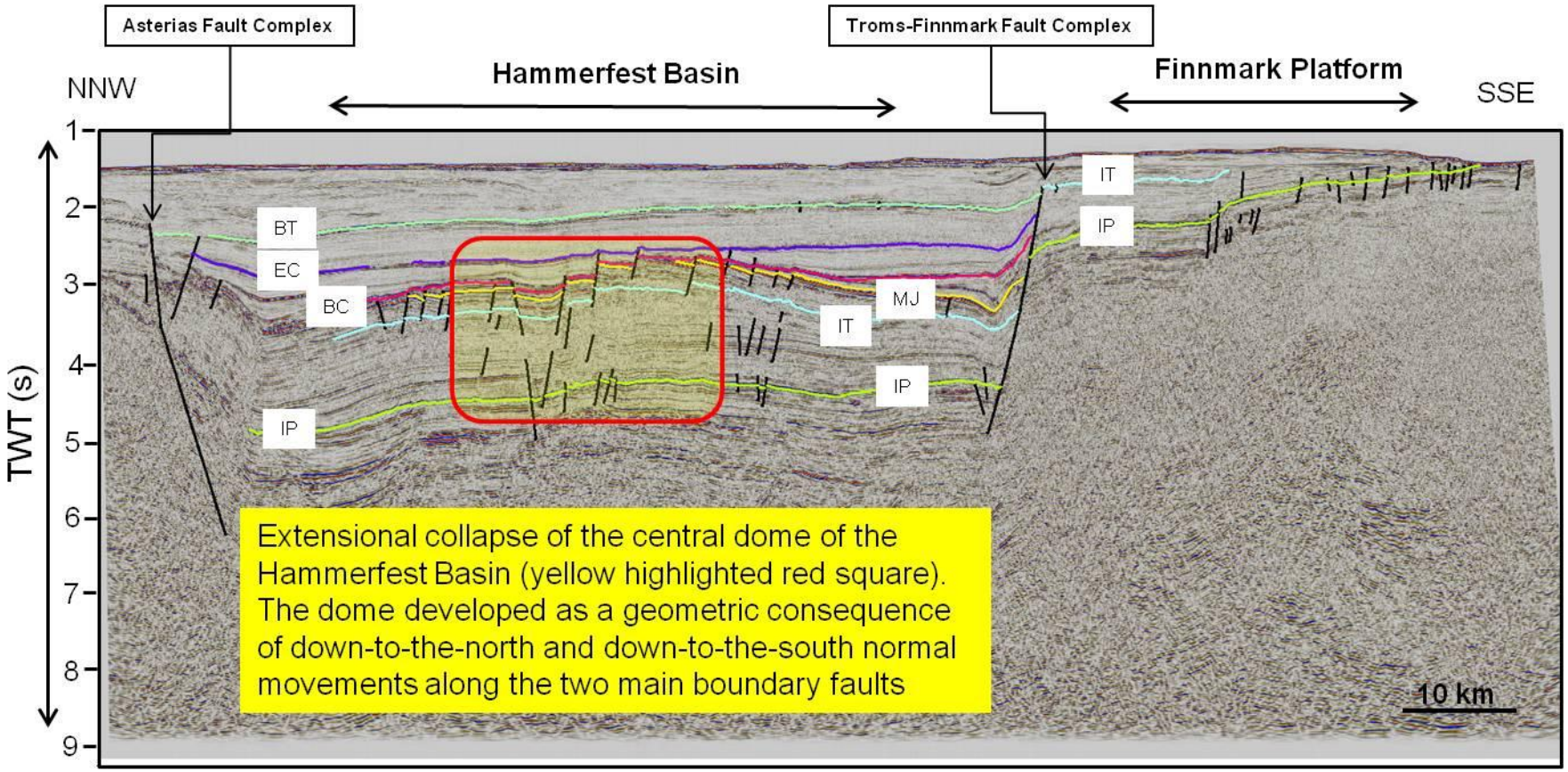

Figure 4.4: A regional cross-section of the Hammerfest Basin along with its bounding master faults. Red square covers the areal extent of the central dome of the basin that is developed as a geometric consequence to the movements along the bounding normal faults. Age of the central dome is coeval with that of the movement along the northern and southern boundary faults. Extensional collapse occurred shortly after deposition of the base Cretaceous reflection. For color codes of the interpreted reflections refer to the Fig. 3.3. BT: Base Tertiary, EC: Early Cretaceous, BC: Base Cretaceous, MJ: Middle Jurassic, IT: Intra Triassic, IP: Intra Permian.

4.2 Relationship of the hanging-wall geometries with the fault plane

It is pertinent to note at this stage that the cross-sections *(key profiles 1-8; Fig. 3.10 – Fig. 3.17)* described in the previous chapter (Descriptive Analysis) are displayed in time-depth (twt) domain and hence the fault plane geometries are not truly representative of what they may look like in the true-depth domain. Therefore, in order to understand whether there exists a certain relationship between the fault plane geometry and the geometry of the deformed hanging-wall adjacent to the fault plane, restoration of the two key profiles *(key profiles 2 & 6, Fig. 3.11 a & Fig. 3.15)* using the technique of geometric section-balancing was undertaken after depth-conversion. The two key profiles (2 & 6) were selected to represent the master fault segments MF2 & MF3 and their restoration yielded vital information regarding the linkage of the fault plane and the associated hanging-wall geometries *(Fig. 3.9).*

The underlying purpose of such a geometric section balancing is to relate the hanging-wall shape to the fault geometry and hence, obtain a cross-section that restores to a geologically reasonable format (Roberts & Yielding, 1994). The pivotal assumption around which all extensional section-balancing methods revolve is that all deformation associated with the fault-slip is exclusively restricted to the hanging-wall, while rigid body rotation related to the foot-wall can be accommodated. A variety of techniques for extensional section-balancing exist, with different principles about the deformation associated with the hanging-wall. The oldest of such a technique is the Chevron construction (Verall, 1981) which assumes that vertical simple shear is responsible for the deformation in the hanging-wall and magnitude of extension is same as the heave of the fault plane and is considered as constant. Consequently, fault-slip is considered to decrease with decreasing fault-dip (Roberts & Yielding, 1994). Various modifications to this constant-heave method were developed later, which included White et al. (1986), Grosshong (1989), White (1987), White & Yielding (1991) and Roberts & Yielding (1994). Another construction method devised by Gibbs (1983) necessitates constant fault-slip and variable fault-heave which requires elongation of the bed-length within the roll-over *(Fig. 4.5).* Alternatively, Davison (1986) proposed that bed-length could be preserved, if fault-slip and heave are allowed to vary.

Comparison between the rotation of main faults and the bedding provides information for the internal block deformation (Fossen & Gabrielsen, 1996). If the fault blocks experience the rigid rotation, the initial angular relationship between the main faults and the bedding is maintained. This angular relationship is used by some authors as the fundamental supposition

for reconstruction of the initial fault dips (e.g. Jackson 1987, as cited in Fossen & Gabrielsen, 1996). However, since deformation is compensated at wider range of scales, internal block deformation cannot be negligible. The differential rotation of the bedding and the main faults ('tilt discrepancy' by Westaway & Kusznir, 1993) is thus an estimate of the internal or distributed deformation of the rotated fault block. The nature of block-internal deformation has been a topic of much debate and anticipated models include distributed vertical shear (Verral, 1981; Gibbs, 1983; Westaway & Kusznir, 1993; as cited in Fossen & Gabrielsen, 1996), oblique shear (White et al., 1986) and bedding-parallel slip (Higgs et al., 1991; as cited in Fossen & Gabrielsen, 1996).

Some authors still consider the rigid-body rotation model for block faulting where internal deformation is either absent or negligible (e.g. Jackson, 1987; Jackson et al., 1988; Moretti & Colletta, 1988; as cited in Fossen & Gabrielsen, 1996). However, extensional faulting experiments of Fossen & Gabrielsen (1996) with the plaster as the deforming medium, argues that the rigid-body rotation alone fails to explain the mechanism for internal block deformation. Their experimental work concludes that the vertical shear cannot explain all of the internal ductile block deformation and as the bedding parallel slip does not work in plaster medium so the oblique shear is the most likely candidate for controlling the internal block deformation, which is in accordance with observations of Ellis & McClay (1988) (Fossen & Gabrielsen, 1996). Therefore, any reconstruction exercise neglecting the internal block deformation that undergoes stretching would not yield the geometrically viable results.

Nevertheless, neither of above-mentioned section balancing techniques geometrically conserves hanging-wall portion during deformation hence geologically invalid in their simplest mode (Wheeler, 1987; as cited in Roberts & Yielding, 1994). Briefly, all restoration techniques can be implemented in two ways. If the fault geometry is known, forward modeling of the hanging-wall can be predicted or conversely fault-plane geometry can be constructed from the shape of the roll-over which is called inverse modeling (Roberts & Yielding, 1994). During the present study, forward modeling approach for the reconstruction of roll-over geometry from the already known fault-plane geometry was applied to understand their mutual relationship *(Fig. 4.9 & Fig. 4.10).*

The two selected key profiles (key profile 2 & 6, refer to *Fig. 3.11 a, b & Fig. 3.15*) were first domain-converted (time-depth) using velocity information from the available borehole's check-shot data (boreholes 7120/9-2, 7120/12-4 & 7121/5-3) *(Figs. 4.6, 4.7 & 4.8).* An

average velocity of 3000 m/s is used for the depth conversion which implies that the time (twt) of 1 s corresponds to the depth of 1500 m and so on.

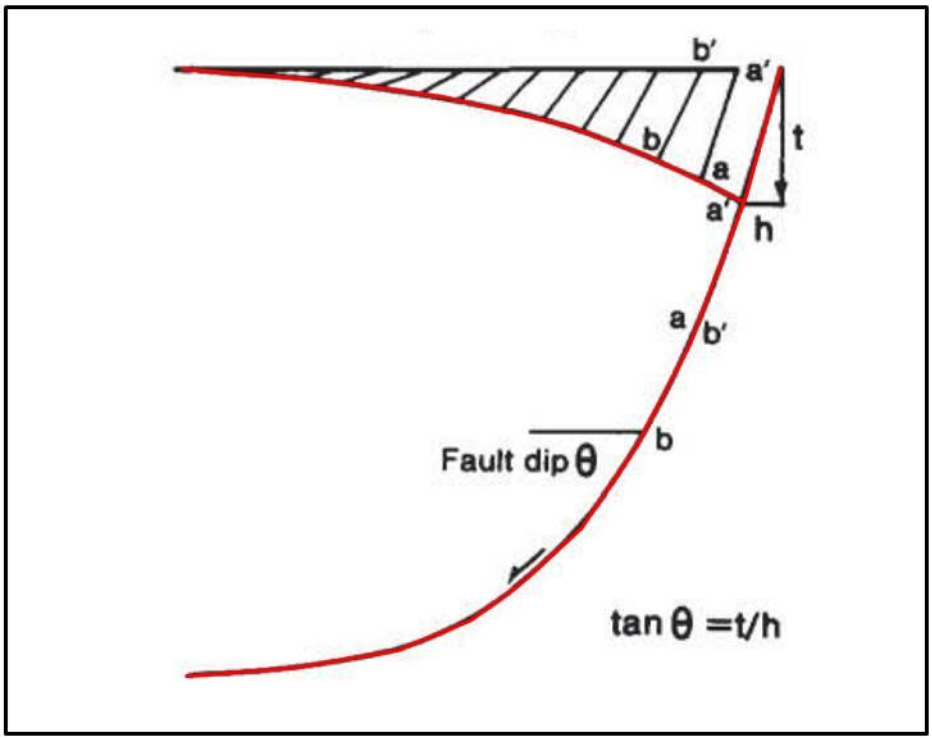

Figure 4.5: An example of geometric reconstruction of the fault-plane from the roll-over geometry proposed by Gibbs (1983).

Similarly, before embarking on to the actual reconstruction it was deemed necessary to obtain the similar horizontal and the vertical scales (1:1) which further enhanced the spatial relationship of the subsurface geometries *(Fig. 4.12 & Fig. 4.13).* The fault-plane from such a depth-converted and equal-scaled (1:1) profile was traced along its length. Heaves of the fault plane were then plotted at a uniform interval of 1km after which perpendiculars were drawn on all fault-heaves. Interestingly, the length of these perpendiculars decreased with the diminishing fault-plane dip. Subsequently, the perpendiculars derived from the heaves of the fault-plane were projected on to a reference datum and plotted as downward vectors *(Fig. 4.9, Fig. 4.10).*

Finally, the points obtained from these downward projected vertical vectors were joined and the resultant geometry was observed which evidently pointed to the hanging-wall folding *(Fig. 4.9 & Fig. 4.10).* Afterwards, the roll-over geometries constructed from the fault-plane were compared by superimposing the constructed geometries on top of the interpreted geometries in depth-converted key profiles 2 & 6 *(Fig. 4.9, Fig. 4.10, Fig. 4.12 & Fig. 4.13).*

An excellent match exists between the constructed rollover geometry by forward modeling solution and the one observed on the depth converted key profile 6, representing the master fault segment MF3 of the large array of the Troms-Finnmark Fault Complex *(Fig. 4.10 & Fig. 4.13).*

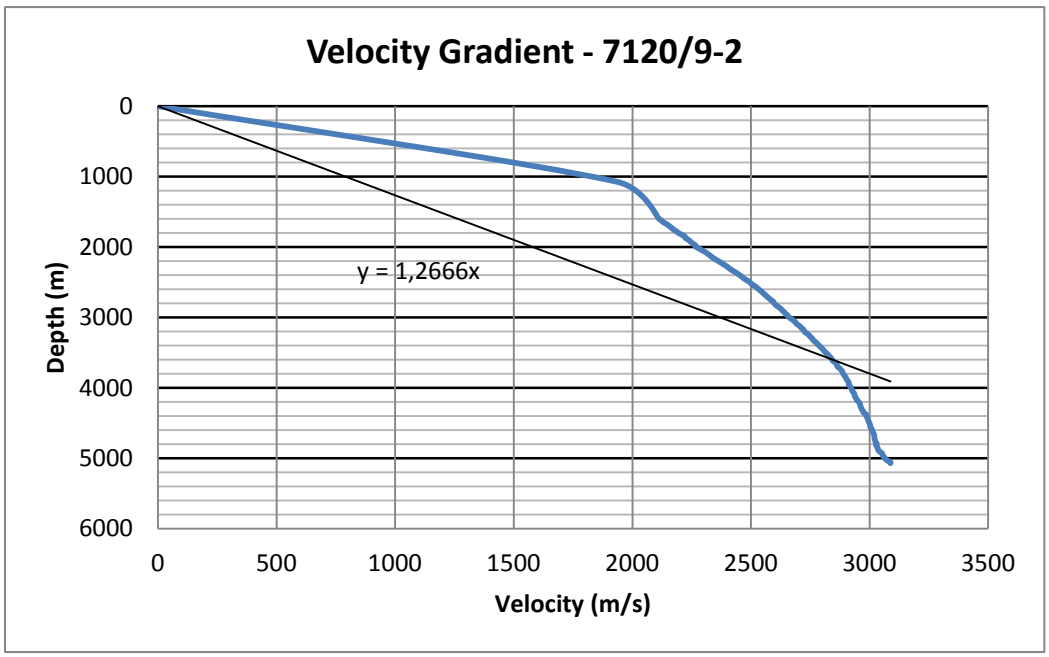

Figure 4.6: Velocity-Depth relationship of the borehole 7120/9-2 used for domain conversion.

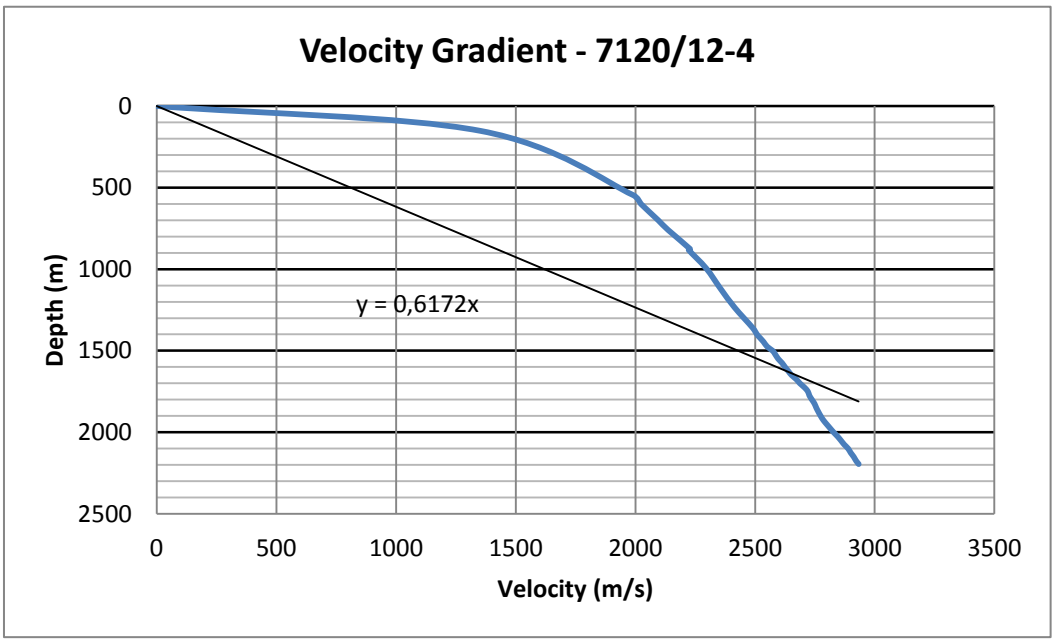

Figure 4.7: Velocity-Depth relationship of the borehole 7120/12-4 used for domain conversion.

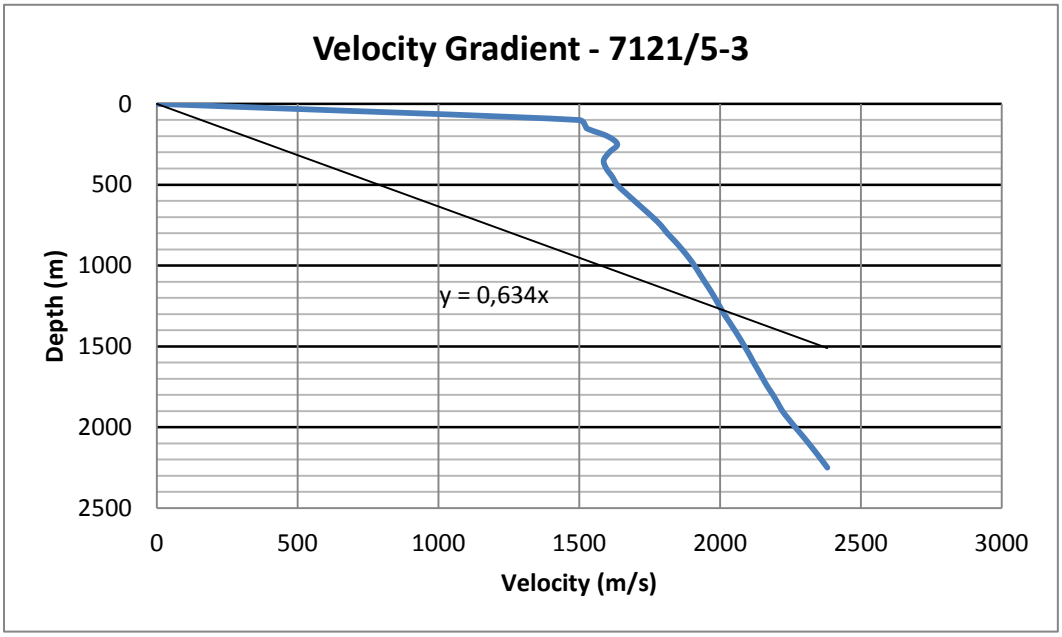

Figure 4.8: Velocity-Depth relationship of the borehole 7120/5-3 used for domain conversion.

Similarly, the comparison of constructed and interpreted roll-over geometries for the key profile 2 generally demonstrates a good match however, certain important differences do exist *(Fig. 4.9 & Fig. 4.12).*

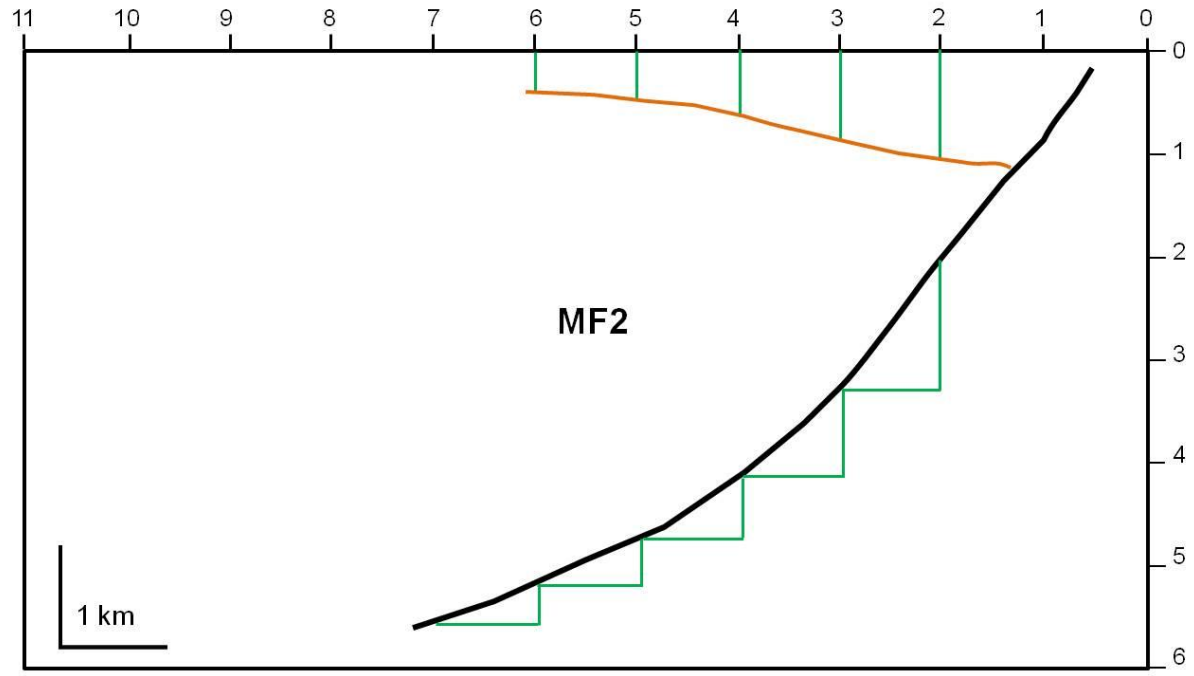

Figure 4.9: Forward modeling solution (construction of roll-over geometry from the fault plane) for the key profile 2 representing the master fault segment MF2.

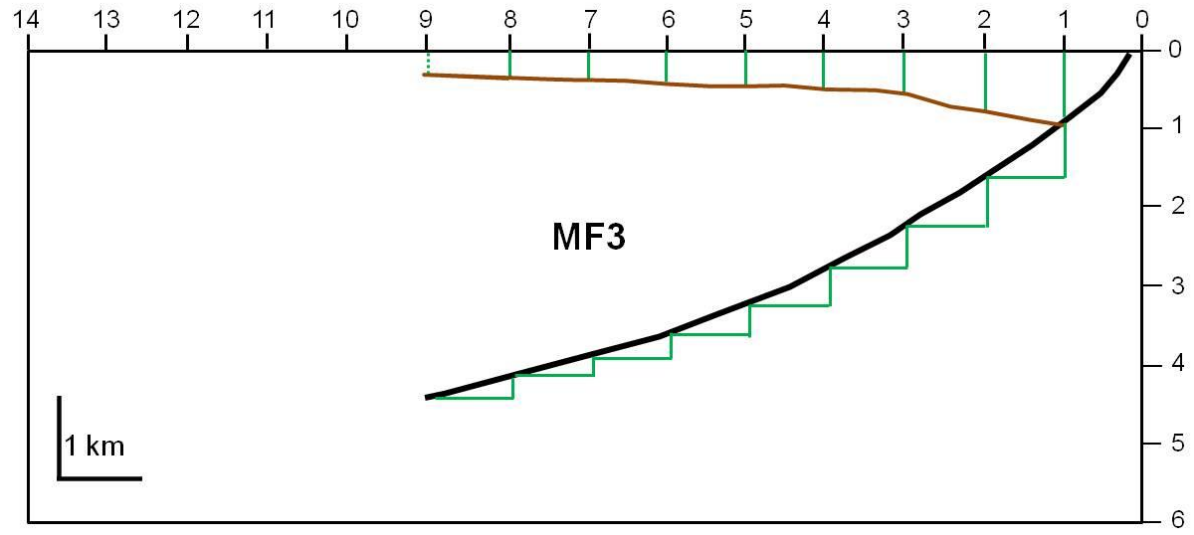

Figure 4.10: Forward modeling solution (construction of roll-over geometry from the fault plane) for the key profile 6, representing the master fault segment MF3.

When superimposed on top of each other, the constructed and interpreted geometries deviate from each other after certain interval due largely to the later extensional collapse of the roll-over anticline observed in this cross-section *(Fig. 4.12).* Therefore, it was concluded that if the effect of extensional collapse of the roll-over geometry was removed, it would bear striking resemblance with the constructed roll-over geometry from the fault plane *(Fig. 4.9).* This restoration exercise determined the linkage between the hanging-wall folding above a curved fault plane by utilizing the forward modeling technique *(construction of the roll-over geometry from the fault-plane)*; however, it is important to note that similar link could also be established by making use of the inverse modeling technique (*construction of the fault plane from the roll-over geometry).*

4.2.1 The Compaction problem

As explained by White (1987) and White & Yielding (1991), ignoring the effects of sediment compaction may yield erroneous results during cross-section balancing in extensional basins.

$\emptyset(z) = \emptyset_0 \exp(-z/\lambda)$*)…….. (a)*

Where, $\emptyset_0$ = initial porosity, λ = porosity decay length

$$F'(x' + h') = F'(x') - R'(x') + B'(x' + h') + \emptyset'_0 \lambda' \{\exp(-F'(x')/\lambda') - \exp(-R'(x')/\lambda') - \exp(-F'(x' + h')/\lambda') + \exp(-B'(x' + h')/\lambda')\} \ldots\ldots\ldots\ldots\ldots\ldots\ldots\ldots\ldots\ldots \textit{(b)}$$

Where, F'(x') & B'(x') are the y' coordinates of the fault and bed at the coordinate x' in a reference frame rotated through ά, h' is the rotated heave, $\emptyset'_0$ is the rotated initial porosity and λ'

is the rotated porosity decay length while R'(x') is the rotated shape of bed before extension *(Fig 4.11)*. Equation (b) can be solved for F when B is given or the vice versa.

However, when porosity approaches to zero i.e., $Ø_0 = 0$, equation (b) assumes a simplified form, as given below:

F'(x ' + h') = F'(x') - R'(x') + B'(x' + h')…… *(c)*

The equation (a) explains an empirical relationship of porosity and depth (Scalter & Christie, 1980; as cited in White & Yielding, 1991). While equation (b) defines the deformation of the hanging-wall related to the fault geometry with loss in initial porosity playing a significant role in determining the fault and bed coordinates i.e., the change in porosity trend will influence the determination of fault plane geometry from the bedding and vice versa. However, when porosity approaches to zero (*equation c*) the determination of the fault plane geometry from the bedding becomes a function of the initial orientation of the bedding and the rotated shape of the bed after extension.

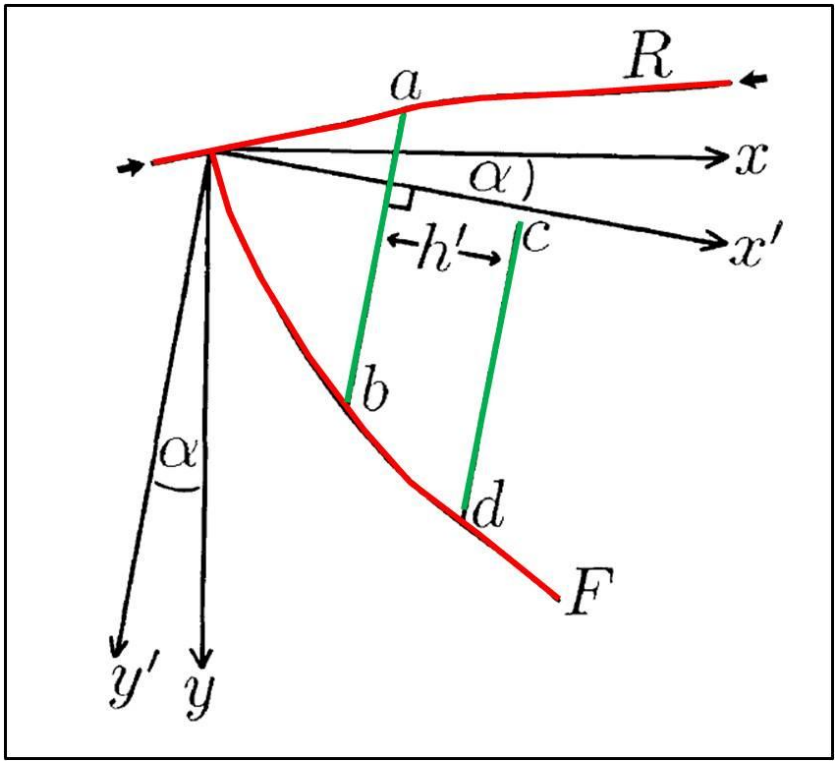

Figure 4.11: Geometry and coordinates employed to derive the **equation *(b)*** while the black arrows at the top define the pre-deformational geometry of the bedding. The symbols used in the diagram are explained under the description of equation *(b)* (modified form White & Yielding, 1991).

During the present study however, the compaction constraint has not been accounted for largely because of the following two reasons:

i) As discussed earlier in the section, compaction modeling involves several parameters to work with before the algorithms defined in equations (a,b,c) can be applied. Time constraint of the present study largely impeded to further explore the influence of compaction on reconstruction of the roll-over fold from the fault plane geometry.

ii) The results obtained in the present study without incorporating the effects of compaction have yielded fairly reasonable results in relation to determine the bedding geometry from the already known fault plane geometry through a forward modeling technique. Additionally, the difference of the reconstructed roll-over fold geometry from the fault plane in *Figure 4.12* is attributed to the later extensional collapse of the anticline.

4.3 Comments on the fault's strike-wise length and displacement

The maximum theoretical strike-length of a normal fault surface has yet to be proven by modeling studies, however, Jackson & White (1989) and Roberts & Jackson (1991), have observed that the maximum strike-length of an active, normal fault surface does not exceed c. 25 km and further commented that such a length could be the upper limit for a normal fault to accommodate slip during a single rupture event (Roberts & Yielding, 1994). The present study differs from this perspective as the mapped faults' (MF2 & MF3) strike-wise lengths clearly traverses the threshold of c.25 km *(Fig. 4.14 b),* however, an important constraint for the present study is the coarse grid of 2D seismic data set, which is approximately 8x9 km across *(Fig. 3.2).* There is a likelihood that with addition of more seismic data amid the present grid, the interpreted master fault segments (MF2 & MF3) may become discontinuous along their strike-lengths and auxiliary fault segments may arise out of the these larger fault strands, possibly showing overlapping characteristics.

According to Schultz et al (2008), the faults follow a power-law slope of approximately n = 1 and therefore maximum displacement is a linear function of the fault's length ($D_{max} = \gamma L^n$, where γ is related to the host rock stiffness and driving stress) i.e., displacement increases with increase in the faults' strike-wise length *(Fig. 4.14 a).*

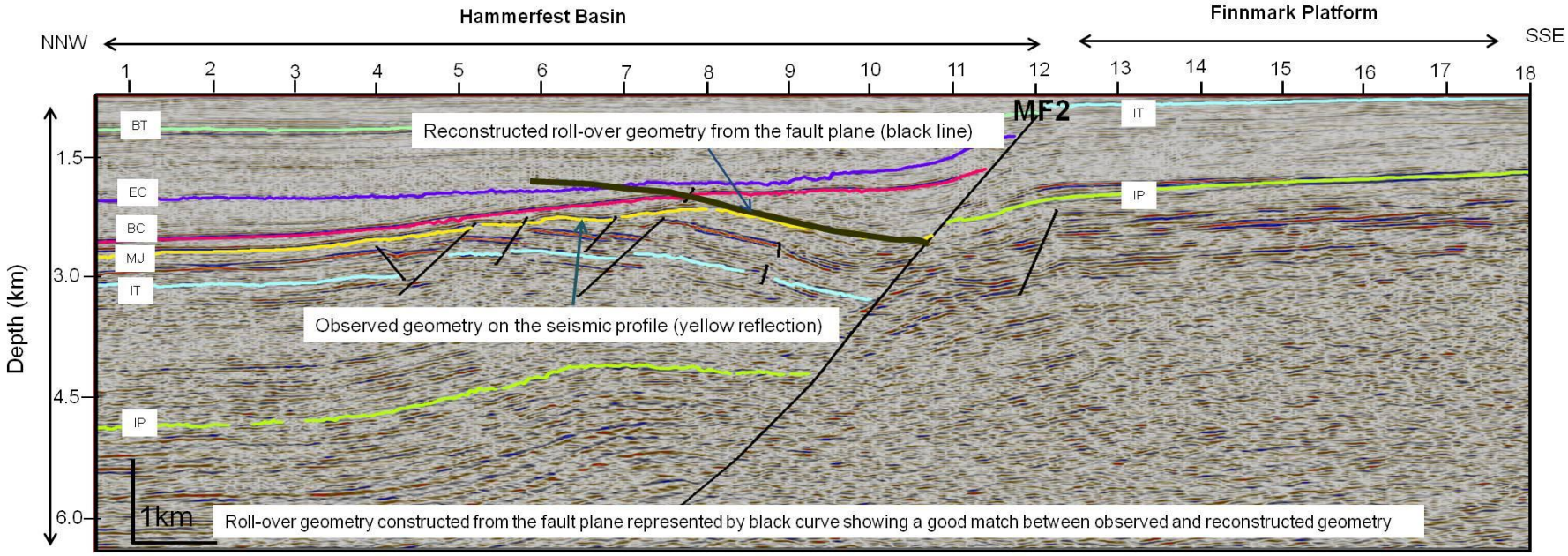

Figure 4.12: Comparison of the interpreted roll-over geometry with the constructed rollover geometry from the fault-plane (Fig. 4.8) is made by superimposing the two. The constructed roll-over geometry is represented by the bold black line dipping towards the fault. The cross-section is depth converted using an average velocity of 3 km/s. Note the distinctive extensional collapse of the interpreted roll-over anticline represented by yellow reflection corresponding to the mid Jurassic. For identification of the color codes of the interpreted reflections, refer to Fig. 3.3. BT: Base Tertiary, EC: Early Cretaceous, BC: Base Cretaceous, MJ: Middle Jurassic, IT: Intra Triassic, IP: Intra Permian.

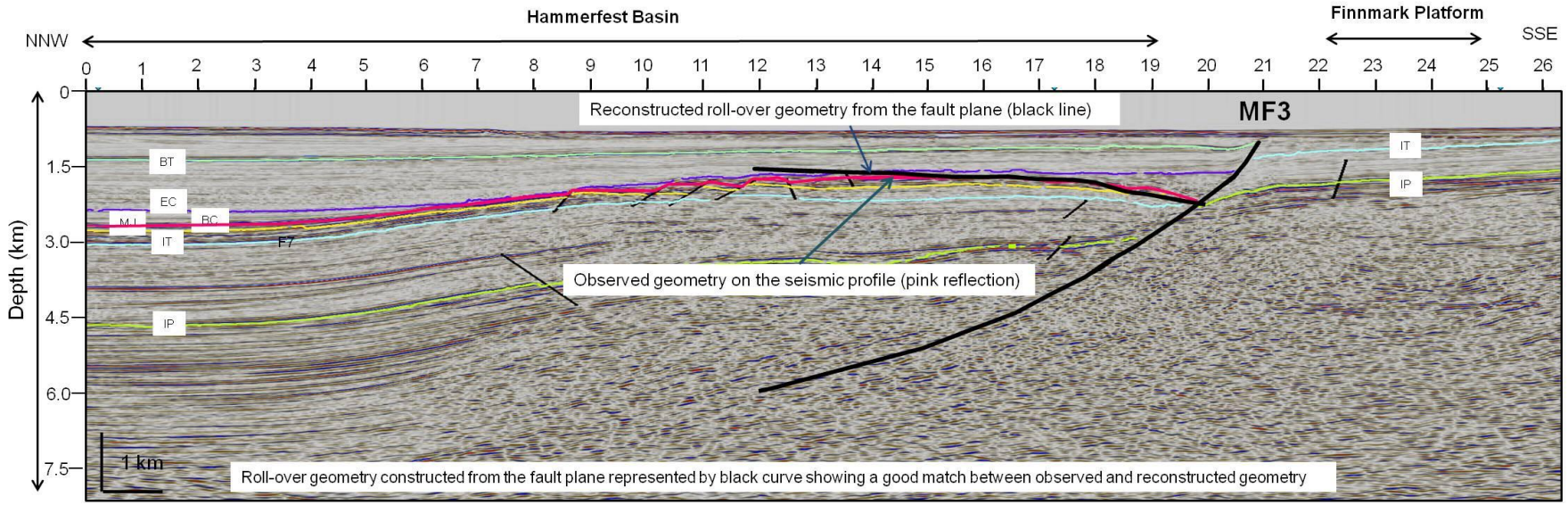

Figure 4.13: Comparison of the interpreted roll-over geometry with the constructed roll-over geometry from the fault-plane (Fig. 4.9) is made by superimposing the two, which results in a very good match. The constructed roll-over geometry is represented by the bold black line dipping towards the fault. The cross-section is depth converted using an average velocity of 3 km/s. The interpreted roll-over anticline is represented by the pink reflection corresponding to the base Cretaceous. For identification of the color codes of the interpreted reflections, refer to Fig. 3.3. BT: Base Tertiary, EC: Early-Cretaceous, BC: Base Cretaceous, MJ: Middle Jurassic, IT: Intra Triassic, IP: Intra Permian.

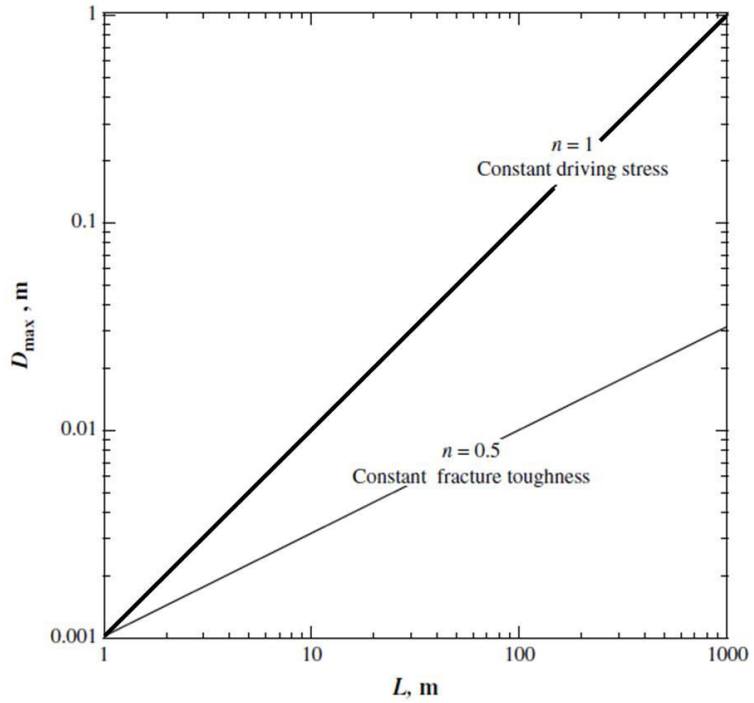

Figure 4.14a: Length-displacement linear relationship for faults that obeys power law slope n=1 is shown in the bold line while the second gradient corresponds to scaling relation n=0.5 for joints & veins (not discussed in the text) (modified from Schultz et al., 2008). See text for details.

Similarly, fault-displacement analysis at the intra Permian level is based on plotting and contouring the fault displacement data in time (twt) for the already discussed key profiles 1-8 *(Fig. 3.10 – Fig. 3.17 & Fig. 4.14b).* It shows a distinctive characteristic of normal faults with increasing displacement towards the fault centre. The maximum fault displacement is associated with the central fault strand MF2 where the displacement values exceed 1.8 s (twt) towards the centre of the master fault *(olive green contours in Fig. 4.14b).* Similarly, the maximum fault displacement values for the fault segment MF3 towards the centre are slightly above 1 s (twt) *(red contours in Fig. 4.14 b).* This observation is supplemented by the analysis of the structure map (twt) at this level which shows greater time values contrast across the master fault strand MF2 as compared to the master fault MF3 *(Fig. 3.8).*

The length-displacement relationship ($D_{max} = \gamma L^n$) proposed by Schultz et al. (2008) could not be tested because the intercept "γ" in *Fig. 4.14a* is a function of the host rock's elastic moduli (i.e., Young's modulus, Poisson's ration) and the driving stress. Since, all the parameters that define the "intercept" are unknown therefore; the present time-bound study does not allow testing the validity of this model in the study area.

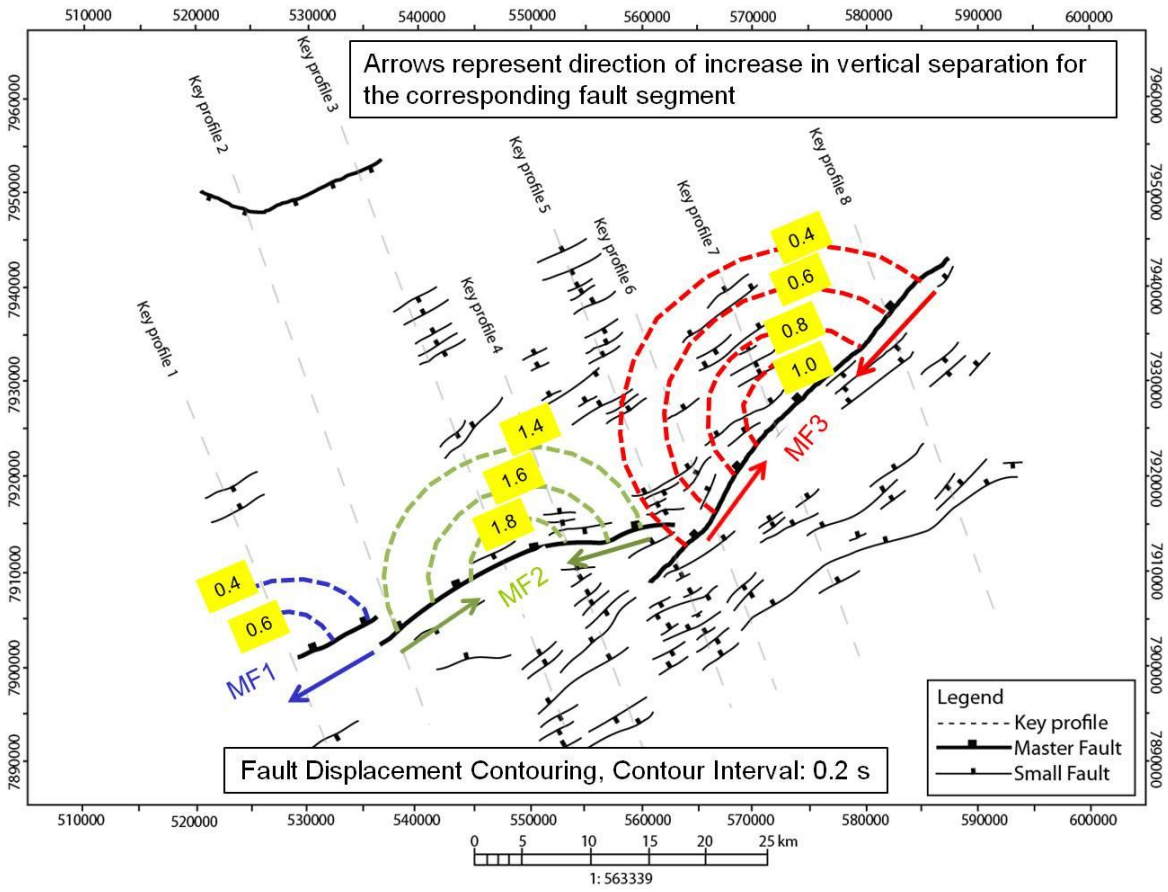

Figure 4.14b: Strike-lengths of the interpreted master fault segments MF1, MF2 & MF3, based on the available 2D seismic reflection data. Note the lengths of MF2 & MF3 exceeding the upper bound c. 25 km limit proposed by Jackson & White (1989) and Roberts & Jackson (1991). Red, Green and blue contours represent the displacement in seconds (twt) (intra Permian level) experienced by different fault segments strike-wise. Also note the increase in dip values towards the center of the isolated fault segments.

4.4 Fault Dating

In order to understand the interplay between the fault movement and sedimentation three established methods of kinematic analysis of growth faults were tested which are:

i) Expansion (Growth) Index Analysis

ii) Throw/Depth Plot Analysis

iii) Stratigraphic Dating

The growth or expansion index is the ratio of the stratigraphic thickness between the hanging-wall and the foot-wall (Thorsen, 1963; as cited in Amogu et al., 2011). It determines period of the most considerable growth however, it lacks the exact information about absolute displacement since this is merely a ratio (Edwards, 1995; Cartwright et al., 1998). Therefore, local variation in sedimentation rates can lead to different growth index results for faults with

the same slip amount (Amogu et al., 2011). In the present study, this technique could only be applied for the interval between the interpreted intra Permian and the intra Triassic reflections as these reflections were present across the master faults in the study area *(Fig. 4.15 & Fig. 4.16).*

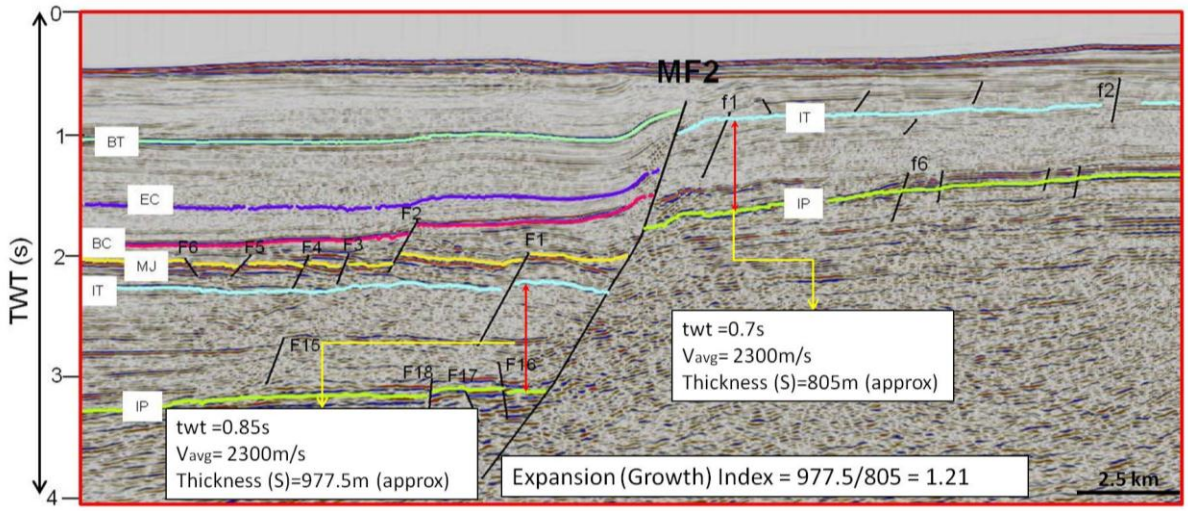

Figure 4.15: Application of the expansion index (E.I) to understand the growth fault behavior, E.I is the ratio of the stratigraphic thicknesses in the hanging-wall to the foot-wall, where E.I =1 suggests non-growth and E.I > 1 represents growth faulting. Average velocities used in the figure have their origin from the velocity cross-plots derived from the well's check-shot data already shown in Fig. 4.6, Fig. 4.7 & Fig. 4.8.

Two representative cross-sections *(key profiles 4 & 7, Fig. 3.13 a,b & Fig. 3.16 a,b)* of the master fault segments MF2 & MF3 were analyzed for the growth index examination. Both the sections yielded the E.I (expansion index) values above 1 which indicate the fault-related growth strata *(Fig. 4.15 & Fig. 4.16).* However, this increase in thickness across the fault keeps on growing towards the more distal part of the basin and the maximum thickness encountered by this interval is evident in the northern and north-western parts of the basin as indicated by the isopach map between these intervals *(Fig. 3.28).* Therefore, E.I method did not resolve the problem of absolute growth strata identification particularly due to the two reasons:

i) Absence of younger than the intra Triassic reflection on the Finnmark Platform impedes the application of this technique for the younger intervals.

ii) This method inherently lacks information on absolute displacement as it is simply a ratio (Cartwright et al., 1998).

Another interesting technique for the identification of growth strata is the use of vertical separation versus depth plot (throw/depth: Amogu et al., 2011). It is a high resolution technique which identifies growth section where it is not obvious in the seismic data by employing the borehole's true stratigraphic thicknesses (Cartwright et al., 1998; Tearpock & Bischke, 1991; Bischke, 1994). This technique however, could not be applied for identification of the growth sequence in the present study because of the absence of multiple closely spaced adjacent wells across the master faults and also largely due to the fact that the present study is based on 2D seismic reflection data. Therefore, throw versus depth plots did not help to resolve the issue of growth sequence identification in the present study.

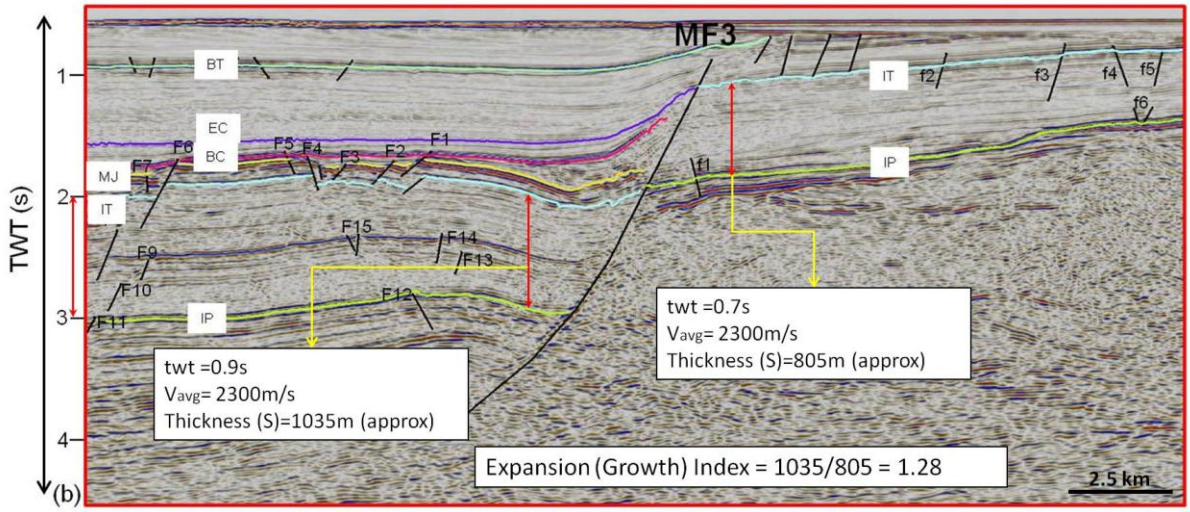

Figure 4.16: Application of the expansion index (E.I) to understand the growth fault behavior, E.I =1 suggests non-growth and E.I > 1 represents growth faulting. Average velocities used in the figure have their origin from the velocity cross-plots derived from the well's check-shot data already shown in Fig. 4.6, Fig. 4.7 & Fig. 4.8.

Stratigraphic dating allows to bracket the age of faulting or the age can be determined accurately by considering the stratal ages affected or unaffected by faults (Angelier, 1994). Recognition of syn-depositional faulting provides valuable information about the age of faulting as it is synchronous to the age of rock unit being deposited. Whenever, fault movement and deposition have interacted over a long period of time, syn-depositional faulting can accurately be reconstructed (Angelier, 1994). In the present study, this technique has provided invaluable information about the age of faulting as the identification of growth sequence was quite evident on all the interpreted cross-sections *(Fig. 3.10 to Fig. 3.17).*

Therefore, in order to make this particular growth sequence clearer on the already discussed key profiles *(key profiles 1-8, Fig. 3.10-Fig. 3.17),* one cross-section for the master fault segment MF1 and three zoomed-in cross-sections for the master faults MF2 & MF3 each, are presented *(Fig. 4.17 & Fig. 4.18).* The NE-SW trending master fault segment MF1 *(Fig. 3.9),* interpreted in the key-profile 1 *(Fig. 3.10),* reveals the presence of a syn-sedimentary wedge between the interpreted middle Jurassic and the base Cretaceous reflection *(Fig. 4.17 a).* Therefore, an age of middle-to-late Jurassic has been assigned to this fault segment.

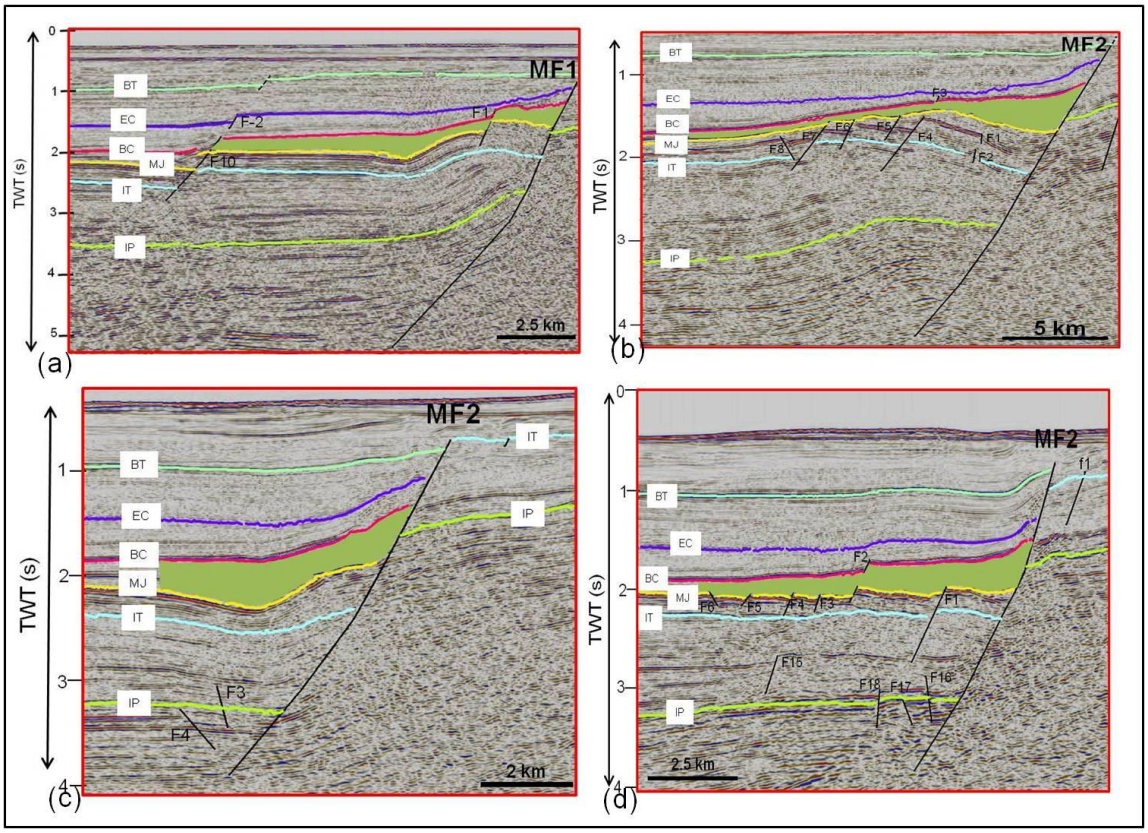

Figure 4.17: Montage of the interpreted growth strata (green highlighted area) on the pre-described key profiles (1-4) (Fig. 3.10 to Fig. 3.13). For color codes of the interpreted reflections refer to the Fig. 3.3. BT: Base Tertiary, EC: Early Cretaceous, BC: Base Cretaceous, MJ: Middle Jurassic, IT: Intra Triassic, IP: Intra Permian.

The master fault segment MF2 *(Fig. 3.9),* interpreted in the key-profiles 2-5 *(Fig .3.11 - Fig 3.14),* reveals the presence of a syn-sedimentary wedge between the interpreted middle Jurassic and the base Cretaceous reflection *(Fig. 4.17 b,c,d).* However, near the tip of the master fault MF2 where it forms an en-echelon characteristic with the master fault segment MF3 *(Fig. 3.9),* growth sequence is found to be associated between the interpreted base Cretaceous and the early Cretaceous reflections *(Fig. 4.18 a),* thereby, representing a bicyclic

kinematic behavior. The ENE-WNW trending master fault MF2 shows two distinctive growth sequence associations from the West to the East strike-wise, therefore, an age of the middle/late Jurassic-early Cretaceous has been assigned to this fault segment.

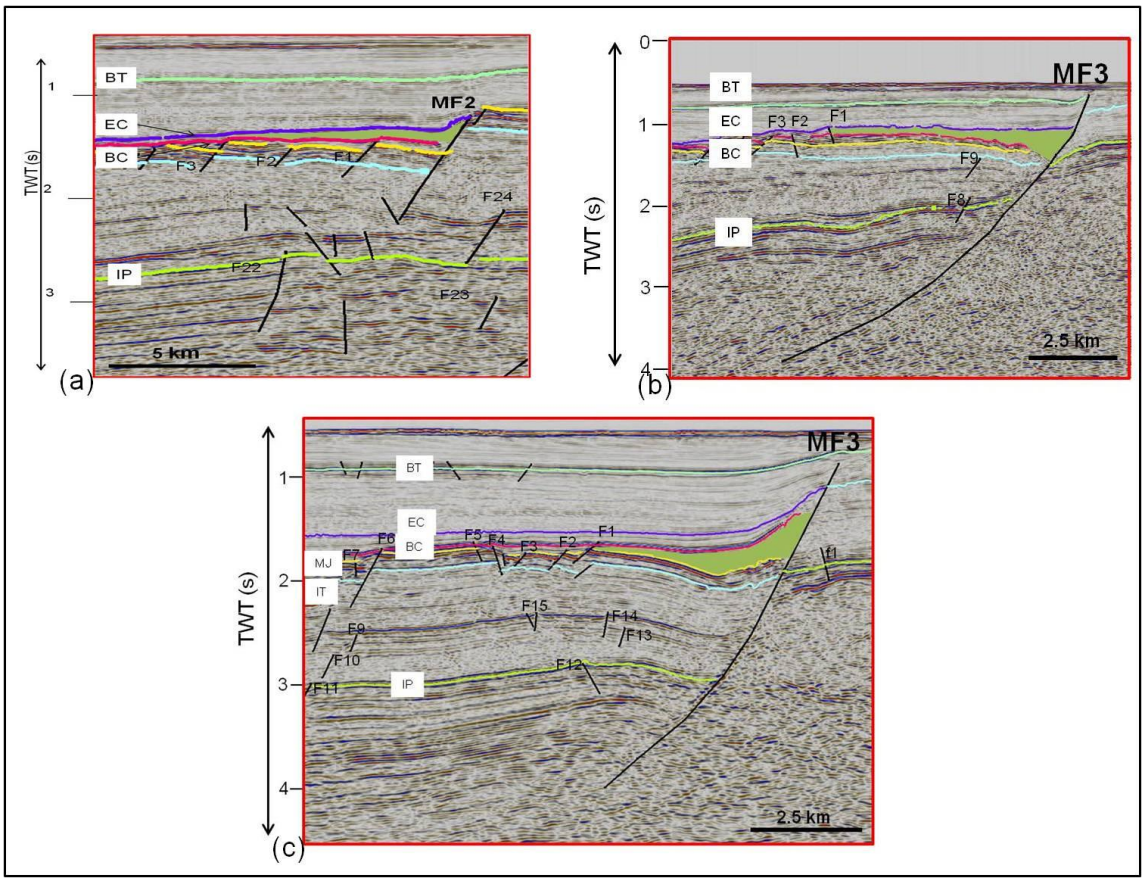

Figure 4.18: Montage of the interpreted growth strata (green highlighted area) on the pre-described key profiles (5-7) (Fig. 3.14 to Fig. 3.16). For color codes of the interpreted reflections refer to the Fig. 3.3. BT: Base Tertiary, EC: Early Cretaceous, BC: Base Cretaceous, MJ: Middle Jurassic, IT: Intra Triassic, IP: Intra Permian.

The NE-SW trending master fault segment MF3 *(Fig. 3.9),* interpreted in the key-profiles 5-8 *(Fig. 3.14 – Fig. 3.17),* reveals the presence of a syn-sedimentary wedge between the interpreted base Cretaceous and the early Cretaceous reflections towards SW *(Fig. 4.18 b)* while nearing the centre of this fault segment and further towards the NE (Fig. 3.9), growth strata is found to be associated with the interpreted middle Jurassic and the base Cretaceous reflections *(Fig. 4.18 c).* Therefore, the master fault segment also presents a case of bicyclic kinematic behavior and hence, an age of the middle/late Jurassic – early Cretaceous has been assigned to this fault segment.

4.5 Analyses of the hanging-wall geometries

During the present study, a great deal of variation observed in the hanging-wall geometries necessitated a thorough analysis. Following major types of hanging-wall geometries are observed:

i) Hanging-wall geometries related to the normal drag
ii) Hanging-wall geometries related to the reverse drag
iii) Narrow folding / snake-head geometries

The examples of normal drag associated with the hanging-wall geometries is scarce *(sensu-stricto)* however, the key profile 5 *(Fig. 4.20 e)* is one such example. This cross-section has been taken at the intersection of softly linked master fault segments (MF2 & MF3), where the master fault segment MF2 becomes the ***"Third-Class"*** fault and the master fault segment MF3 is the ***"First-Class"*** fault in the terminology of Gabrielsen (1984). Hence, this section represents the only example of the normal drag association of the hangingwall geometry which lies close to the tip of both the fault strands *(Fig. 3.9).*

In comparison with the normal drag, the reverse drag is not so uncommon in the study area as shown in the key profiles 1, 2, 6 & 7 *(Fig. 4.20 a,b,f,g).* These reverse drags are responsible for the development of roll-over folds above which the syn-rift sedimentary sequence deposited in essentially the half grabens *(Fig. 4.17 & Fig 4.18).*

Narrow folding / snake-head shaped accommodation structures are frequently occurring phenomenon throughout the strike-lengths of the master fault segments MF1, MF2 & MF3 as shown in their cross-sectional view *(Fig. 4.19, Fig. 4.20 a,b,c,d,g,h).* Such narrow anticlines could be explained by any of the following three plausible mechanisms:

a) Narrow folds may be attributed to the ramp-flat-ramp normal fault, where a geometrical irregularity "flat" in the fault plane can initiate narrow folds.
b) Such accommodation structures may be the consequence of inversion related to the head-on contraction or
c) Strike-slip related inversion

During the present study, observations from the cross-section reconstruction *(section 4.2)* recount that the fault plane geometries control the shape of roll-over folds present in the hanging-wall which are broad and small amplitude structures *(Fig. 4.12 & Fig. 4.13).* In addition, there is no evidence whatsoever, of the presence of ramp-flat-ramp geometries of the fault plane *(sensu-stricto) (Fig. 3.10 & Fig. 3.17).* Moreover, these narrow folds are found

stratigraphically above the roll-over folds and hence, younger in age and they are also not restricted to the areas where fault plane is curved (Fig. 4.20 a,b,c,d). Therefore, ramp-flat-ramp fault geometries can be set aside as it cannot explain the development of the narrow folds found in the study area.

The other two likely candidates responsible for the development of the narrow folds frequently found in the study area are both inversion-related. Hence a brief review of structural inversion is carried out before doing a small exercise to propose the most suitable mechanism responsible for the formation of such accommodation structures.

4.5.1 Review of the structural inversion

The term "inversion" serves to define the process of slip reversal i.e., regions that change from being the sites of subsidence to the sites of uplift or vice versa are described to have experienced "inversion". The term "positive inversion" is used for the regions that have been shifted from subsidence to uplift while "negative inversion" describes the areas that have transformed from the uplift to subsidence (Hayward & Graham, 1989).

Coward (1994) has classified various origins of structural inversion which are briefly discussed below.

i) Inversion related to isostatic forces, which is caused by elimination of the glacial overburden or by the removal of a mountain belt through erosion. In both the cases, uplift will occur to compensate for the lost loading.

ii) Inversion can also accompany the diapiric action of salt during which both the positive and negative inversion may result depending on the movement of salt up-dip or down-dip of the already tilted fault block.

iii) When plates move across the hotspots they could experience the uplift of 1-2 km and the resultant inversion structures are quite large in extent. Later, during thermal cooling the previously uplifted areas will subside.

iv) Inversion can also be associated with extensional faulting when the crust and the upper mantle (lithosphere) experience differential stretching, foot-wall uplift may occur which is termed as extension-related inversion.

v) Horizontal plate movements (tectonic inversion) lead to the plate collision processes and the oblique plate collision is considered to be the most significant of them all.

vi) Strike-slip tectonics may also result in inversion, particularly along the restraining bends of the major strike-slip faults.

vii) Inversion can also occur due to the rotational block faulting. For instance, the original extensional faults within a shear couple could rotate in a way that they align themselves closer to the orientation of the shear system, the result would be the lengthening of the block but however, if they rotate away from the shear couple's orientation the result would be the shortening. Therefore, a shear couple could induce extension or rotational-block faulting-related inversion.

viii) Inversion can also be related to the collision tectonics which is precisely termed as contraction-related inversion.

Coward (1994) further explained that when the original faults are normal growth faults, inversion leaves characteristic imprints to identify such a structure i.e., upper level of displacement along the fault resembles that of reverse fault geometry or compressive folding, whereas, at depth the net displacement may be that of extension. In the present study, several such instances are available, where the expulsion of syn-rift sequence is quite evident *(Fig. 4.19).* The syn-rift sequence and the younger overlying post-rift early Cretaceous package seem to move outward and upward towards the fault which together constitutes the typical accommodation structures of the inverted growth fault (Hayward & Graham, 1989) *(Fig. 4.20 a, b,c).*

Similarly, in order to ascertain whether the mechanism responsible for the inversion is head-on contraction or strike-slip related, a "litmus-test" / "rule of thumb" could be the analysis of the narrow fold geometries and orientations. If the axis of the fold strikes parallel to the main fault then the fold under consideration is likely to reflect a head-on contractional inversion whereas, in case of the strike-slip related inversion the fold axes are oriented obliquely to the master fault to constitute an en-echelon array of folds. Therefore, an exercise was done which dealt with the application of such a "rule of thumb" for identification of the most likely candidate for the inversion-related narrow anticlines. During the exercise, the base Cretaceous fault map was used as the base map. It was followed by mapping of the narrow folds on the key profiles where they were present, and then additional seismic lines were revisited to confirm the presence of these features. For every narrow fold identified on a seismic line, a symbol was plotted at its corresponding location on the base map and their fold axes were determined on the basis of presence of these structures on the two adjacent

lines. When such control was not available, the location of fold axes was projected *(shown in dotted red line in Fig 4.21).* At the end an interesting image evolved which predominantly showed the main-fault parallel fold-axes for the narrow folds implying contraction-related inversion *(Fig. 4.21).*

Therefore, there is a compelling evidence to believe that that the inversion structures found in the present study, are related to head-on contraction instead of strike-slip movement *(Fig. 4.21).* Additionally, instead of an array of en-echelon folds, transpressional stress systems leave other diagnostic imprints in the form of the positive flower structures of which the study area is devoid of.

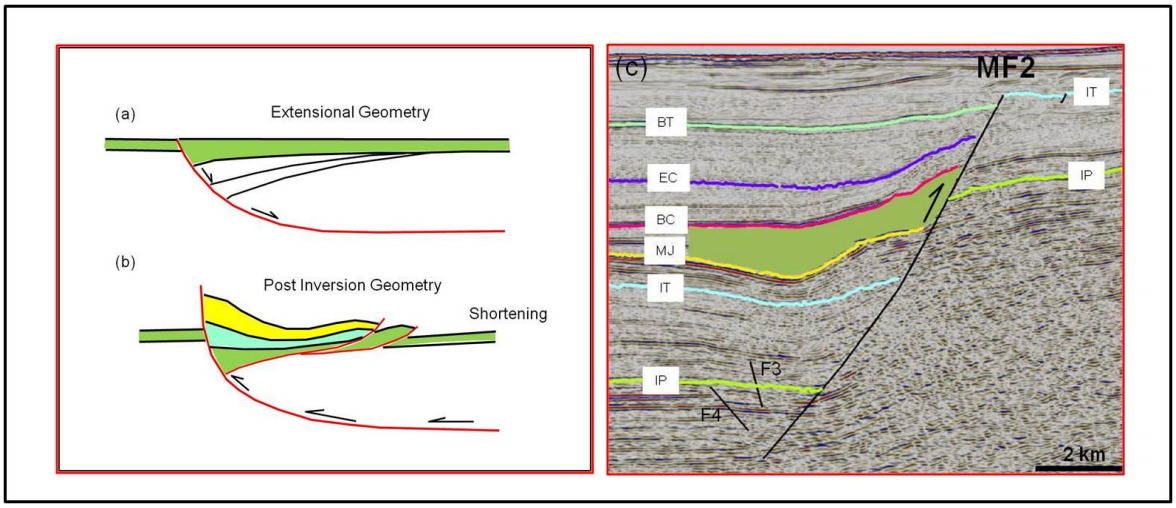

Figure 4.19: Comparison of typical inversion structure with an example from the study area. **(a)** Growth fault geometry of a typical extensional fault resulting in the formation of a half graben. **(b)** Geometrical relationship of a positively inverted extensional fault with expulsion of syn-rift strata (modified from Hayward & Graham, 1989). **(c)** Accommodation structures developed during inversion of the syn-rift sequence, notice the green highlighted package and the early Cretaceous reflection (see text for details).

At the same time however, it is relevant to consider that the present study is based on 2D reflection seismic data and all the structural analyses have been carried out on the seismic "dip-lines" that are widely apart (6-8 km). Similarly, the effects of the following mechanisms (Coward, 1994) which could also have contributed to the inversion in the study area include:

a) Foot-wall uplift related to differential stretching of lithosphere (requires a basin modeling exercise).
b) Foot-wall uplift related to isostatic adjustments in response to removal of large overburden (Tertiary uplift in the study area is very well documented, Nyland et al, 1992)

Briefly, the present comment on the orientation of the fold-axis of the narrow anticlines and the consequent interpretation of head-on contraction inversion is susceptible to errors which could only be improved by incorporating more closely spaced seismic dip-lines which are not available during this study. An age of the mid Jurassic is proposed by Gabrielsen et al. (1990) for the inversion associated with the Troms-Finnmark Fault Complex. Association of narrow folding in the hanging-wall has been found in the interpreted mid Jurassic to the early Cretaceous reflections *(Fig. 4.20 a,b,c)* while the late Jurassic to the late Cretaceous interpreted reflections also record structural inversion *(Fig. 4.20 d).* Therefore, the present study places this episodic event in the mid Jurassic through the late Jurassic to the late Cretaceous, on the basis of identification of related structural configurations.

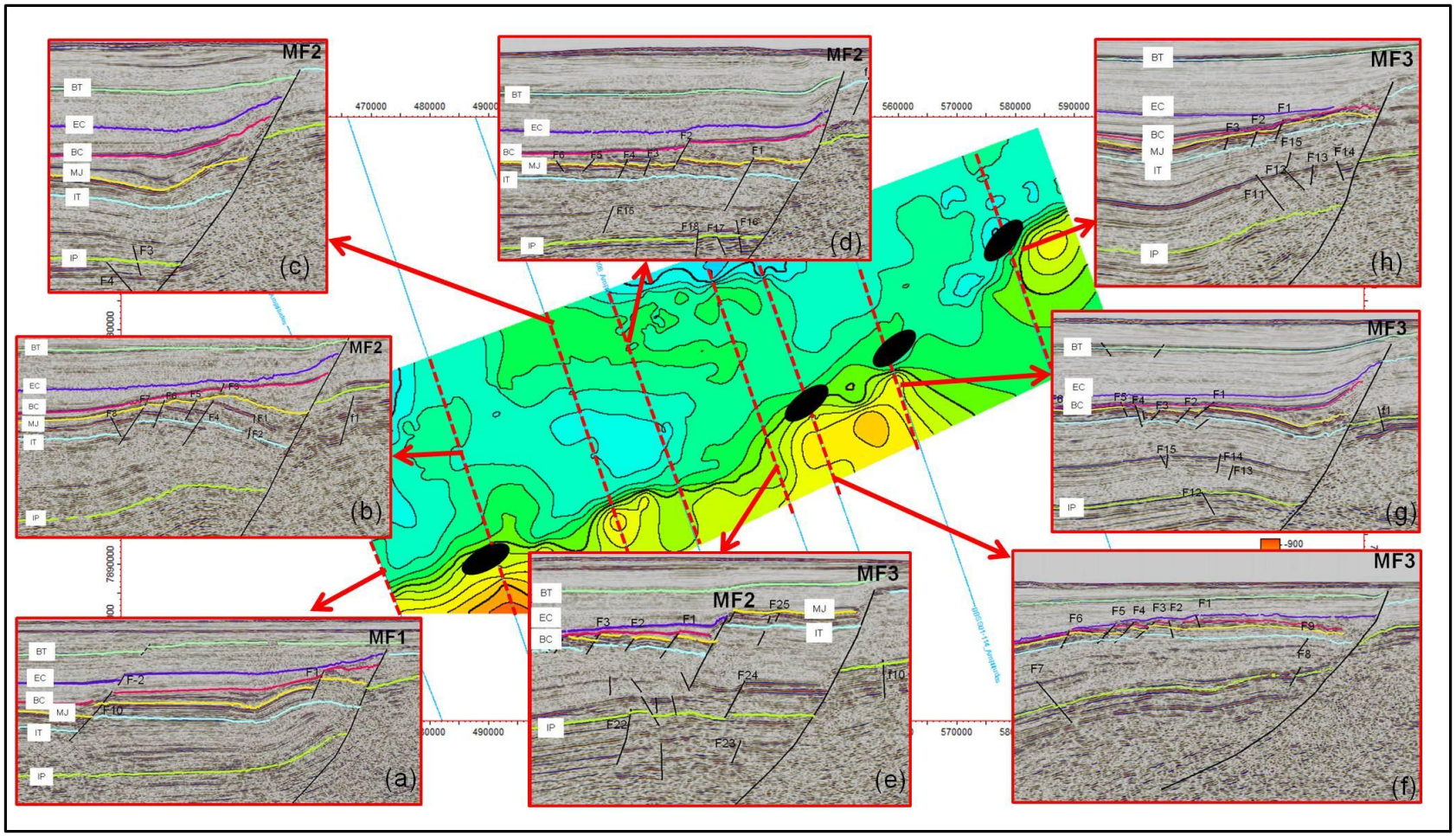

Figure 4.20: Time-structure map at the interpreted Base Cretaceous level showing the hangingwall's roll-over folds (black colored) parallel to the strike of the main boundary fault interpreted at this level. Figs. (a-h) represent the parts of the key profiles 1-8 already discussed in Chapter 3. Different hanging-wall geometries are found to be associated with the length of the fault segments ranging, such as the normal drag (inset "e"), the reverse drag (insets "f &h") and the anomalous snake-head geometries (insets "b, c, d, g").

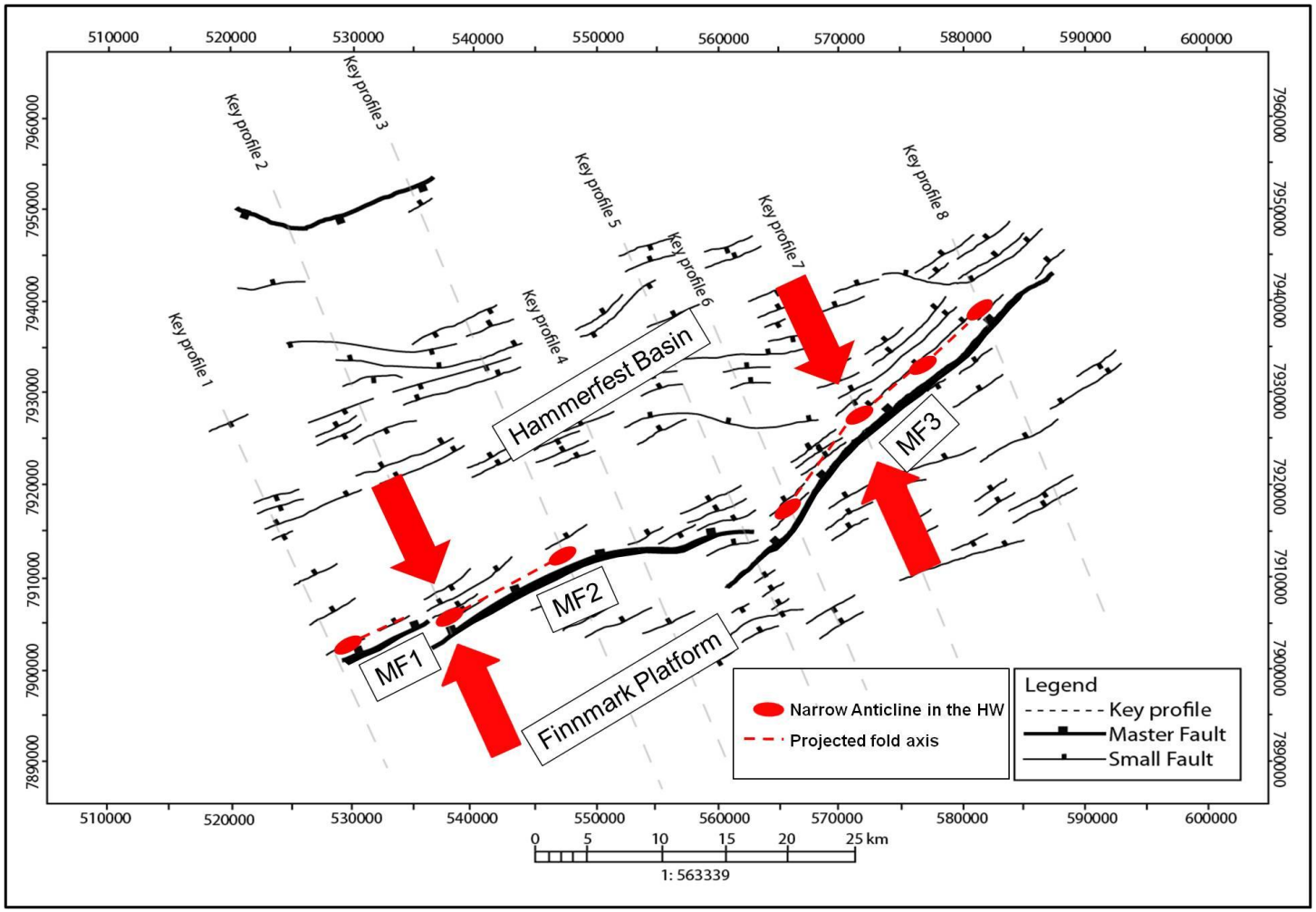

Figure 4.21: Fault Map at the interpreted Base Cretaceous level showing the orientation of kinematic indicators of inversion (narrow folds - red colored, red arrows show the direction of σ_1) striking parallel to the main boundary fault. The master fault segments (MF1, MF2, and MF3) are shown with the horizontal displacement increasing toward the centre of the faults. A novel approach to differentiate between the head-on-contraction related inversion and strike-slip related inversion is the analysis of strike of the folds' axis orientation (see text for details).

4.6 Genesis of the Troms-Finnmark Fault Complex

The area under investigation lies on the Caledonian basement which strikes in the NE-SW direction (Gabrielsen et al., 1990). Ritzman & Faleide (2007) have mapped offshore continuation of the Caledonian structures and subdivided them into the remnant of Laurantien Crust, the Scandian phase collision zone and the Fennoscandian crystalline basement of the Baltica. The closure of the Iapetus Ocean started in the Cambrian and lasted until the Devonian however, the major collision stage between the Baltica and Laurentia occurred between the Silurian to the early Devonian which is referred to as the Scandian phase of Caledonides (Roberts & Gee, 1985; Barrere et al., 2009). Different crustal units in the Barents Shelf are characterized by varying rock's physical properties (density, thermal conductivity & rheology etc) which subsequently influenced the later evolution of the sedimentary basins by controlling the processes such as regional subsidence rates, deformation styles and geothermal gradients (Gabrielsen, 1984; Ritzman & Faleide, 2007). The offshore extension of the Norwegian Caledonides is bordered on the East by the late Neoproterozoic Timanide Foldbelt. The Trollfjord-Komagelv Fault separates the Baltican Platform from the Timanian basement complex and it can be followed to the southeast into the Timan Range *(Fig. 2.3)* (Barrere et al., 2009). The northeast Atlantic rift during late Paleozoic developed within the Caledonian Foldbelt and its position and structural architecture was predominantly controlled by the pre-existing Caledonian trends (Gudlaugsson et al., 1998). The continuity of trends between the underlying Caledonian basement and the later rifting is attributed to the fact that pre-existing structural grain controls the subsequent structural development of the area (Gabrielsen 1984; Gudlaugsson et al., 1998).

The narrative put forth so far, tends to explain the type and the age of the basement on which the study area is situated. It also serves to elaborate that the older weakness zones control the later structural framework of the area by accommodating the deformation along the pre-existing structural trends. During the Devonian, extensional collapse of the Caledonides occurred (McClay et al., 1986; Norton, 1986 in Gudlaugsson et al., 1998); this event however is hard to grasp in the present study largely due to the poor signal-to-noise ratio at the pre-Permian reflection *(Fig. 4.4, Fig. 4.12 & Fig. 4.13).* Except the master fault strands MF1, MF2 & MF3 of the larger array of Troms-Finnmark Fault Complex which are the basement involved structures of regional significance and hence termed as the "***First-Class***" faults (*sensu* Gabrielsen, 1984), there is no evidence of extensional collapse in the study area either

because it has not affected the part of the Barents Shelf under investigation or the resolution of 2D used in the study, data does not warrant to identify any such feature.

The development of the Barents Sea rift system is linked with the evolution of the north-east Atlantic and Arctic rifts during the late Paleozoic (Gudlaugsson et al., 1998). Lithospheric stretching was perhaps initiated at the end of Devonian while the major rifting period belongs to the middle Carboniferous and Permian (Surlyk et al., 1984, Stemmerik & Håkansson, 1991 as cited in Gudlaugsson et al., 1998) *(Fig. 4.25).* A rift phase belonging to the Permian-early Triassic is assigned to the structural development of the western Barents Sea while an age of middle-Carboniferous has been put forward for the south-western Barents Sea (Gudlaugsson et al., 1998) of which the present study area is a small part. During the present study tectonic subsidence belonging to the late Paleozoic could not be well constrained, as the interpreted reflection at this level lacks fault-related growth sedimentary strata. However, the kinematic analysis of fault by making use of the "Expansion/Growth Index" for the key profiles 4 & 7 yielded the values of above 1; which points to the activity along the fault at the interpreted intra-Permian to the intra-Triassic reflections *(Fig. 4.15 & Fig. 4.16).* Nevertheless, interesting information is observed to be associated with the interpreted "PF fault" on the Finnmark Platform *(Fig. 4.23).* This fault documents the growth strata related to the pre-Permian deposition and provides pivotal information about the tectonic activity that influenced this area in the pre-Permian time. Gabrielsen & Færseth (1988) argued that activity along the Troms-Finnmark Fault Complex is coeval with the activity along the Vargsundet Fault that runs parallel to it on the mainland Norway which is thought to be active in the late Caledonian time. The present study cannot conclude any pre-Permian activity along the different strands (MF1, MF2 & MF3) of the Troms-Finnmark Fault Complex with confidence due to the reasons already explained. However, the Finnmark Platform in the southeast of the study area in the proximity of the master fault segment MF3, does bear the marks of pre-Permian activity documented by the "PF fault". It is therefore inferred from the information collected from the activity on the "PF Fault" that the master fault segments lying further northward to this fault might have experienced the similar kind of activity in the pre-Permian time *(Fig. 4.23).*

The Barents Shelf experienced another rifting episode during the mid Jurassic which culminated in late Jurassic to early Cretaceous periods *(Fig 4.25).* This rift phase is considered to have resulted in the formation of major basins and highs of the present day Barents Shelf (Gabrielsen et al., 1990; Faleide et al., 1993). However, structural development

associated with this rifting is quite complex with extreme tectonic subsidence in the Tromsø Basin and western part of the Bjørnøya Basin during the early Cretaceous while indications of local inversion during the early Cretaceous are also found along the Ringvassøy-Loppa Fault Complex and its intersection with the Asterias Fault Complex *(Fig. 2.1)* (Gabrielsen et al., 1990). In the study area, stratigraphic dating of the fault segments MF1, MF2 & MF3 *(Fig. 3.9)* carried out on all key profiles (1-8) *(Fig. 3.10 – Fig. 3.17)* allowed the identification of growth strata associated with the interpreted mid Jurassic through the late Jurassic to the early Cretaceous helped in bracketing the age of the fault movement *(Fig. 4.17 & Fig. 4.18).*

Gabrielsen (1984) discussed the presence of a dome shaped, elongated structure in the central part of the Hammerfest Basin which is associated with the E-W trending normal faults. Zeigler et al. (1986) proposed that some strike-slip deformation is associated with the central E-W trending fault segments of the Hammerfest Basin, while Berglund et al. (1986) suggested that transpressional movements are responsible for the doming of the central part of the Hammerfest Basin in the middle Jurassic, which later down-faulted. However, observation based on the present study, combined with the observation of another recent study on the northern main boundary fault of the basin (Mongat, 2011; master's thesis), central doming is believed to be the product of probably synchronous movements on the northward and the southward dipping Troms-Finnmark Fault Complex and the Asterias Fault Complex respectively during the mid/late Jurassic-early Cretaceous. Fault controlled thickness of the early Cretaceous sequence gives clue about the dating of the extensional collapse of the central dome of the Hammerfest Basin *(Fig. 4.4).*

Ziegler et al. (1986) associated reactivation of the Troms-Finnmark Fault Complex and the Asterias Fault Complex with the gravity induced transverse movement of the Hammerfest Basin towards the west (Tromsø Basin) while the northern and the southern main boundary faults experienced dextral and sinistral strike-slip movements respectively, in the late Cretaceous and the early Tertiary. Berglund et al. (1986) have supported the argument of Ziegler et al. (1986) that the northern main boundary fault experienced the dextral shear which resulted in doming and formation of a half flower structure towards its northwestern margin, that collapsed later on *(Fig. 4.22).* However, if the Hammerfest Basin moved westward owing to the dextral and sinistral shear couple, there must be some strike-slip deformational signature associated with the boundary faults i.e., positive flower structures at the restraining bends and the negative flower structures at the releasing bends. Towards the

southern boundary fault of the Hammerfest Basin, no such evidence has been recorded during this study, rather the deformation in the southern master fault segments (MF1, MF2 & MF3) shows typical geometries of extensional normal faults *(Fig. 4.20 a-h).* The half flower structure associated with the northwestern margin of the Asterias Fault Complex proposed by Ziegler et al. (1986) and Berglund et al. (1986) has been contested by Mongat (2011, master's thesis), who described this feature as a rollover fold associated with the ramp-flat geometry of extensional normal fault, based primarily on the newly available 3D seismic data *(Fig. 4.22).* Gabrielsen et al. (1990) have proposed reverse faulting and folding combined with extensional faulting in some areas of the Barents Shelf towards the end of the Cretaceous period *(Fig. 4.25).* There is no evidence of Cretaceous reverse faulting in the area under investigation, however; this study augments the observation of Gabrielsen et al. (1990) regarding the presence of folding in the late Cretaceous which is an inversion-related phenomenon *(Fig. 4.19c & Fig. 4.20 a b c d)*

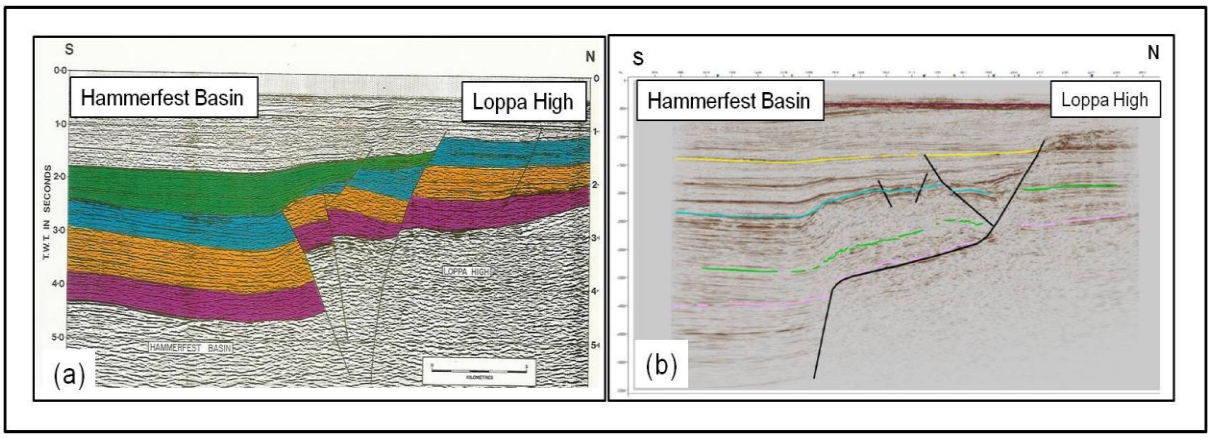

Figure 4.22: Comparison of interpreted structural geometries of the western margin of the Asterias Fault Complex (a) Ziegler et al. (1986) argued that wrenching resulted in the development of positive half flower structure (b) Mongat (2011; master's thesis) interpreted the domal feature on the 3D seismic data, as the rollover fold developed on the ramp-flat normal fault geometry.

Gabrielsen et al. (2011) explained that the Barents Sea has experienced episodes of minor tectonic inversion however; E-W extension dominated the western Barents Sea from the late Paleozoic to early Cenozoic. Additionally, Gabrielsen et al. (1990) proposed mild inversion related to the large-scale rotation, for the north-eastern segment of the Troms-Finnmark Fault Complex. The present study registers several such instances where the positive structural inversion has affected the area and it is found to be associated with all the master fault segments (MF1, MF2 & MF3) and concludes that this phenomenon is related to the head-on contraction *(Fig. 4.19 & Fig. 4.20) (see section 4.6 for discussion on structural inversion).*

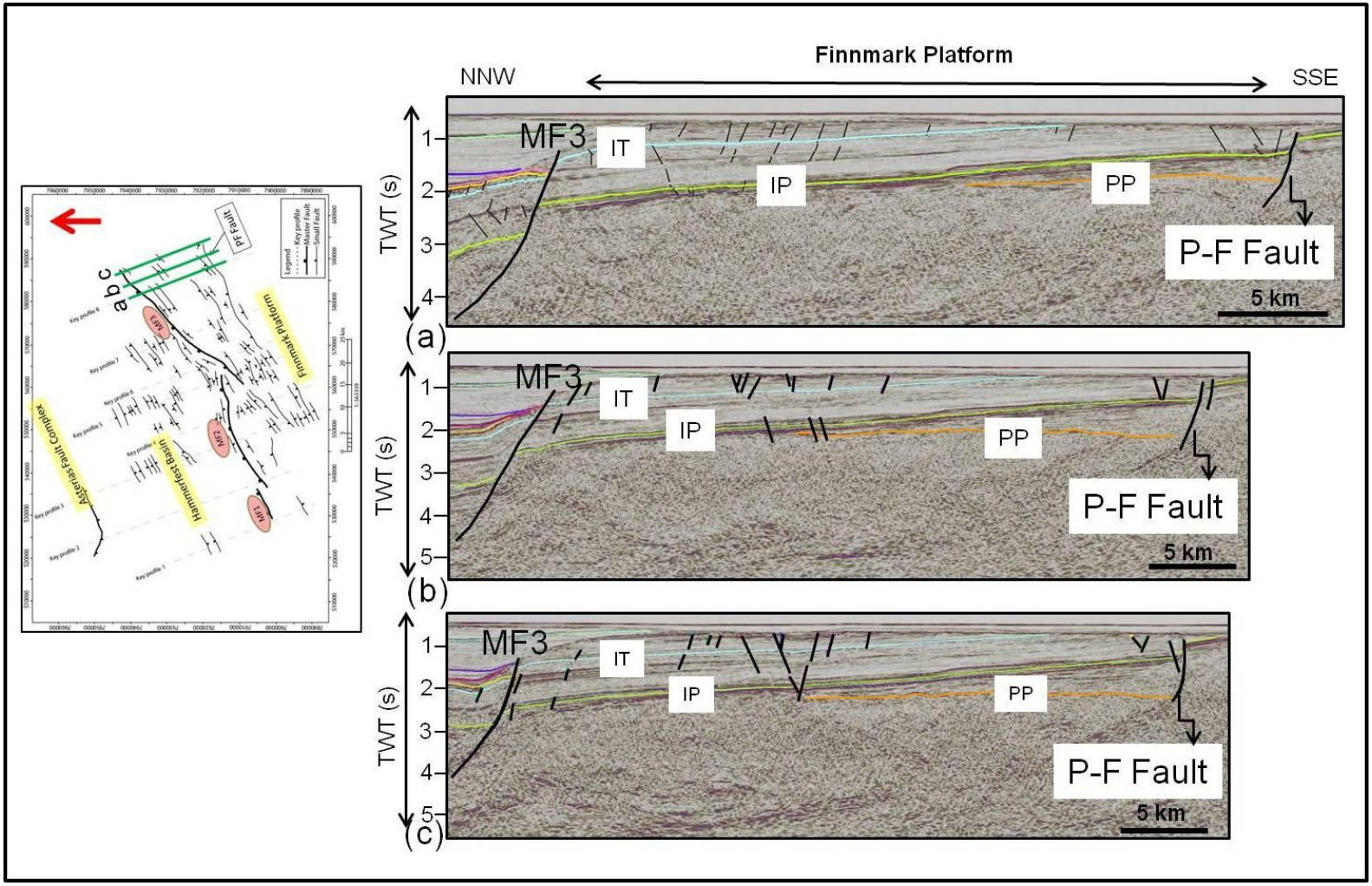

Figure 4.23: A set of three cross-sections (a,b,c) taken from the north-eastern segment (MF3) of the Troms-Finnmark Fault Complex, location and extent of the lines are shown in green color on the Permian fault map shown in the inset. Geometry of the PF Fault along with the associated syn-rift sedimentation between interpreted intra-Permian and the pre-Permian fault. This fault is interpreted on the footwall side of the fault segment MF3 on the Finnmark Platform, and is representative of pre-Permian tectonic activity in the study area.

The key profile 7 *(Fig. 3.17 a,b)* clearly demonstrates the development of reverse drag and it shows the presence of a syn-rift sequence enclosed in the mid-Jurassic to the base-Cretaceous reflections, however, the reverse drag is overlain by a narrow contractional fold registering slip-reversal *(see section 4.6 for details of structural inversion)* which is shown by all the interpreted reflections younger than the intra-Triassic. It is therefore believed that the formation of rollover anticline and the associated syn-rift fill is followed shortly by the mild positive structural inversion during which the slip-reversal occurred that resulted in the formation of a narrow fold in this cross-section *(Fig. 3.17ab, Fig. 4.20g).* Similarly, there are instances where the interpreted late-Jurassic to the early-Cretaceous reflections records structural inversion *(Fig. 4.20).* Therefore, the present study places the head-on contraction related inversion in the mid-Jurassic through the late-Jurassic to the late-Cretaceous, on the basis of identification of related structural configurations.

Gabrielsen & Færseth (1989) proposed the large scale rotation around a vertical axis to be responsible for the inversion related to the Troms-Finnmark Fault Complex while the present study on the basis of analysis of kinematic indicators of inversion structures *(Fig. 4.21)* postulates that the compressive stresses acting perpendicular to the master faults are the most likely candidates. The origin of such a stress system which is coeval with an overall extensional tectonic regime could be explained by the "Gabrielsen's matchbox experiment" in which a far-field stress system could result in simultaneous extension, contraction and along-strike movements of the match boxes and the major deformation is focused on the boundaries rather than intra-matchbox area *(*Gabrielsen, 2010; Class Lectures, Geo 4230*).* Therefore, such an analogy can explain the complex interaction of contractional features associated with the Troms-Finnmark Fault Complex in a regional extensional tectonic framework.

Early Tertiary lithospheric stretching related to rift-related opening of Norwegian-Greenland Sea is a significant structural development in the Barents Sea region (Faleide et al., 1993a). Reactivation of the master fault segments MF1, MF2 & MF3 of the large array of Troms-Finnmark Fault Complex in the Tertiary is attributed to this rifting process and the present study clearly shows that the master fault segments affect the strata of the Paleogene *(Fig. 3.10 to Fig. 3.17, Fig. 4.4 & Fig. 4.20).* Significant uplift and erosion in the Barents Sea during Tertiary is confirmed by the studies of vitrinite reflectance, apatite fission tracks, shale compaction curves and diagenesis of clay minerals as well as by the comparison of seismic sequence geometries with the syn-rift rock volumes (Nyland et al., 1992) *(Fig. 4.25).*

4.7 Paleo-stress Analysis

Quality information on the development of stress system is mandatory in order to comprehend the tectonic evolution of the crust (Gruenthal & Stromeyer, 1986 in H. W. van Gent et al., 2009). There are several methods to determine the contemporary in-situ stress system such as, the earthquake focal mechanisms and analysis of the borehole breakouts and related methods; however, quantifying the paleo-stress is quite challenging (H. W. van Gent et al., 2009). The classical literature on the paleo-stress analysis is based on the observations recorded in the outcrops (e.g., Angelier, 1994). An outcrop-based study to analyze the neotectonic stress orientation and magnitudes is conducted in the Finnmark area, northern Norway by Pascal et al. (2005). They made use of stress relief features associated with quarrying and road cuts, such as borehole offsets and vertical fractures in the concave remnants of boreholes and quantified the shallow stress orientations and magnitudes however, such a method is not workable as the present study is based on the reflection seismic data. Nevertheless, some recent literature is also available which uses the reflection seismic data for the reconstruction of paleo-stress systems (e.g., H.W. van Gent et al., 2009). This kind of approach follows the following workflow:

i) High resolution seismic interpretation of faults and reflections employing 3D seismic data in order to record the paleo-slip orientation on individual faults
ii) The 3D reconstruction to remove the effect of younger deformation in order to constrain the slip direction of the older faults.
iii) Analysis of fault displacements and fault orientation data to compute paleo-stress tensor.

However, due to time constraints of the present study, such an analysis could not be performed rather only first order estimate of the orientation of the paleo-stress system is carried out and is presented in the *Figure 4.25,* which obviously does not consider the stress anisotropy. This kind of Andersonian interpretation of a newly formed North-South oriented graben system postulates the vertical σ_1 and an East-West oriented σ_3 thereby disregarding the likelihood of an oblique-slip while the relative size of the principle stresses also remains unknown (H. W. van Gent et al., 2009). Therefore, the local paleo-stress orientations *(Fig. 4.25)* proposed during this study must be viewed along with the constraints described above. A brief correlation of the observed paleo-stress orientations extracted from the present structural analysis with the regional paleo-stress orientations is carried out in the backdrop of the plate tectonic settings of the Barents Sea using the model of Ziegler (1988) as a reference.

According to Ziegler (1988) the Caledonian orogeny (late Cambrian -Silurian time) resulted in the suturing of Laurentia-Greenland and Fennosarmatia. Similarly, it also involved the collision of the Arctic terrane with the northern margin of Laurentia and Greenland *(Fig. 4.24 a).* The Hercynian plate reconstruction points to the back-arc rifting towards the Innuitian foldbelt which includes subsidence of the Sverdrup Basin during the Carboniferous possibly because of the following two reasons:

a) Rifting between the West Siberian Craton and Laurussia.
b) Development of the Norwegian-Greenland Sea rift system.

Similarly, during the Carboniferous, the Uralian orogenic cycle initiated due to the collision between the West Siberian Craton with the Kazakhstan Craton and the eastern margin of Fennosarmatia. This orogeny culminated during the late Permian-early Triassic and resulted in the formation of the Ural-Novaya Zemlya-Taimir and the Altay-Sayan foldbelts *(Fig. 4.24b).* Mosar et al. (2002) interpreted an E-W oriented minimum principal stress orientation for this age *(see the red arrows in Fig. 4.24 b)* while during the present study, based on the analysis of the interpreted Intra-Permian time-structure map *(Fig. 3.9 & Fig. 4.25)* the orientation of a WNW-ESE oriented σ_3 shows considerable variation from the regional stress orientation.

During the mid-Jurassic to early Cretaceous, formation of the Northwest European graben systems was predominantly controlled by the tensional stresses to the Arctic-North Atlantic rifting. During the early Cretaceous, sea-floor spreading axis of the Central Atlantic stretched into the North Atlantic province (Ziegler 1988). Mosar et al. (2002) interpreted a WNW-ESE oriented minimum principal stress orientation for these ages *(see the red arrows in Fig. 4.24 c,d)* whereas, the present study on the basis of interpretation of the structural and the isopach maps, postulates a NE-SW oriented σ_3 during the mid-Jurassic *(Fig. 3.20; Fig. 3.30 & Fig. 4.25),* similarly, the minimum principal stress orientation for the early Cretaceous time is interpreted to be NW-SE *(Fig. 3.24; Fig. 3.30 & Fig. 4.25).*

According to Ziegler (1988), during the late Paleocene-early Eocene, the sea-floor spreading axis of the North Atlantic further stretched into the Baffin Bay, the Norwegian-Greenland Sea, and the Eurasian Basin. It was accompanied by rotation of North America, Greenland, and Eurasia relative to each other which induced the contractional deformation of the eastern Sverdrup Basin along with the western margin of the Barents Shelf that resulted in the formation of the Eurekan and Spitsbergen orogens. Mosar et al. (2002) interpreted a NW-SE

oriented minimum principal stress orientation for this time period *(see the red arrows in Fig. 4.24 f)* whereas, the present study on the basis of interpretation of the structural and the isopach maps, indicates a NW-SE oriented σ_3 during the mid-Tertiary, which is in agreement with the regional interpretation of Mosar et al. (2002) *(Fig. 3.26; Fig. 3.31).*

The discussion presented in the above paragraphs is summarized in the form of a timeline which shows sequential development of regional tectonic framework of the southwestern Barents Sea along with the local tectonics and stress orientations from the present study *(Fig. 4.25).* This event chart is based on the lithostratigraphic interpretation of Glørstad-Clark et al. (2011) while the regional tectonic events and stress orientations are based on the studies of Ziegler (1988) and Mosar et al. (2002) (discussed above) and it serves to conclude the results of the present study as well.

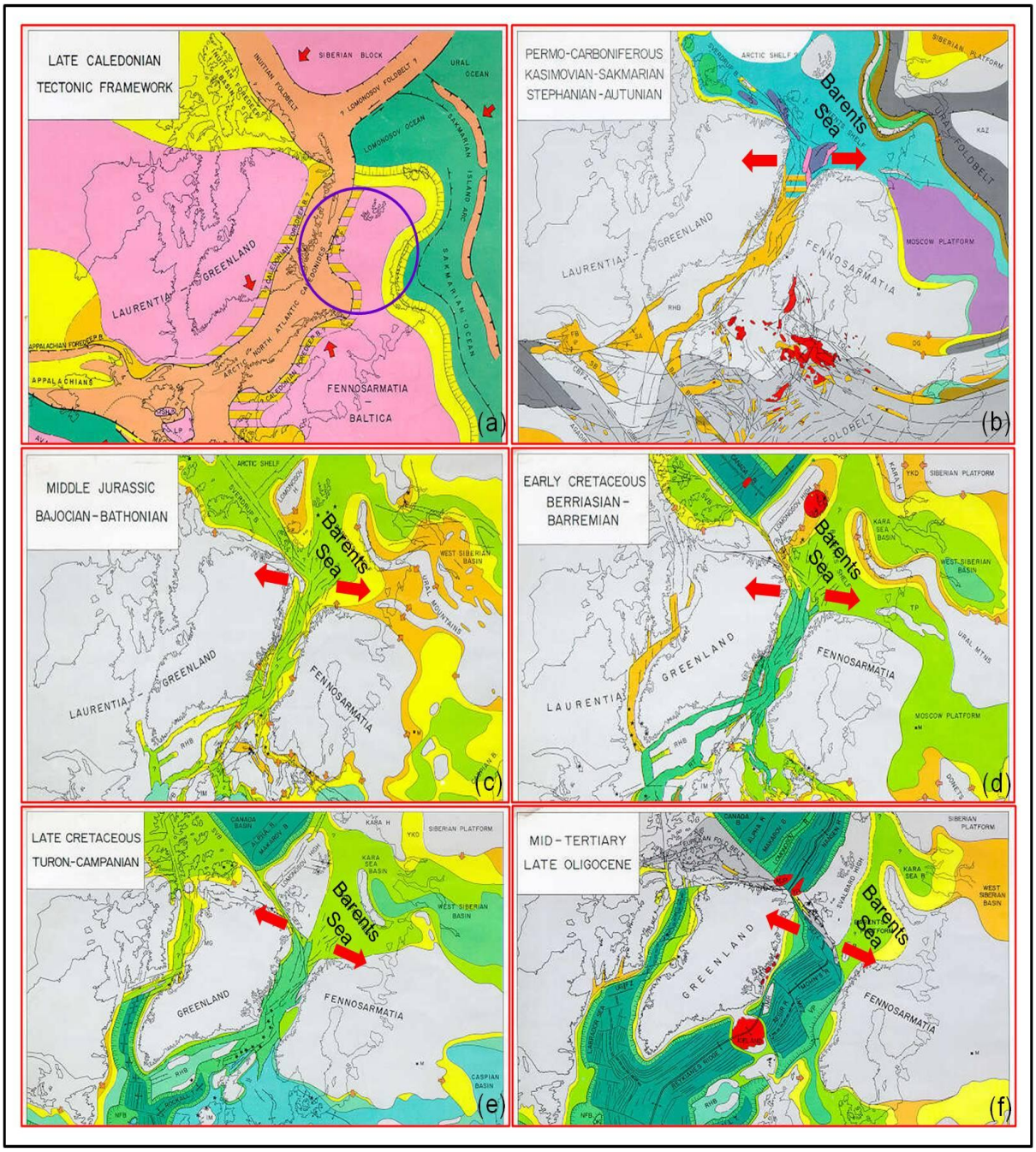

Figure 4.24: Paleo-geographic reconstruction of the surrounding of the Barents Sea and adjacent areas (modified from Ziegler 1988). (a) Late-Caledonian tectonic framework, purple circle indicating the approximate area of future Barents Sea (b) Permo-Carboniferous tectonic framework showing start of Norwegian-Greenland Sea opening, with minimum principal stress orientation in EW direction (c) Middle-Jurassic tectonic arrangement showing change in minimum principal stress orientation from EW to ENE-WSW (d) Early Cretaceous tectonic setup with the same σ_3 orientation as in the previous frame (e) Late Cretaceous tectonic setting, note the change in σ_3 orientation from the previous frame to NW-SE (f) Mid-Tertiary-late Oligocene tectonic framework showing almost complete development of the Norwegian Greenland Sea and the σ_3 orientation remains the same as in the previous frame. The minimum principal stress orientation (σ_3) is derived from Mosar et al. (2002).

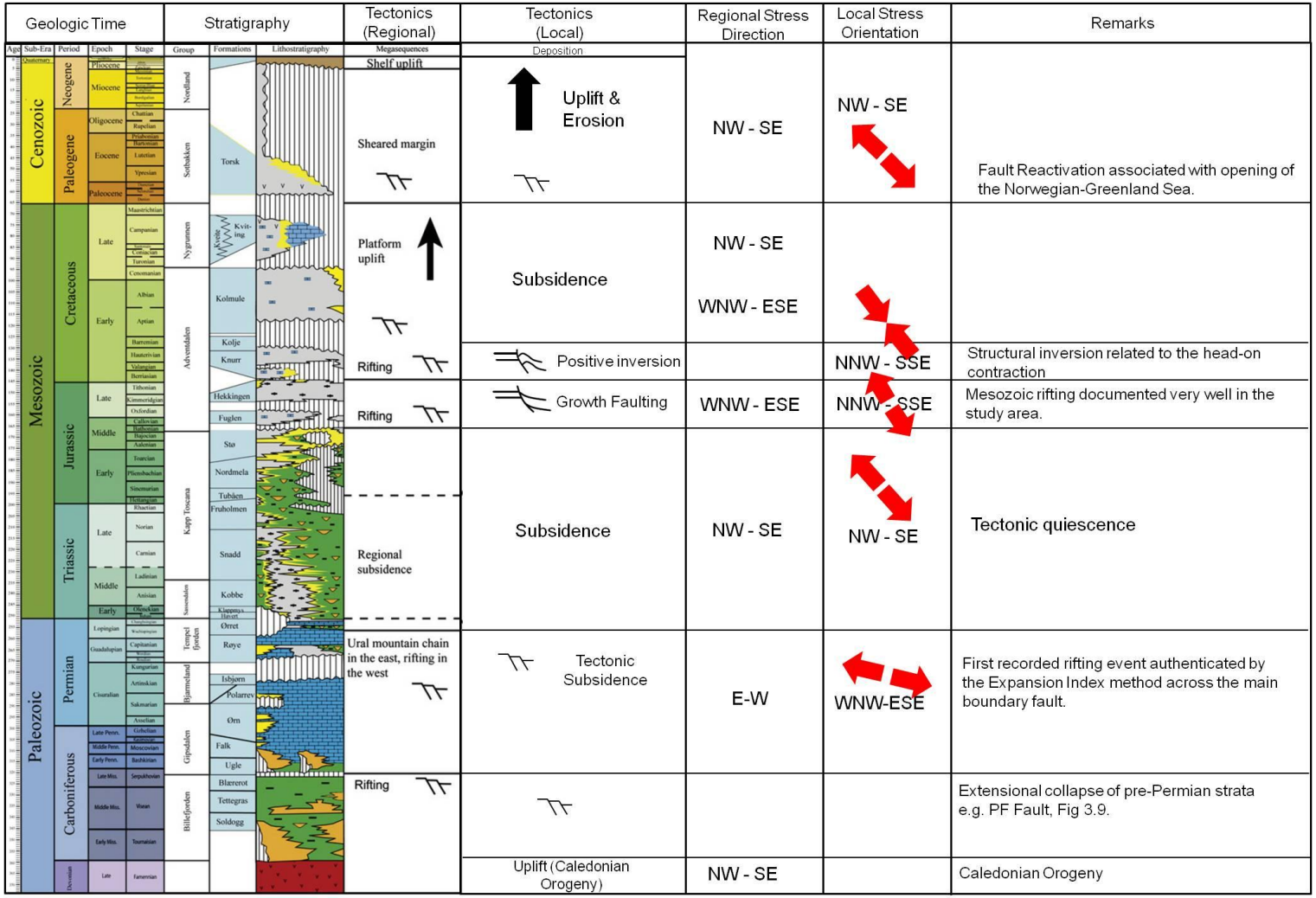

Figure 4.25: A timeline showing regional tectonic events (modified from Glørstad-Clark et al., 2011) in comparison with the local tectonic events in the study area. Regional stress orientations are modified from Ziegler (1988) and Mosar et al. (2002) while the local stress orientations (red arrows) are based on the present study.

Chapter 5
Highlights of the study

5.1 Conclusion

The Troms-Finnmark Fault Complex in the study area comprises of the three fault strands MF1, MF2 and MF3, which constitute together a softly-linked fault system. Their mutual relationship is termed as "approaching-synthetic" which are arranged in an en-echelon pattern. This fault complex has a regional significance as it separates the Hammerfest Basin in the North from the Finnmark Platform in the south. The cross-sections along the fault segments (MF1, MF2 & MF3) display a wide spectrum of the master fault geometries which range from the planar normal fault through the slightly curved normal fault to the typical listric normal fault, which all show a down-to-the-North displacement. Additionally, in the cross-sectional view, these fault segments clearly cuts the pre-Permian strata and continues down-section thereby most likely involving the basement, therefore, the basement-involvement and regional significance of the three fault strands (MF1, MF2 & MF3) qualifies them to be placed in the category of the ***"First-Class"*** faults. The maximum fault displacement is associated with the central fault strand MF2 where the displacement values exceed 2.7 km towards the centre of the master fault, while the maximum fault displacement values for the fault segment MF3 towards the centre are slightly above 2.5 km at the intra Permian level. The cross-section restoration on selected key profiles (2 & 6) by using the forward modeling technique determined that the fault plane geometry and the associated hangingwall folding are kinematically linked.

Fault dating is done by employing the established techniques of growth index examination and identification of syn-rift sedimentation. The expansion index yielded values of above 1 for the sedimentary package between the intra-Permian and the intra-Triassic reflections, across the fault strands MF2 and MF3, which indicates the fault-related growth strata associated with this age. The NE-SW trending master fault segment MF1, on the basis of recognition of growth sequence is assigned an age of middle-to-late Jurassic. The ENE-WNW trending master fault segment MF2 shows two distinctive growth sequence associations from the west to the east strike-wise and it is assigned the age of middle/late Jurassic-early-Cretaceous, representing a bicyclic kinematic behavior. The NE-SW trending master fault segment MF3 also displays a bicyclic kinematic behavior and an age of the middle/late Jurassic – early Cretaceous has been assigned to this fault segment.

The present study registers several instances (narrow folds) where the positive structural inversion has affected the area and it is found to be associated with all the master fault segments (MF1, MF2 & MF3). The analysis of kinematic indicators of inversion structures suggests that the compressive stress system acting perpendicular to the master faults is the most likely mechanism to control inversion in the study area. Therefore, these inversion structures are proposed to be head-on contraction related structures instead of any association with the strike-slip movements. The present study places this episodic event in the mid-Jurassic through the late-Jurassic to the late-Cretaceous on the basis of identification of related structural configurations.

The Troms-Finnmark Fault Complex has experienced repeated reactivations since the Caledonian orogeny. Tectonic subsidence belonging to the late Paleozoic could not be well constrained, as the interpreted reflection at this level lacks fault-related growth sedimentary strata. However, the kinematic analysis of fault by making use of the "Expansion/Growth Index" yielded the values of above 1; which points to the activity along the fault at the interpreted intra-Permian to the intra-Triassic reflections' level. Second regional rifting event recorded in the Barents Sea has also influenced the study area. Stratigraphic dating of the fault segments MF1, MF2 & MF3 carried out on all key profiles (1-8) allowed the identification of growth sequences associated with the interpreted mid Jurassic through the late Jurassic to the early Cretaceous, which helped in bracketing the age of the fault movement. The Troms-Finnmark Fault Complex show reactivation in the Tertiary, constrained by the affect of the master faults on the Paleogene strata.

The first order estimate of the orientation of the paleo-stress system is carried out. During the present study, based on the analysis of the interpreted intra Permian time-structure map and the time thickness map (intra Permian – intra Triassic), the orientation of a WNW-ESE oriented σ_3 is interpreted which shows considerable variation from the regional stress orientation. Similarly, the present study on the basis of interpretation of the structural and the isopach maps, postulates a NE-SW oriented σ_3 during the mid-Jurassic, while the minimum principal stress orientation for the early Cretaceous is interpreted to be NW-SE which is also not in agreement with the regional stress orientation at this age defined by previous authors. Additionally, the present study on the basis of interpretation of the structural and the isopach maps, indicates a NW-SE oriented σ_3 during the mid-Tertiary, which is in agreement with the regional interpretation of stress orientation defined by previous authors.

5.2 Recommendations for relevant future work

The present structural analysis has been accomplished during a limited amount of time (17 weeks). Therefore, a number of relevant issues are left unaddressed which are important to include into any such study which will further help towards better understanding of the area under investigation. They include;

i) Analysis of the tectonic and thermal subsidence for different rift phases that influenced the study area. This exercise will involve basin modeling and will yield significant information on quantification of tectonic and thermal subsidence related to different rifting periods.

ii) Estimation of beta factor in order to constrain the cumulative stretching experienced by the Hammerfest Basin.

iii) Compaction modeling during cross-section restoration in order to obtain the geometrically and geologically realistic results.

iv) There is a need to revisit the mapping of narrow anticlines by adding more seismic dip lines (preferably 3D seismic if possible) in order to understand their relationship with the neighboring master fault.

v) Analysis of other inversion mechanisms which might have contributed to the mid-Jurassic to the late-Cretaceous inversion in the study area, such as, footwall uplift related either to the differential stretching of the lithosphere or the isostatic adjustment in response to the late Tertiary erosion, needs further investigation.

vi) Detailed paleo-stress analysis of the study area following the technique offered by H. W. van Gent et al. (2009).

References

Amogu, D. K., Filbrandt, J., Kadipo, K. O., & Onuoha, K.,, 2011, Seismic interpretation, structural analysis, and fractal study of the Greater Ughelli Depobelt, Niger Delta basin, Nigeria: Leading Edge, v. 30, p. 640-648

Angelier, J., 1994, Fault slip analysis and paleostress reconstruction. In: Hancock, P.L., (Ed.) Continental Deformation, Pergamon Press, Oxford, p. 53-100.

Aydin, A., & Nur, A., 1985, The types and role of stepovers in strike-slip tectonics. In: Biddle, K.T., and Christie-Blick, N., (Eds.), Strike-slip deformation, basin formationand sedimentation: Society of Economic Paleontologists and Mineralogists Special Publication, v. 37, p. 35-44.

Barrere, C., Ebbing, J., & Gernigon, L., 2009, Offshore prolongation of Caledonian structures and basement characterization in the western Barents Sea from geophysical modelling: Tectonophysics, v. 470, p. 71-88.

Beckinsale, R.D., Reading, H. G., & Rex. D. C, 1975, Pottasium-argon dates for basic dykes from east Finnmark: Stratigraphic and Structural implication: Scottish Journal of Geology, v. 12, p. 51-65.

Berglund, L.T., Augustson, J., Farseth, R., Gjelberg. J. & Ramberg-Moe, H., 1986, The evolution of the Hammerfest Basin. In: A. M. Spencere (Ed.), Habitat of Hydrocarbons on the Norwegian Continental Shelf, Graham and Trottman, London, p. 319-338.

Berthelsen, A., & Marker, M., 1986, 1.9-1.8 Ga old strike-slip megashears in the Baltic Shield, and their plate tectonic implications: Tectonophysics, v. 128, p. 163-181.

Bischke, R. E., 1994, Interpreting sedimentary growth structures from well log and seismic data (with examples): AAPG Bulletin, v. 78, p. 873–892.

Bosworth, W., 1985, Geometry of propogating continental rifts: Nature, v. 315, p. 625-627.

Brekke, H., & Riis, F., 1987, Mesozoic tectonics and basin evolution of the Norwegian shelf between 60^0 N and 72^0 N: Norsk Geologisk Tidsskrift, v. 67, p. 295-322.

Cartwright, J., Bouroullec, R., James, D., & Johnson, H., 1998, Polycyclic motion history of some Gulf Coast growth faults from high-resolution displacement analysis: Geology, Geological Society of America, v. 26; no. 9, p. 819–822.

Coward, M., 1994, Inversion tectonics. In: P.L. Hancock, (Ed.) Continental Deformation, Pergamon Press, Oxford p. 289-304.

Dalland, A., Worsley, D., & Ofstad, K.,, 1988, A lithostratigraphic scheme for the Mesozoic and Cenozoic succession offshore mid- and northern Norway: Norwegian Petroleum Directorate, Bulletin no.4, p. 1-65.

Davis, G. H., 1984, Concept of detailed structural analysis. In: G. H. Davis, Structural Geology of Rocks and Regions. John Wiley & Sons, New York., p. 16-35.

Davis, G. H., 1984, Faults. In: G. H. Davis, Structural Geology of Rocks and Regions. John Wiley & Sons, New York., p. 261-324.

Davison, I., 1986, Listric normal fault profiles: calculation using bed-length balance and fault displacement: Journal of Structural Geology, v. 8, p. 209-210.

Davison, I., 1994, Linked fault systems; extensional, strike-slip and contractional. In: Hancok, P.L., (Ed.) Continental Deformation, Pergamon Press, Oxford, p. 121-142.

Dengo, C. A., & Røssland, K. G., 1992, Extensional tectonic history of the western Barents Sea. In: R. M. Larsen, H. Brekke, B. T. Larsen & E. Talleraas (Eds.), Structural and Tectonic Modeling and its applications to Petroleum Geology. Norwegian Petroleum Society, Special Publication v.1, p. 91-107.

Edwards, M. B., 1995, Differential subsidence and preservation potential of shallow-water Tertiary sequences, Northern Gulf Coast Basin, USA. In: Plint, A. G., (Ed.), Sedimentary facies analysis: International Association of Sedimentologists, Special Publication v. 22, p. 265–281.

Ellis, P. G., & McClay, K. R. , 1988, Listric extensional fault systems - results of analogue model experiments: Basin Research, v. 1, p. 55-70.

Faleide, J. I., Bjørlykke, K., & Gabrielsen, R. H., 2010, Geology of the Norwegian Continental Shelf. In: K. Bjørlykke (Ed.). Petroleum Geoscience: From Sedimentary Environment to Rock Physics, Springer, Berlin, p. 467-501.

Faleide, J. I., Gudlaugsson, S. T. & Jacquart, G., 1984, Evolution of the western Barents Sea: Journal of Marine and Petroleum Geology, v. 1, p. 123-150.

Faleide, J. I., Solheim, A., Fiedler, A., Hjelstuen, B.O., Andersen, E.S., & Vanneste, K., 1996, Late Cenozoic evolution of the western Barents Sea Svalbard continental margin: Global and Planetary Change, v. 12, p. 53-74.

Faleide, J. l., Gudlaugsson, S.T., Eldholm, O., Myhre, A.M. & Jackson, H.R., 1991, Deep seismic transects across the sheared western Barents Sea-Svalbard continental margin: Journal of Marine and Petroleum Geology, v. 189, p. 73- 89.

Faleide, J. l., Vlignes, E. & Gudlaugsson, S.T., 1993a, Late Mesozoic-Cenozoic evolution of the southwestern Barents Sea in a regional rift-shear tectonic setting: Journal of Marine and Petroleum Geology, v. 10, p. 186-214.

Faleide, J. l., Vlignes, E. & Gudlaugsson, S. T., 1993b, Late Mesozoic-Cenozoic evolution of the southwestern Barents Sea. In: J. R. Parker (Ed). Petroleum Geolgoy of Northwest Europe: Proceedings of the 4th conference,The Geological Society London, p. 933- 950.

Fossen, H., & Gabrielsen R. H. , 1996, Experimental modeling of extensional fault systems by use of plaster: Journal of Structural Geology, v. 18, p. 673-687.

Fønstelien, S., & Horvei, A., 1979, Thoughts and considerations arising from the study of a "prospective" feature in the Troms I area. Proceedings, Norwegian Sea Symposium, Tromso: Norwegian Petroleum Society, v. NSS/20, p. 1-10.

Gabrielsen, R. H., 1984, Long-lived fault zones and their influence on the tectonic development of the southwestern Barents Sea: Journal of the Geological Society, London, v. 141, p. 651-662.

Gabrielsen, R. H., 2010, The structure and hydrcarbon traps of sedimentary basins. In: K. Bjørlykke, (Ed.) Petroleum Geoscience: From Sedimentary Environments to Rock Physics. Springer, Berlin, p. 299 – 327.

Gabrielsen, R. H., 2009, Class Lecture – Geo 4230. Structural Analysis, Tectonic Regimes and Plate Tectonics. University of Oslo, Norway.

Gabrielsen, R. H., & Faerseth, R. B., 1988, Cretaceous and Tertiary reactivation of master fault zones of the Barents Sea (extended abstract). In: W. K. Dallman, Y. Ohta & A. Adnresen (Eds.) Tertiary Tectonics of Svalbard. Extended abstracts from Symposium held in Oslo 26 & 27 April 1988. Norsk Polarinstitutt, Report Series 46, p. 93-97.

Gabrielsen, R. H., & Faerseth, R. B., 1989, The inner shelf of North Cape, Norway and its implications for the Barents Shelf-Finnmark Caledonide boundary. A comment: Norsk Geologisk Tidsskrift, v. 69, p. 57-62.

Gabrielsen, R. H., Faerseth, R. B., Hammar. G., & Ronnevik, H., 1984, Nomenclature of the main structural features on the Norwegian Continental Shelf north of 62nd parallel. In: A. M. Spencer et al., (Eds.), Petroleum Geology of the North European Margin. Norwegian Petroleum Society, Graham & Trotman, London, p. 40-60.

Gabrielsen, R. H., Faerseth, R. B., Jensen, L. N., Kalheim, J. E., & Riis, F, 1990, Structural elements of the Norwegian continental shelf. Part 1: The Barents Sea region: Norwegian Petroleum Directorate, Bulletin no. 6, p. 1-33.

Gabrielsen, R. H., Faleide, J. I., Pascal.C. & Torsvik,T. H., 2011, Plate tectonics and tectonic inversion in the Barents Sea, Abstract: AAPG 3P Arctic, The Polar Petroleum Potential Conference & Exhbition, 30 August – 2 September, Halifax, Nova Scotia, Canada, Search and Discovery Article # 90130

Gabrielsen, R. H., Grunnaleite, I., & Rasmussent, E., 1997, Cretaceous and Tertiary inversion in the Bjornoyrenna Fault Complex, south-western Barents Sea: Marine and Petroleum Geology, v. 14 No. 2, p. 165-178.

Gabrielsen, R.H., Klovjan, O.S., Rasmussen, A., & Stolan, T., 1992, Interaction between halokinesis and faulting: structuring of the margins of the Nordkapp Basin, Barents Sea region. In: R. M. Larsen, H. Brekke, B. T. Larsen & E. Talleraas (Eds.) Structural and Tectonic Modelling and its applications to Petroleum Geology, Norwegian Petroleum Society Special Publication, v. 1, p. 121-131.

Gibbs, A. D., 1983, Balanced cross-section construction from seismic lines in areas of extensional tectonics: Journal of Structural Geology, v. 5, p. 153-160.

Glørstad-Clark, E., Birkeland, E. P., Nystuen, J. P., Faleide, J. I., and Midtkandal, I., 2011, Triassic platform-margin deltas in the western Barents Sea: Marine and Petroleum Geology, v. 28, p. 1294-1314.

Glørstad-Clark, E., Faleide, J. I., Lundschien, B. A. & Nystuen, J. P. , 2010, Triassic seismic sequence stratigraphy and paleogeography of the western Barents Sea area: Marine and Petroleum Geology, v. 27, p. 1448-1475.

Grosshong, R.H., 1989, Half-graben structures: balanced models of extensional fault-bend folds: Geological Society America, Bulletin, v. 101, p. 96-105.

Gruenthal, G., & Stromeyer, D., 1986, Stress pattern in Central Europe and adjacent areas: Gerlands Beitraege zur Geophysik, v. 95, p. 443–452.

Gudlaugsson, S. T., Faleide, J. I, Fanavoll, S. & Johansen, B., 1987, Deep seismic refleciton profiles across the western Barents Sea: Geophysical Journal of Royal Astronomical Society, v. 89, p. 273-278.

Gudlaugsson, S. T., Faleide, J. I., Johansen, S. E., & Breivik, A. J, 1998, Late Paleozoic structural development of the south-western Barents Sea: Marine and Petroleum Geology, v. 15, p. 73-102.

H. W. van Gent, B., S., Urai, J. L., Kukla, P. A., & Reicherter, K., 2009, Paleostresses of the Groningen area, the Netherlands-Results of a seismic based structural reconstruction: Tectonophysics, v. 470, p. 147–161.

Handin, J., 1969, On the Cooulomb-Mohr failure creiterion: Journal of Geophysical Research, v. 74, p. 5343-5348.

Hanisch, J., 1984a, West Spitzbergen Fold Belt and Cretaceous opening of the Northeast Atlantic: In: A. M. Spencer et al. (Ed.) Petroleum Geology of the North European continental Margin. Norwegian Petroleum Society, Graham & Trotman, London, p. 187-198.

Hanisch, J., 1984b, The Cretaceous opening of the Northeast Atlantic: Tectonophysics, v. 101, p. 1-23.

Harland, W.B., 1969, Contribution of Svalbard to the evolution of the North Atlantic region. In: MCKAY (Eds.), North Atlantic Geology and Continental Drift. American Association of Petroleum Geologists Memoir, v. 12, p. 817-857.

Harland, W.B., 1985, Caledonides Svalbard. In: D.G. Gee and B.A. Staut (Eds.), The Caledonides Orogeny – Scandinavia and Related Areas. John Wiley and Sons, Chichester, p. 999-1016.

Harland, W.B., Cutbill, J. L., Friend, P. F., Gobbett, D. J., Holliday, D. W., Maton, P. I., Parker, J. R. & Wallis. R. H., 1974, The Billefjorden Fault Zone, Spitsbergen. The long history of a major tectonic lineament: Norsk Polarinstitutt Skrifter, v. 161, p. 72.

Hayward, A.B., & Graham, R. H., 1989, Some geometrical characterstics of inversion. In: M. A. Cooper & G. D.Williams, (Eds.) Inversion Tectonics . Special Publication, Geological Society London, v. 44, p. 17-40.

Higgs, W.G., Williams, G. D. & Powell, C. M., 1991, Evidence for flexural shear folding associated with extensional faults: Bull. geol. Soc. Am., v. 103, p. 710 -717.

Jackson, H.R., Faleide, J. I., & Eldholm, O., 1990, Crustal structure of the sheared south-wesetern Barents Sea continental margin. In: Arctic Geoscience. J.R. Weber. D.A. Forsyth. A.F. Embry. and S.M. Blasco (Eds.), Marine Geology, v. 93, p. 119-146.

Jackson, J.A., 1987, Normal faulting and crustal extension. In: Coward, M.P., Dewey, J.F., & Hancock, P.L.(Eds.), Continental Extensional Tectonics, Special Publication, Geological Society London, p. 3-18.

Jackson, J.A., & White, N. J. , 1989, Normal faulting in the upper continental crust: observations from regions of active extension: Journal of Structural Geology, v. 11, p. 1-36. .

Jackson, J. A., White, N. J., Garfunkel, Z., & Anderson, A., 1988, Relation between normal fault geometry, tilting and vertical motions in extensional terrains, an example from the southern Gulf of Suez: Journal of Structural Geology, v. 10, p. 155-170.

Jensen, L. N., & Broks, T. M., 1988, Late movements on the Trollfjord-Komagelv Fault Zone and rifting in the Nordkapp Basin. Abstract, 6th Annual TSGS meeting. Institute of Geology, University of Oslo, Intern Skriftserie, v. 54, p. 24-25.

Johansen, S. E., Henningsen, T., Rundhovde, E.,Saether, B. M., Fichler, C., & Rueslatten, H. G., 1994, Continuation of the Caledonides north of Norway: seismic reflectors within the basement beneath the southern Barents Sea: Marine and Petroleum Geology, v. 11, no. 2.

Johansen, S. E., Ostisty, B. K., Birkeland, Ø., Fedorovski, Y. F., Martirosjan, V. N., Christensen, O. B., Cheredeev, S. I., Ignatenko, E. A. & Margulis, L. S. , 1993, Hydrocarbon potential in the Barents Sea region: play distribution and potential. In: T. O. Vorren, E. Bergsager, Ø. A. Dahl-Stamnes, E. Holter, B. Johansen, E. Lie, & T. B. Lund, (Eds.), Arctic Geology and Petroleum, Potential Norwegian Petroleum Society Special Publication No. 2, Elsevier, Amsterdam, p. 273-320.

Johnson, H. D., Levell, B. K., & Seidlecki, S., 1978, Late Precambrian sedimentary rocks in east Finnmark, north Norway and their relationship to the Trollfjord-Komagelv fault: Journal of the Geological Society of London, v. 135, p. 517-533.

Kjøde, J., Storetvedt, K. M., Roberts, D., & Gidskehaug, A., 1978, Paleomagnetic evidence for large scale dextral movement along the Trollfjord-Komagelv Fault, Finnmark, North Norway: Physics Earth Planetary Interiors, v. 16, p. 132-144.

Larssen, G. B., Elvebakk, G., Henriksen, L. B., Kristensen, S. E., Nilsson, I., Samuelsberg, T.A., Stemmerik, L., & Worsely, D., 2002, Upper Paleozoic lithostratigraphy of the southern Norwegian Barents Sea: Norsk Geologisk Undersøkelser, Bulletin 444, 43. Geological Survey of Norway, Trondheim.

McClay, K.R., Norton, M. G., Coney, P., & Davis, G. H., 1986, Collapse of the Caledonian orogen and the Old Red Sandstone: Nature v. 323, p. 147-149.

Milani, E.J., & Davison, I., 1988, Basement Control and transfer tectonics in the Reconcavo-Tucano Jatoba Basin, NE Brazil: Tectonophysics, v. 154, p. 41-70.

Moe, A., 1974, Continental shelf north of 62^0 latitude. Offshore North Sea 1974: Technology Conference and Exhibition, Stavanger, G-IV/5, p. 1-18.

Mongat, M. M., 2011, Structural analysis of the Asterias Fault Complex in the SW Barents Sea, M.Sc. Thesis, University of Oslo, (NBN: no 29780).

Moretti, I., & Colletta, B., 1988, Fault-block tilting: the Gebel Zeit example. Gulf of Suez: Journal of Structural Geology, v. 10, p. 9-19.

Morley, C. K., Nelson, R. A., Pattion, T. L., & Munn, S. G., 1990 Transfer zones in the East African Rift System and their relevance to hydrocarbon exploration in rifts: AAPG Bulletin, v. 74, p. 1234-1253.

Mosar, J., Torsvik, T. H., & the Bat Team, 2002, Opening the Norwegian and Greenland Seas: Plate tectonics in Mid Norway since the Late Permian. In: E. A. Eide, (coord.), BATLAS—Mid Norway Plate Reconstruction Atlas With Global and Atlantic Perspectives, Nor. Geol. Unders, p. 48-61.

Myhre, A. M., Eldholm, O. & Sundvor, E., 1982, The margin between Senja and Spitsbergen Fracture Zones - Implications from Plate Tectonics: Tectonophysics, v. 89, p. 33-50.

Mørk, A., Embry, A. F., & Weitschat, W., 1989, Triassic Transgressive-Regressive cycles in the Sverdrup Basin, Svalbard and the Barents Shelf. In: J. D. Collinson, (Ed.) Correlation in hydrocarbon exploration. Graham & Trottman, London, p. 113-130.

Norton, M.G., 1986, Late Caledonide extension western Norway: a response to extreme crustal thickening: Tectonics v. 5, p. 195-204.

Nyland, B., Jensen, L.N., Skagen, J. I., Skarpnes O., & Vorren, T., 1992, Tertiary uplift and erosion in the Barents Sea: magnitude, timing and consequences. In: R.M. Larsen et al. (Eds.): Structural and tectonic modelling and its application to petroleum geology, Amsterdam: Elsevier., p. 153–162.

Pascal, C., Roberts, D. & Gabrielsen, R. H., 2005, Quantification of neotectonic stress orientations and magnitudes from field observations in Finnmark, northern Norway: Journal of Structural Geology, v. 27, p. 859-870.

Ramsay, J.G., & Huber, M. I., 1987, The techniques of modern structural geology: Folds and Fractures: London, Academic Press, v. 2, p. 700

Rider, M., 1988, Play potentials of the Barents Shelf: Oil and Gas Journal, p. 87-90.

Ritzmann, O., & Faleide, J. I., 2007, Caledonian basement of the western Barents Sea: Tectonics, v. 26, TC5014.

Roberts, A., & Yielding, G. , 1994, Continental extensional tectonics. In: P. L. Hancock, (Ed.) Continental Deformation, Pergamon Press, Oxford p. 223-251.

Roberts, D., 1971, Patterns of folding and fracturing in northeast Soroy: Norges geologiske undersokelse, v. 269, p. 89-95.

Roberts, D., 1972, Tectonic deformation in the Barents Sea region of Varanger peninsula, Finnmark: Norges geologiske undersokelse, v. 282, p. 1-39.

Roberts, D., & Gee, D. G., 1985, An introduction to the study of the Scandinavian Caledonides. In: D.G.Gee & B.A.Sturt (Eds.), The Caledonide Orogen - Scandinavia and related areas. (Wiley & Sons), p. 485-497.

Roberts, D., & Sturt, B. A., 1980, Caledonian deformation in Norway: Journal of the Geological Society of London, v. 137, p. 241-250.

Roberts, S., & Jackson, J. A. , 1991, Active normal faulting in Central Greece- An overview. In: A. M. Roberts, G. Yielding, & B. Freeman, (Eds.), The Geometry of Normal Faults, Special Publication, Geological Society of London, v. 56, p. 125-142.

Roufosse, M. C., 1987, The formation and evolution of sedimentary basins in the Western Barents Sea. In: J. Brooks & K. Glennie (Eds.), Petroleum Geology of North West Europe , Graham & Trotman, London, p. 1149-1161.

Rønnevik, H. C., & Jacobsen, H. P., 1984, Structures and basins in the western Barents Sea. In: A. M. Spencer (Ed.) Petroleum Geology of the North European Margin, p. 19-32.

Rønnevik, H. C., Beskow, B., & Jacobsen, H. P., 1982, Structural and stratigraphic evolution of the Barents Sea: Canadian Society of Petroleum Geologists Memoir, No. 8, p. 431-440.

Schultz, R. A., Soliva, R., Fossen, H., Okubo, C. H., & Reeves, D. M., 2008, Dependence of displacement–length scaling relations for fractures and deformation bands on the volumetric changes across them: Journal of Structural Geology, v. 30, p. 1405-1411.

Sclater, J. G., & Christie, P. A. F., 1980, Continental stretching: An explanation of the post-mid-Cretaceous subsidence of the Central North Sea Basin: Journal of Geophysical Research, v. 85, p. 3711 - 3739.

Siedlecka, A., 1975, Late Precambrian stratigraphy and structure of the northeastern margin of the Fennoscandian shield Norg: Geol. Unders. Bull. 316, p. 313-348.

Siedlecka, A., & Siedlicki, S. , 1972, Lithostratigraphic correlation and sedimentology of the Late Precambrian of Varanger Peninsula and neighbouring areas of East Finnmark, northern Norway. In: 24th InternationalGeological Congress Section 6, p. 349-358.

Steel, R. J., & Worsley, D., 1984, Svalbard's post-Caledonian strata an atlas of sedimentological patterns and paleogeographic evolution. In: A. M. Spencer (Ed.), Petroleum Geology of the North European Margin, p. 109-135.

Stemmerik, L., & Håkansson, E., 1991, Carboniferous and Permian history of the Wandel Sea Basin, North Greenland. In: J. S. Peel, & M. Sønerholm (Eds.) Sedimentary basins of North Greenland, Grønlands geol. Unders. Bull, v. 160, p. 141-151.

Sturt, B. A., Pringle, I. R., & Ramsay, D. M, 1978, The Finnmarkian phase of Caledonian Orogeny: Journal of Geological Society, v. 135, p. 597-610.

Sund, T., Skarpnes, O., Jensen, L. N. & Larsen, R. M., 1986, Tectonic development and hydrocarbon potential offshore Troms, northern Norway. In: M. T. Halbouty (Ed.) Future petroleum provinces of the World. AAPG Memoir, v. 40, p. 616-627.

Surlyk, F., Piasecki, S., Rolle. F., Stemmerik, L., Thomsen, E., & Wrang, P., 1984, The Permian basin of East Greenland. In: A. M. Specner (Ed.) Petroleum Geology of the North European Margin, Graham & Trotman, London, p. 303-315.

Syrstad, E., Tallleraas, E., & Bergseth, S., 1976, Gravity modelling offshore Troms, northern Norway. Offshore North Sea 1976: Exploration Geology and Geophysics, Technology Conference and Exhibition, Stavanger, 1976. .

Talleraas, E., 1979, The Hammerfest Basin – an aulacogen? Proceedings, Norwegian Sea Symposium: Norwgeian Petroleum Society, v. NSS/18, p. 1-13.

Tearpock, D. J., & R. E. Bischke, 1991, Applied subsurface geological mapping: New York Prentice-Hall, p. 648.

Thorsen, C. E., 1963, Age of growth faulting in Southeast Louisiana: Transactions - Gulf Coast Association of Geological Societies, v. 13, p. 103–110.

Townsend, C., 1987, Thrust transport directions and thrust sheet restoration in the Caledonides of Finnmark North Norway: Journal of Structural Geology, v. 9, p. 345-352.

Trudgill, B., & Cartwright, J., 1994, Relay-ramp forms and normal-fault linkages, Canyonland National Park, Utah: Geological Society of America Bulletin, v. 106, p. 1143-1157.

Verrall, P., 1981, Structural interpretation with application to North Sea problems, Course Notes No. 3: JAPEC, U.K.

Vorren, T.O., Kristoffersen, Y, & Andreassen, K., 1986, Geology of the inner shlf west of North Cape, Norway. : Norsk geologisk tidsskrift, v. 66, p. 99-105.

Walsh, J. J., &Watterson, J., 1991, Geometric and kinematic coherence and scale effects in normal fault systems. In: A. M., Yielding, G., and Freeman, B., (Eds.), The geometry of normal faults: Geological Society of London Special Publication, v. 56, p. 193-206.

Westaway, R., & Kusznir, N., 1993, Fault and bed ‘rotation’ during continental extension: block rotation or vertical shear: Journal of Structural Geology, v. 15, p. 753-770.

Wheeler, J., 1987, Variable-heave models of deformation above listric normal faults, the importance of area conservation: Journal of Structural Geology, v. 9, p. 1047-1050.

White, N. J., 1987, Constraints on the measurement of extension in the brittle upper crust: Norsk Geol. Tidsskr., v. 67, p. 269-279.

White, N. J., & Yielding, G. , 1991, Calculating normal fault geometries at depth: theory and examples. In: A. M., Yielding, G., & Freeman, B., (Eds.) The Geometry of Normal Faults, Special Publications, Geological Society London, v. 56, p. 251-260.

Whtie, N. J., Jackson, J. A. & McKenzie, D. P., 1986, The relationship between the geometry of normal faults and that of the sedimentary layers in their hangingwalls: Journal of Structural Geology, v. 8, p. 897 – 909.

Worsley, D., Johansen, R, & Kristensen, S. E., 1988, A Lithostratigraphic Scheme for the Mesozoic and Cenozoic Succession Offshore Mid & Northern Norway: Norwegian Petroleum Directorate, v. 4, p. 42-65.

Worthing, M. A., 1984, Fracture patterns on eastern Seiland, north Norway and their possible relationships to regional faulting: Norges geologiske undersokelse, v. 396, p. 35-41.

Ziegler, P. A., 1986, Geodynamic model for the Palaeozoic crnstal consolidation of Western and Central Europe: Tectonophysics, v. 126, p. 303-328.

Ziegler, P. A., 1988, Evolution of the Arctic-North Atlantic and the Western Tethys: AAPG Memoir, v. 43, p. 198.

Ziegler, W. H., Doery, R. and Scott, J. , 1986, Tectonic habitat of Norwegian oil and gas. In: A. M. Spencer (Ed.) Habitat of Hydrocarbons on the Norwegian Continental Shelf, Graham and Trotman, London, p. 3-19. .

Øvrebø, O., & Talleraas, E., 1976, The structural geology of the Troms area. In: Exploraiton Geology and Geophysics. Offshore North Sea Conference, Norwegian Petroleum Society, Article G/TV-6.

Øvrebø, O., & Talleraas, E., 1977, The structural geology of the Troms area Barents Sea: Geojournal, v. 1, p. 47-54.

http://en.wikipedia.org/wiki/File:Barents_Sea_map.png. Last accessed 10th February, 2012

http://factpages.npd.no/factpages/Default.aspx?culture=en. Last accessed 10th February, 2012.

http://www.slb.com/services/software/geo/petrel.aspx. Last accessed 10th February, 2012.